Technische Universität München

Fakultät für Medizin

Institut für Medizinische Mikrobiologie, Immunologie und Hygiene

Molecular and functional changes induced by mutations transform the tumor suppressor RNF43 into an oncogene

Martina Isabell Grandl, M.Sc. (TUM)

Vollständiger Abdruck der von der Fakultät für Medizin der Technischen Universität München zur Erlangung des akademischen Grades eines

Doktors der Naturwissenschaften **(Dr. rer. nat.)**

genehmigten Dissertation.

Vorsitzender:	Prof. Dr. Dirk Busch
Prüfer der Dissertation:	1. Prof. Dr. Markus Gerhard
	2. Prof. Dr. Martin Hrabé de Angelis
	3. Prof. Dr. David Horst

Die Dissertation wurde am 14.03.2016 bei der Technischen Universität München eingereicht und durch die Fakultät für Medizin am 12.10.2016 angenommen

Diese Arbeit wurde in der Zeit von Dezember 2011 bis März 2016 im Institut für Medizinische Mikrobiologie, Immunologie und Hygiene der Technischen Universität München unter Anleitung von Herrn Prof. Dr. Markus Gerhard durchgeführt

Munich, 14th March 2016

All truths are easy to understand once they are discovered;
the point is to discover them.

(Galileo Galilei, 1564-1642)

Table of contents

1 Abstract

Colorectal cancer is one of the most common solid tumors worldwide. Despite advances in diagnosis and treatment colorectal cancer often has a poor prognosis for cancer patients. A better understanding of the molecular mechanisms behind colorectal carcinogenesis is essential for developing new therapies and improving survival. Molecular studies have already revealed that genetic alterations in genes encoding for members of the Wnt pathway, which maintains the intestinal tissue homeostasis, promote carcinogenesis. However, targeting Wnt signaling by therapeutic inhibition is difficult, because most substances act upstream of the oncogenic mutations in the Wnt pathway, being only applicable to a small subset of colorectal cancer patients. The RING finger protein 43 (RNF43) is an E3 ubiquitin ligase, which was originally identified in intestinal stem cells. Studies showed that RNF43 is overexpressed in colonic adenomas and adenocarcinomas. RNF43 has been reported to function as an oncogene as well as a tumor suppressor, being localized either in the nuclear compartment or at the cellular membrane. In this study, the subcellular localization of RNF43 under overexpression as well as endogenous conditions was analyzed. RNF43 was detected primarily in the nucleus of human and murine intestinal crypts as well as in human cancer cells. Furthermore, functional analysis of endogenous RNF43 revealed that RNF43 acts as a tumor suppressor by inhibiting Wnt signaling and suppressing the tumorigenic capacity of tumor cells. RNF43 was found to physically interact with T cell factor 4 (TCF4) in human cells by sequestering TCF4 to the nuclear membrane, thus silencing TCF4 transcriptional activity in the presence of constitutively active mutants of APC and β-catenin. Finally, the impact of mutations in RNF43, identified in human gastrointestinal tumors, was studied. Most analyzed mutants impaired the Wnt inhibitory mechanism due to mislocalization of mutated RNF43. More interestingly, mutating the RING domain of RNF43 transactivated Wnt signaling *in vitro*. This was confirmed *in vivo* using a new mouse model in which the RING mutation H292R/H295R was introduced in the genomic locus of *Rnf43*. These mutations induced intestinal lesions and increased proliferation of cells. These findings indicate that RNF43 inhibits Wnt signaling downstream of activating oncogenic mutations. Furthermore, mutations in RNF43 were identified, which lead to loss of function or even changing the tumor suppressor activity to an oncogenic activity of RNF43. Validating RNF43 as a biomarker and mimicking the inhibitory activity of RNF43 may help to develop new strategies for patients suffering from colorectal cancers with hyperactive Wnt signaling due to mutations in the pathway.

Zusammenfassung

Weltweit zählt das kolorektale Karzinom zu den häufigsten bösartigen Tumoren. Trotz guter Fortschritte bei der Diagnose und Behandlung von Patienten mit kolorektalen Tumoren steht diese Krankheit in den meisten Fällen für eine schlechte Prognose. Die Erforschung des molekularen Hintergrundes kolorektaler Tumore ist unabdingbar für das Verständnis dieser Krankheit, um neue Therapien zu entwickeln und damit das Überleben der Patient zu verbessern. Wissenschaftliche Studien auf molekularer Ebene haben bereits gezeigt, dass genetische Veränderungen im Wnt Signalweg die Karzinogenese fördern, da dieser zur Aufrechterhaltung der Homöostase des Intestinaltrakts sehr wichtig ist. Es hat sich jedoch gezeigt, dass eine therapeutische Behandlung, welche auf den Wnt Signalweg zielt, sehr schwierig ist. Die meisten Medikamente setzen oberhalb genetischer Mutationen im Wnt Signalweg an und sind daher nur für eine kleine Untergruppe von Patienten mit kolorektalen Karzinomen verwendbar. Die E3 Ubiquitinligase RING finger protein 43 (RNF43) wurde in den Stammzellen des Intestinaltrakts entdeckt. Studien zeigen, dass RNF43 vermehrt in Kolonadenomen gefunden wird und im Kolon Adenokarzinom stark überexprimiert ist. Zudem, wurde RNF43 sowohl als Onkogen als auch als Tumorsuppressor beschrieben. Darüber hinaus wurde RNF43 in einigen Veröffentlichungen im Zellkern lokalisiert und in anderen an der Zellmembran. In dieser Arbeit wurde versucht, die zelluläre Lokalisation von überexprimierten und endogenem RNF43 aufzuklären. Dabei wurde RNF43 ausschließlich im Zellkern der Krypten sowohl von humanen und murinen intestinalen Geweben als auch von humanen Krebszellen gefunden. Untersuchungen über die Funktion von RNF43 zeigten, dass RNF43 als Tumorsuppressor den Wnt Signalweg inhibiert und das karzinogene Potenzial von Krebszellen unterdrückt. Dabei interagiert RNF43 direkt mit dem T cell factor 4 (TCF4), indem es TCF4 an die Zellkernmembran bindet und damit seine transkriptionelle Aktivität in Tumorzellen mit konstitutiv-aktiven Mutanten von APC und β-catenin verhindert. Abschließend wurde der Einfluss von einigen RNF43 Mutationen, welche in gastrointestinalen Tumoren gefunden wurde, analysiert. Viele Mutationen hoben die Wnt-inhibitorische Wirkung durch veränderte Lokalisation von RNF43 auf. Interessanterweise verursachte eine Mutationskombination in der RING Domäne von RNF43 eine zusätzliche Aktivierung des Wnt Signalwegs. Die Einführung der H292R/H295R Mutationen in die genomische *Rnf43* Sequenz von Mäusen verursachte Darmläsionen im Intestinaltrakt und führte zu erhöhter Zellproliferation. Diese Ergebnisse zeigen deutlich, dass RNF43 als Tumorsuppressor unterhalb onkogener Mutationen im Wnt Signalweg wirkt. Darüber hinaus wurde gezeigt, dass Mutationen in *RNF43* nicht nur zum Verlust der Tumorsuppressorwirkung führen, sondern dabei auch eine onkogene Wirkung verursachen können. Die Validierung von RNF43 als Biomarker und das Nachahmen der inhibitorischen Wirkung von RNF43 auf den Wnt

Signalweg kann dabei helfen Patienten mit kolorektalen Tumoren, welche aus mutationsbedingter Wnt Hyperaktivität entstanden sind, gezielter und erfolgreicher zu behandeln.

2 Introduction

2.1 Anatomy and physiology of the intestine

The gastrointestinal (GI) tract is important for the human digestive system. It is responsible for the uptake and digestion of food, for the absorption of nutrients, for the expulsion of indigestible food components and immune surveillance.

Anatomically, the upper GI tract combines mouth, pharynx, esophagus and stomach, where the ingestion and the first phase of digestion occur. The main digestive function is, however, localized in the lower GI tract, which includes the small and large intestine.
The small intestine is structurally divided into three parts: the duodenum, the jejunum, and the ileum. Every segment of the small intestine performs different digesting functions. The duodenum is the first and shortest segment of the small intestine. It receives partially digested food, which is known as chyme, from the stomach. In preparation for absorption the chyme undergoes chemical digestion with the help of digestive enzymes and intestinal juices secreted by cells of the intestinal wall. To facilitate the chemical digestion, chemical secretions from the pancreas, liver and gallbladder are mixed with the chyme. The jejunum and the ileum absorb nutrients and transport them into the bloodstream. The inner lining of the small intestine is folded back and forth to maximize the surface area for better nutrient absorption. In addition, the high density of bacteria in the small intestine, which increases towards the large intestine, helps in the enzymatic processing of food material.
The large intestine, synonymously called colon, is the distal part of the lower gastrointestinal tract and responsible for the fine-tuned absorption of electrolytes and water from the chyme. The colon is larger in diameter than the small intestine and is divided into six sections: cecum with the appendix, ascending colon, transverse colon, descending colon, sigmoid colon, and rectum. The cecum absorbs fluids and salts that remain after intestinal digestion, while mixing its contents with lubricating mucus. The ascending colon carries feces from the cecum to the transverse colon meanwhile bacteria digest the transitory material in order to release vitamins. The main absorption and feces formation takes place in the transverse colon, where bacteria further break down the food matter in a process called fermentation. The descending and sigmoid colon stores the feces to be emptied into the rectum by absorbing the rest water. The rectum stores fecal matter produced in the colon until the body is ready to eliminate the waste through the process of defecation (**Figure 1**).

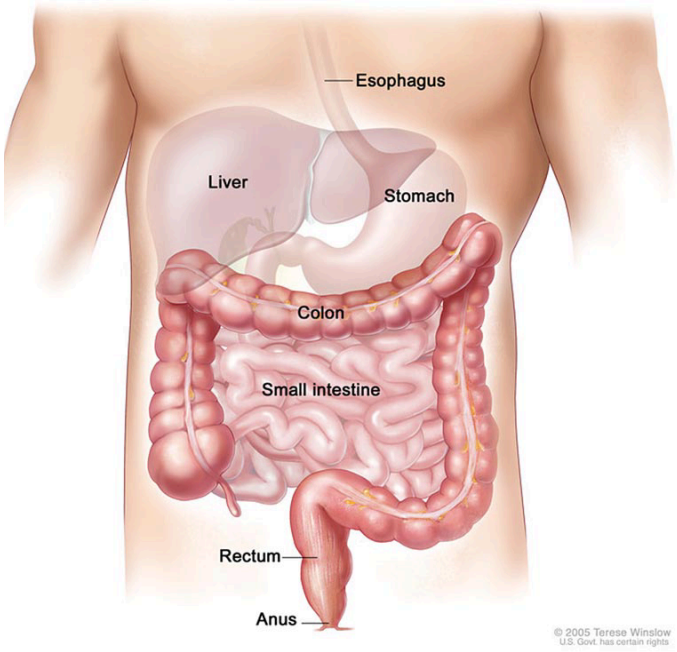

Figure 1: Schematic representation of the gastrointestinal tract.
Reprinted with permission from NIH medlineplus Spring 2009 Issue: Volume 4 Number 2 Pages 7 – 8.

Histologically, the intestine is a smooth muscular tube consisting of four concentric tissue layers: on the luminal side, the *Tunica mucosa*, followed by the *Tela submucosa* and the *Tunica muscularis* and finally, on the peritoneal side, the *Tunica serosa*. The latter is made of connective tissue and covered by a simple squamous epithelium. It produces mucus, which prevents friction damage from the intestine. The *Tunica muscularis* is composed of circular and longitudinal smooth muscles whose coordinated contraction ensures the directed transport of chyme and feces. This so-called peristalsis is controlled by highly autonomous enteric nervous system located in the *Tunica muscularis* and the *Tela submucosa*. Furthermore, this layer of fibrous connective tissue harbors a large number of blood and lymph vessels. The luminal side is formed by the *Tunica mucosa,* which can be divided further into the *Lamina epithelialis mucosae*, the *Lamina propria mucosae*, and the *Lamina muscularis mucosae*. The *Lamina muscularis mucosae* is a thin layer of smooth musculature defining the border of the mucosa. The *Lamina propria mucosae* contains many blood and lymph vessels. The *Lamina epithelialis mucosae* is the epithelial tissue layer surrounding the lumen. In the small intestine the epithelium is occupied with a high number of microscopic finger-like projections, which are called villi, to maximize the surface for absorption and digestion. In contrast, the colon has a flat epithelial surface, where chyme and feces pass through and from where electrolytes and water are absorbed[1,2] (**Figure 2**).

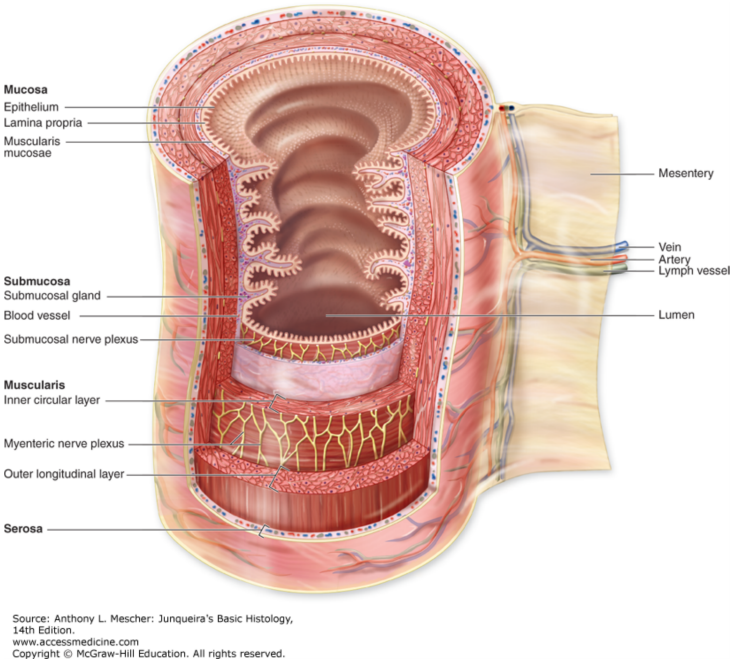

Figure 2: Schematic representation of major layers and organization of the digestive tract.
Diagram shows the intestinal wall. The lamina propria of the small intestine is folded and occupied with villi to extend the surface, whereas the mucosa of the large intestine has a flat surface. Reprinted with permission from McGraw-Hill Education: Major layers and organization of the digestive tract, Junqueira's Basic Histology: Text and Atlas e14 (2016).

2.2 Intestinal homeostasis

The intestinal epithelium has the well-defined architecture of a simple columnar epithelium. It forms characteristic so-called Lieberkühn crypts, where proliferative crypt base columnar (CBC) stem cells occupy the bottom of the crypts, and differentiated non-proliferative cells constitute the epithelium on the top and between the crypts. It is a classical self-renewing tissue with very high cell turnover. The average life span of an intestinal epithelial cell is less than a week with exception of Paneth cells, which survive around 20 days[3]. The undifferentiated crypt progenitor cells divide every 12 to 16 hours and give rise to approximately 200 cells per crypt per day[4]. Rapidly proliferating transit-amplifying (TA) cells, generated by stem cells constantly migrate up towards surface epithelium of the intestine. During their migration, the cells differentiate acquiring their absorptive function before they undergo anoikis and are shed into the lumen[5]. According to different functions of small and large intestine the epithelium is based on different cells.

Small intestine

The most abundant cells in the small intestine are absorptive enterocytes, which secrete hydrolytic enzymes to digest the food exiting the stomach. In addition, goblet cells are found in between the enterocyte population. Goblet cells secret high glycosylated mucins to

generate mucus, which supports the passage of the food material. A small population of enteroendocrine cells are spread as single cells in between other epithelial cells secreting hormones e.g. somatostatin, motilin, cholecystokinin, neurotensin, vasoactive intestinal peptide, and enteroglucagon[6,7]. Paneth cells are located at the bottom of the crypts between intestinal stem cells. They are filled with granules containing antimicrobial peptides such as cryptdins and α-defensins[8]. The granules are discharged into the crypt lumen in response to the entry of bacteria or food-related stimulation by acetylcholine[4,8,9]. Finally, three other cell types are found in the epithelium, which are poorly defined up to now: cup cells, tuft cells and Peyer's patch-associated M cells[10] (**Figure 3**).

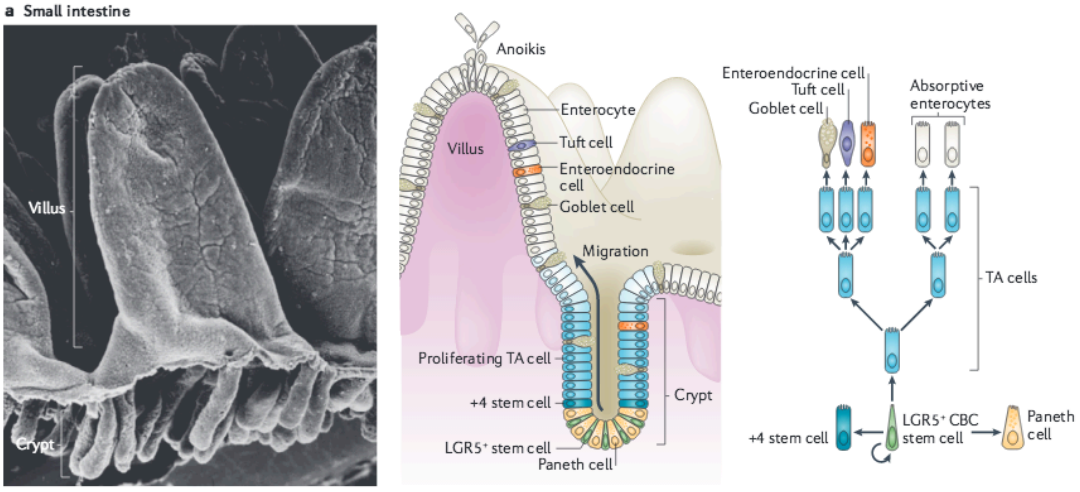

Figure 3: Epithelial self-renewal in the small intestine

Scanning electron micrograph of the small intestine (left panel). LGR5$^+$ crypt base columnar stem cells are intercalated with Paneth cells at the crypt base. Next to the stem cell compartment are proliferating transit-amplifying (TA) cells differentiating into the various functional cells on the villi (enterocytes, tuft cells, goblet cells and enteroendocrine cells). The +4 'reserve' stem cells can restore the LGR5$^+$ CBC stem cell compartment (middle panel). Differentiating cell hierarchy is shown in the tree on the right panel. Reprinted with permission from Macmillan Publisher Ltd: [Nature Reviews|Molecular Cell Biology] (Nat Rev Mol Cell Biol. 2014; 15:19-33) copyright (2014).

Large intestine

The colon is specialized for generation of compacting stool and rapid excretion. Therefore, the colonic epithelium has a flat luminal surface without any villi. In contrast to the small intestine, the most abundant colonic epithelial cells are goblet cells. Here, they provide the extra lubrication needed to facilitate the passage of water-free material towards the rectum. In addition, very few absorptive enterocytes, enteroendocine cells and tuft cells are found. Characteristic for the colonic crypt is the absence of Paneth cells (**Figure 4**).

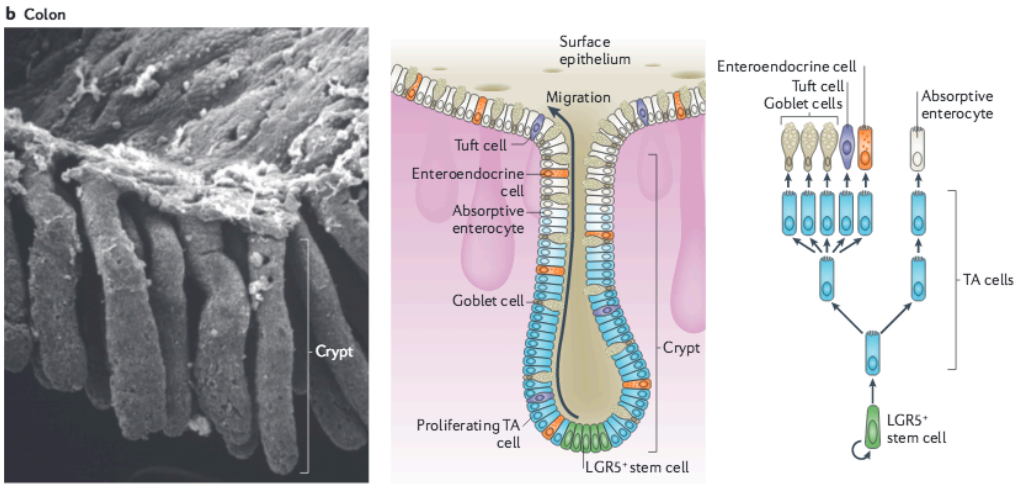

Figure 4: Epithelial self-renewal in colon epithelium.
Scanning electron micrograph of the colonic epithelium (left panel). LGR5^{+} stem cells at the crypt base generate rapidly proliferating TA cells (middle panel). TA cells subsequently differentiate into goblet cells, enterocytes, enteroendocrine cells and tuft cells (right panel). Reprinted with permission from Macmillan Publisher Ltd: [Nature Reviews|Molecular Cell Biology] (Nat Rev Mol Cell Biol. 2014; 15:19-33) copyright (2014).

In order to ensure intestinal homeostasis, mechanisms are required that tightly regulate proliferation, migration and apoptosis. Interestingly, these processes are controlled only by a relatively small number of signaling pathways including the Wnt[11], Notch[12], TGFβ/BMP[13] and Hedgehog[14] pathways. On the one hand these signaling cascades are known to play important roles during embryogenesis and organ development. On the other hand, the same pathways are also involved in the regulation and control of multiple self-renewing processes. For example, high levels of β-catenin induced by Wnt signaling keep crypt base cells in stem cell–like state. During migration of these cells, β-catenin levels decrease and the cells consequently lose their stem cell phenotype differentiating into functional enterocytes. In recent years, large experimental evidence has demonstrated that disturbances of these fine-regulated pathways can lead to disease and tumor formation[15-19].

2.3 Colorectal cancer

2.3.1 Epidemiology of colorectal cancer

Cancer is one of the leading cause of death worldwide[20]. An estimated 14.1 million new cancer cases and 8.2 million cancer deaths occurred in 2012 worldwide according to the World Cancer Report 2014[21]. Among them, colorectal cancer (CRC) is the third most common cancer in men (incidence of 746.300 cases, representing 10 % of all new cancers) and the second most common in women (incidence of 614,300 cases, representing 9.2 % of all new cancers) worldwide according to GLOBOCAN 2012[22], International Agency for Research on

Cancer. The highest rates are estimated in Australia and New Zealand, Western Europe, and North America (45 % for men and 32 % for women of all new cancers), the lowest in Middle and West Africa and (< 5 % of all new cancers). The rates are higher in men than in women. This means that the overall lifetime risk is about 4.7 % for men and 4.4 % for women. In general, colon cancer upstream the rectum is approximately two-fold more frequent than rectal cancer. While mortality from CRC has been decreasing in Western countries, presumably due to improved treatment, increased awareness, and early detection, mortality continues to increase in countries with poor health infrastructure[21-24]. Furthermore, CRC incidence depends on the patient's age being low in patients under the age of 45 years (2 per 100,000), but increasing to 150 per 100,000 in patients over 65 years[20,25-27].

2.3.2 Etiology of colorectal cancer

CRC is a multifactorial disease. Exogenous factors, inflammatory conditions, and genetic factors are involved in the development of colorectal cancer. Generally, colorectal cancer is divided into two basic etiologic categories: hereditary and sporadic cancer. Sporadic – nonhereditary – colorectal cancer is defined as cancer without any family cases of colorectal cancer and the patient being above the age of 50 years. It occurs more frequently than hereditary colorectal cancer. Epidemiologic studies have linked increased risk of sporadic colorectal cancer to exogenous factors as diet high in red meat and animal fat, low-fiber diets, and low overall intake of fruits and vegetables[28]. Furthermore, obesity, overweight, and lifestyle choices such as cigarette smoking, excessive alcohol consumption, and sedentary habits have also been associated with increased risk for colorectal cancer[29-31]. Although less is known about colorectal cancer genetics, current research indicates that genetic factors have the greatest correlation to colorectal cancer. However, only 5 to 10 % of CRC cases are attributed to well characterized hereditary syndromes with increased lifetime risk of 80 % to 100 %[32-35]. One of them is known as familial adenomatous polyposis (FAP). Affected individuals carry an almost 100 % risk of developing colon cancer by age of 40 years[36]. Another well know syndrome is the hereditary non-polyposis colon cancer syndrome (HNPCC), also known as Lynch syndrome, which possess about a 40 % lifetime risk for developing colorectal cancer[35,37,38]. Moreover, recent twin studies suggested that up to 30 % of all CRC cases might have genetic etiology, which has been poorly understood to date[39-41]. For instance, patients with chronic inflammatory bowel disease, this is Crohn's disease (CD) or ulcerative colitis (UC), show an elevated risk for developing CRC[42,43]. Other syndromes such as MUTYH-associated polyposis (MAP)[44], Peutz-Jeghers syndrome (PJS)[45,46], juvenile polyposis syndrome (JPS)[47], and hyperplastic polyposis (HPP)[48] are attributed to less than 1 % of CRCs[49].

2.4 Development of colorectal cancer

2.4.1 Genetic model of colorectal cancer

CRC mostly develops sporadically, which accounts for 75 % of all colon cancer cases. In 1990, Eric Fearon and Bert Vogelstein proposed a multi-step genetic model for colorectal carcinogenesis[50] in which they described how most of sporadic tumors arise from previously healthy tissue. The model is based on four assumptions. Firstly, colorectal tumors are clonal entities and arise as a result of mutational activation of oncogenes coupled with the mutational inactivation of tumor suppressor genes. Secondly, mutations in at least four to five genes are required for the formation of a malignant tumor. Thirdly, the final accumulation of mutations does not have to happen in a specific order, and fourthly, mutant tumor suppressor genes appear to exert a phenotypic effect even when present in the heterozygous state[50].

Microscopically, the first lesions observed seem to be aberrant crypt foci (ACF), which are clusters of abnormal tube-like glands in the colon mucosa. These ACF develop from single mutated cells, which typically begin with mutation-derived inactivation of the *APC* gene. Subsequent activating mutations of oncogenes and inactivation of tumor suppressor genes as well as DNA hypermethylation lead to additional growth advantages causing adenomas. Finally, loss of heterozygosity (LOH) in chromosomal regions encoding for important tumor suppressor genes such as p53 opens the last door for the development of carcinoma (**Figure 5**).

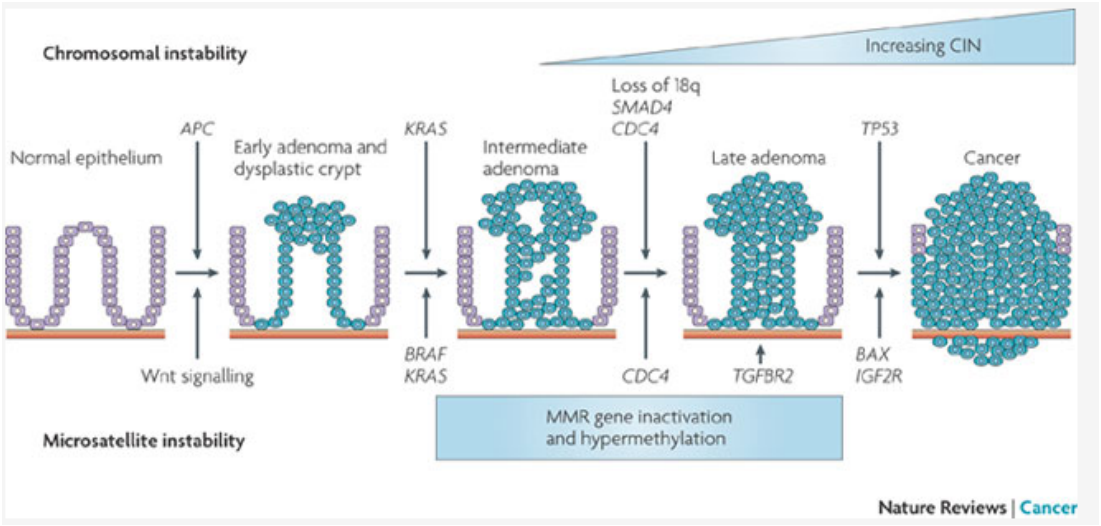

Figure 5: Schematic representation of the multi-step tumor progression model proposed by Bert Vogelstein and Eric Fearon.
APC mutations initiate the neoplastic process. Tumor progression results from DNA hypermethylation, activation of the oncogene *K-ras* and inactivation of genes on the chromosome locus 18q21. Finally, loss of the tumor suppressor gene p53 leads to carcinogenesis. During the process levels of nuclear β-catenin and probability of chromosomal instability increase permanently. Reprinted with permission from Macmillan Publisher Ltd: [Nature Reviews|Cancer] (Nat Rev Cancer. 2009; 9: 489499-33) copyright (2009)

2.4.2 Genetic mutations in colorectal cancer

In terms of colorectal cancer disease, the model of Bert Vogelstein and Eric Fearon has become widely accepted. Up to now, several mutations in oncogenes, tumor suppressor genes, and stability genes have been identified, which are strongly associated with the development of colorectal cancer.

Tumor suppressors:

APC: Adenomatous polypsis coli promotes the degradation of β-catenin, thereby regulating the transcription of Wnt target genes involved in cell cycle[51-53]. Inactivated *APC* leads to a growth advantage of the affected cells resulting in a neoplastic epithelium or in case of germline mutations leads to FAP. Approximately 70-80 % of sporadic colorectal adenomas and carcinomas have somatic inactivating *APC* mutations. Allelic losses, many point mutations at two hot spot regions (codon 1061 and 1309), and truncating mutations have been found in chromosome 5q21 where *APC* is localized[52,54,55].

SMAD4: SMAD family member 4 – also referred to as DPC4[56] - belongs to the Smad family, which mediates TGF-β signaling pathway. Inactivating *SMAD4* point mutations are found in ~10–35 % of colorectal tumors[57-60], resulting in juvenile polyposis syndrome[47]. Also, loss of *SMAD4* has been reported to associate with poor prognosis[61].

CDC4: Cell division control protein 4 (also known as Fbxw7) was identified as an E3 ubiquitin ligase targeting cyclin E, c-Myc, c-Jun and Notch for degradation[62,63]. Somatic *CDC4* mutations were detected in 9 % of HNPCC and FAP carcinomas, and in 10 % of sporadic carcinomas[64] with R465C being the most prominent mutation[65]. In addition, loss of *CDC4* induces chromosomal instability (CIN)[66,67].

TP53: Tumor protein 53 (p53) plays a crucial role in apoptosis, genomic stability, and inhibition of angiogenesis. *TP53* is located on chromosome 17q[68], where loss of heterozygosity is frequently observed in colorectal cancer as late event in tumorigenesis[69]. In addition, approximately 50 % of colorectal cancer cases harbor different *TP53* mutations with high frequencies observed in distal colon and rectal tumors[70]. Over 50 publications described mutations in the *TP53* gene with their relevance in colorectal cancer[71-74].

Oncogenes:

KRAS: Kirsten rat sarcoma viral oncogene homolog regulates primarily cell division. Mutated KRAS is found in 33 % of sporadic CRC, where it is mainly mutated in exon 2 (codons 12 and 13) and to a lesser extent in exon 3 (codon 61)[75-79]. Interestingly, the chronological order of mutation in regard to *KRAS* and *APC* is important. If the mutation occurs after a primary *APC*

mutation, it will progress to cancer[80]. Otherwise, *KRAS* mutations lead to non-dysplastic lesions and hyperplastic polyps[81,82].

BRAF: B-Raf is a member of RAF family of serine/threonine kinases and mediates cellular responses to growth signals. Over 30 activating mutations of the *BRAF* gene related to different human cancers have been identified. The mutation frequency in colorectal cancer is reported from 5 to 10 %[83,84], with the vast majority being a V600E hotspot mutation[83,85]. Mutations in *BRAF* were found to be mutually exclusive with mutations in *KRAS*[84,86].

CTNNB1: β-catenin is bound to membrane-associated E-cadherin and essential for its correct positioning and function[87,88]. In addition, activated Wnt signaling leads to cytoplasmic and subsequent nuclear accumulation of β-catenin[89]. According to the cosmic database approximately 400 studies describe *CTNNB1* mutations and their effect on different cancer types[65]. In colorectal cancer S33Y-, T41A-, and S45F point mutations in β-catenin are the most frequent mutations[65,90-93].

Stability genes:

MSH2, MSH6, MLH1, and PMS1/2: These five genes belong to the DNA mismatch repair (MMR) family[94-99]. Defective mismatch repair genes have been linked to hereditary nonpolyposis colon cancer (HNPCC) as well as to sporadic cancers that exhibit length polymorphisms in simple repeat (microsatellite) DNA sequences[33,100,101]. Germline mutations in one of four major HNPCC-associated MMR genes are detected in 2 % to 4 % of CRC patients[102,103]. Approximately 70 % of known mutations in HNPCC are truncated MLH1 and MSH2 proteins, whereas *MSH6* mutations are more commonly in endometrial cancer predisposition, and *PMS2* mutations are rare in HNPCC[103,104]. Moreover, in sporadic cancers up to 15 % of all colon cancers somatic mutations inactivate both mismatch repair alleles[102,105].

2.4.3 Altered signaling pathways in CRC

Cancer development arises as a consequence of genetic alterations to cellular genes, which may be inherited or evolve spontaneously. Among thousands of mutations, only two to eight are typically driver mutations that cause progression of the cancer[106]. The genetic alterations in cancer cells can be connected to signaling pathways that control processes associated with tumorigenesis. Moreover, single signaling pathways cross talk[107,108] and can be placed in signaling networks (**Figure 6**), thereby driving tumor progression. Oncogenic mutations result in constitutively activated proteins and tumor suppressor mutations reduce the activity of negatively regulated proteins. They are often involved in signaling pathways regulating

cellular processes, such as cell cycle (e.g. TGFβ[13,109]), proliferation (e.g., Ras/MAPK[110]), survival (e.g. Akt[111,112]), DNA damage and apoptosis[71] (e.g. p53), and mobilization of resources (e.g. receptor tyrosine kinases, RTK, and Cytokine receptors, GPCR). In addition, components of developmental signaling pathways, such as Wnt, Hedgehog (Hh), Hippo, and Notch can also be affected. Thus, different signaling pathways are involved in development and progression of colon cancer. However, the most important pathway linked to colorectal cancer is the Wnt signaling pathway.

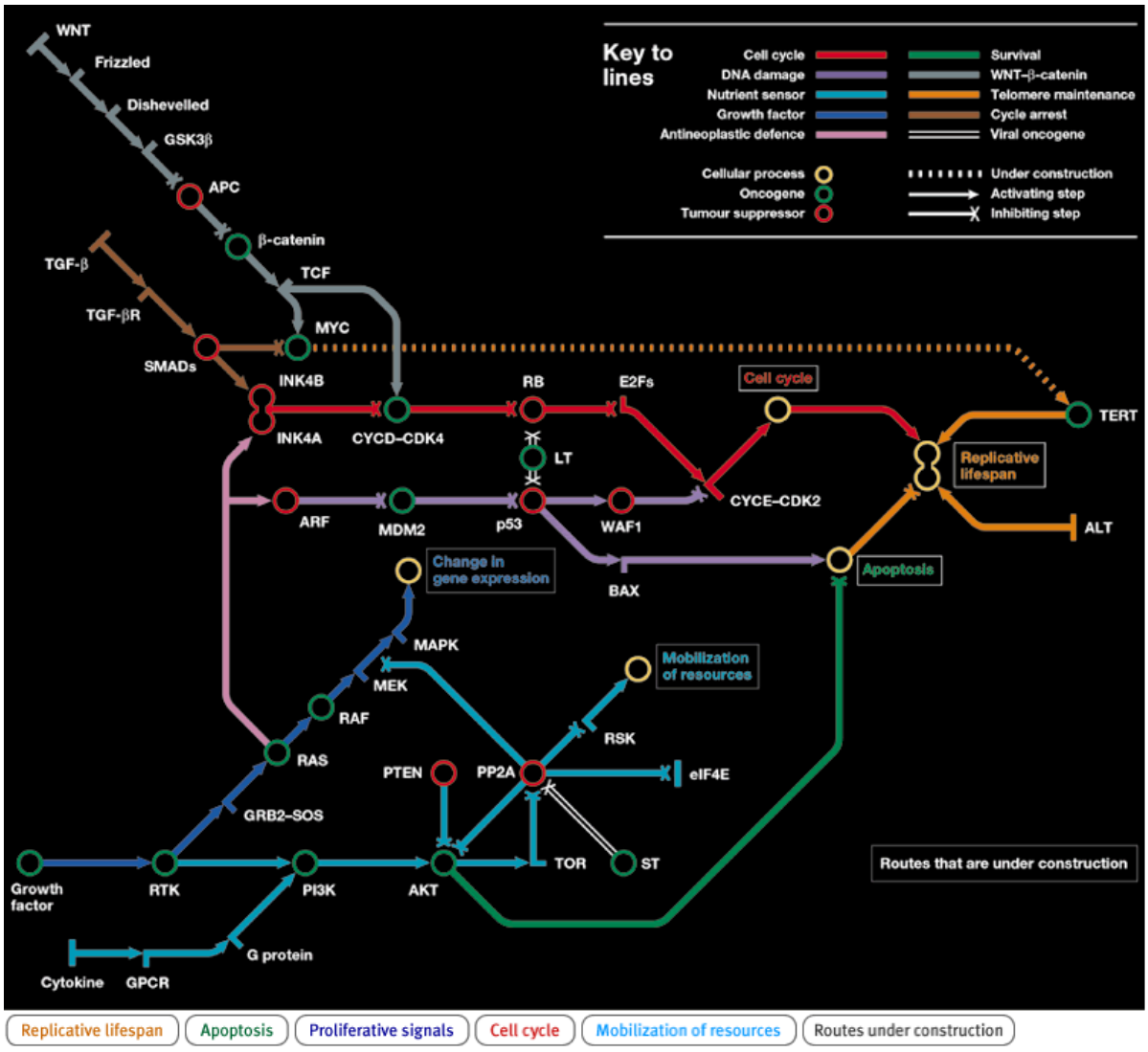

Figure 6: Schematic representation of signaling pathway networks in cancer.

Reprinted with permission from Macmillan Publisher Ltd: [Nature Reviews|Cancer] (Nat Rev Cancer 2002; 2; No5) copyright (2002)

2.5 Wnt signaling pathway

2.5.1 Wnt pathway

Since the early 1990s, the Wnt pathway has become one of the best-studied signaling cascades in the intestinal (patho)physiology. Rijsewijk *et al*. identified the *Drosophila* segment polarity gene *wingless* (wg) as the orthologous of the mouse mammary oncogene *int-1*[53]. The combination of both terms led to the neologism Wnt. Numerous subsequent *in vitro* and *in vivo* studies revealed that this pathway is evolutionarily highly conserved[113-116]. Up to now 19 *Wnt* genes in man and mice have been described, which encode for secreted cysteine-rich glycoproteins[115]. Murine WNT3A was the first purified and characterized Wnt protein[117]. Wnt proteins act in cell-to-cell communication by binding to members of the seven-span transmembrane receptor family named Frizzled (Fzd)[118,119] and the low density lipoprotein (LDL) receptor-related proteins 5 and 6 (LRP5/6)[120-122]. Activation of these receptor complexes leads to intracellular responses that regulate cell proliferation, cell polarity as well as cell fate determination during embryonic development[122,123] and in adult intestinal homeostasis[119]. Several studies have classified Wnt signaling into two types: one canonical (β-catenin-dependent) and two non-canonical (β-catenin-independent) pathways.

Canonical Wnt signaling

The binding of Wnt proteins to the Frizzled-LRP5/6 receptor complex[121] induces the canonical Wnt pathway. This leads to activation of the adaptor proteins of the Dishevelled (Dvl) family[124], which then inhibits formation of the protein complex including the scaffold protein axin, the kinase Glycogen synthase kinase 3β (GSK-3β), casein kinase 1 (CK1), and the APC[125]. Blocking of axin/GSK-3β/CK1/APC-complex stabilizes β-catenin, resulting in accumulation of this protein in the cytoplasm. Thereafter, β-catenin translocates to the nucleus, where it interacts with members of the TCF/LEF family of DNA-binding proteins[89]. After β-catenin binding, TCF/LEF transforms the DNA binding complex from a transcriptional repressor to an activator of Wnt target genes[89,126]. In the absence of Wnt signaling, CK1 and GSK3β sequentially phosphorylate the amino terminal region of β-catenin, resulting in β-catenin recognition by E3 ubiquitin ligase β-TrCP and subsequent ubiquitination and proteasomal degradation[127-129] (**Figure 7**).

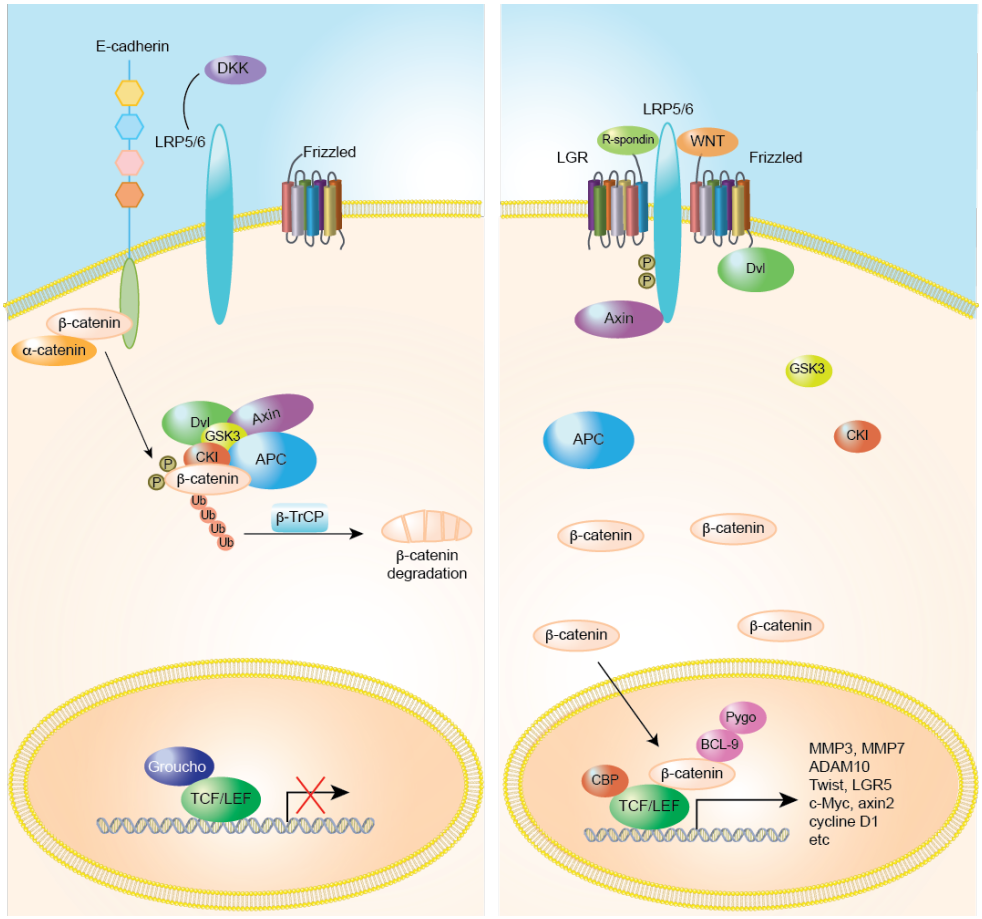

Figure 7: Schematic representation of the Wnt signaling pathway.
Left panel shows inactivated Wnt pathway. β-catenin is degraded after ubiquitination by β-TrCP. Right panel shows the Wnt or R-spondin activated pathway. β-catenin accumulates in the cytoplasm and subsequently translocates to the nucleus activating the TCF/LEF transcription complex.

Non-canonical Wnt signaling

The planar cell polarity (PCP) pathway, which is one of two non-canonical pathways, mediates cell polarity and cell motility during gastrulation[130,131]. The signal transduction takes place through the PDZ and DEP domains of Dvl followed by activation of the small GTPases Rho and Rac, which leads to stimulation of Rho-associated kinase (ROCK) and Jun kinase (JNK)[132,133]. Activation of these kinases subsequently leads to modifications of the actin cytoskeleton and the transcription factor JUN. The other non-canonical pathway is the Wnt/Ca^{2+} pathway. Wnt/Ca^{2+} signaling is thought to influence both the canonical and non-canonical pathway. Activation of this pathway leads to release of intracellular calcium via G-proteins, which involves activation of phospholipase C (PLC). The activation of PLC by Dvl leads to the cleavage of phosphatidylinositol-4,5-bisphosphate (PtdIns(4,5)P_2) into inositol trisphosphate ($InsP_3$) and diacylglycerol (DAG). DAG, together with calcium, activates PKC,

whereas $InsP_3$ increases the release of cytoplasmic free calcium, which in turn activates calmodulin-dependent kinase II (CamKII) and the phosphatase Calcineurin. Calcineurin activates nuclear factor of activated T cells (NFAT) by de-phosphorylation, resulting in translocation into the nucleus[134-136] (**Figure 8**).

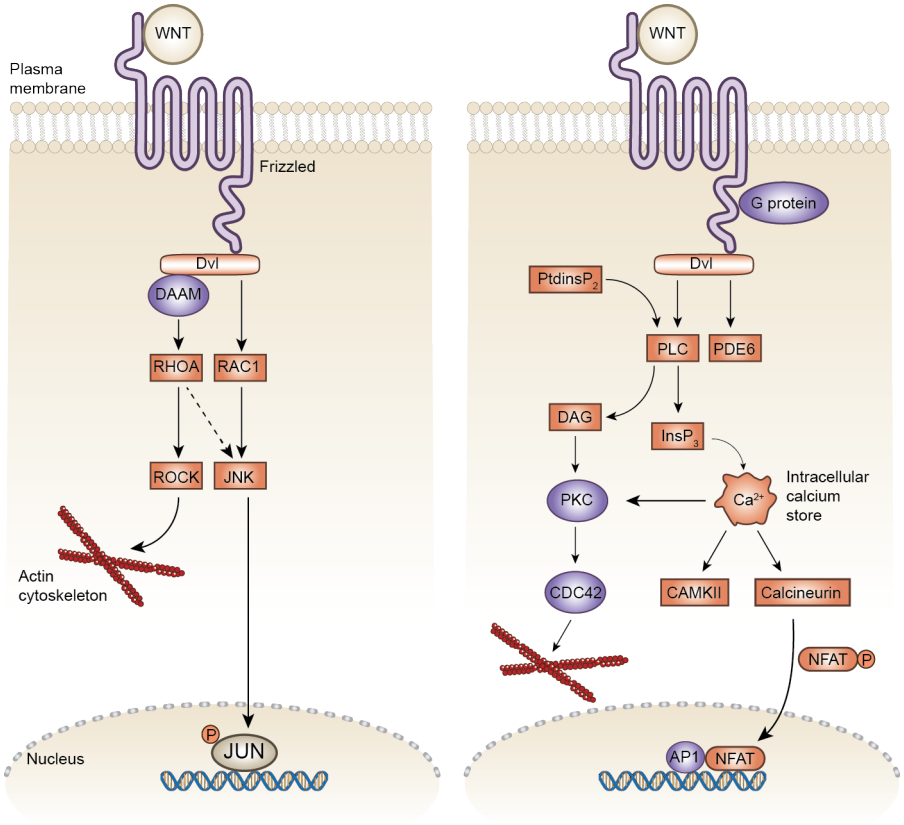

Figure 8: Schematic representation of non-canonical Wnt pathways.
Planar cell polarity (PCP) signaling activates the stress kinases JNK and ROCK resulting in remodeling of the cytoskeleton and changes in cell adhesion and motility (left panel). WNT/Ca^{2+} signaling activates the kinases PKC and CAMKII and the phosphatase calcineurin by releasing Ca^{2+}, resulting in activation of NFAT (right panel). AP1, activator protein 1; CDC42, cell-division cycle 42; NFAT, nuclear factor of activated T cells; PDE6, phosphodiesterase 6. Adapted by permission from Macmillan Publisher Ltd: [Nature Reviews|Immunology] (Nat Rev Immunology. 8, 581-593) copyright (2008).

2.5.2 Wnt agonists and antagonists

Several small protein families modulate Wnt signaling by inhibition or activation. These effectors act either intracellularly to modulate the signal transduction machinery or extracellularly to modulate ligand-receptor interaction. Both antagonists and agonists play an important role because they control the fine-tuning of the Wnt signaling.

Wnt agonists

Apart from Wnt proteins, the two families of Norrin and R-spondin (Rspo) proteins are agonists for Wnt signaling. Secreted Norrin proteins function like Wnt molecules, although they are not structurally related. Norrin specifically binds with high-affinity to Fzd4 and to LRP5/6[137,138], thereby activating the signal cascade downstream to TCF/LEF mediated transcription[121]. The R-spondin family comprises four members (Rspo 1-4), which have the ability to activate canonical Wnt signaling. They synergize with Wnt and require their presence to activate the signaling cascade[139-141]. For some years the nature of their specific receptor was controversially discussed. It has been reported that Rspo binds to both Fzd and LRP6[142], to LRP6 primarly[141], or neither of them[143,144]. However, recently, different studies showed the LGR5 and its homolog LGR4 are Rspo receptors[145-147]. The proposed mechanism of action suggests that Rspo activates Wnt signaling by inhibiting the transmembrane E3 ubiquitin ligase ZNRF3, thereby preventing the internalization of the receptors, resulting in the accumulation of Wnt receptors at the cell membrane[148]. Moreover, R-spondins not only amplify canonical Wnt signaling, they also stimulate Wnt/PCP signaling[147,149].

Wnt antagonists

Currently, six families of secreted inhibitors: Dickkopf proteins (Dkks), secreted Frizzled-related proteins (sFRPs), Wnt-inhibitory factor 1 (WIF-1), Wise, Cerberus, and insulin-like growth-factor binding protein 4 (IGFBP-4); and four families of transmembrane Wnt antagonists: Shisa, Wnt-activated inhibitory factor 1(Waif1/5T4), adenomatosis polyposis coli down-regulated 1 (APCDD1), and Tiki1, are described. Among them the Dkk protein family, comprising four members, Dkk1-4, is the best characterized[150]. Both Dkk1 and Dkk2 bind with high affinity to LRP5 and 6, whereas Dkk4 binds only to LRP6[151]. In contrast, Dkk3 does not bind to LRPs[152], but is involved in the regulation of transforming growth factor–β (TGF-β) signaling[153,154]. A number of studies observed epigenetic silencing of *Dkk* family genes implicating a contribution to Wnt signaling activation and colon cancer disease[155]. The largest family of secreted Wnt inhibitors consists of sFRP proteins, comprising five members, sFRP1-5[156]. Several studies propose that sFRPs inhibit Wnt signaling by sequestering Wnts in the cytoplasm. It has been shown that sFRP1-4 bind to WNT3A. In addition, sFRP1/2 and 5, but not sFRP3 and 4, interact with WNT5A[157,158] inhibiting also the non-canonical Wnt/PCP signaling[158,159]. Similar to sFRPs, WIF-1 prevents canonical and non-canonical Wnts, including WNT3A, WNT4, WNT5A, WNT7A, WNT9A, and WNT11, from binding to their receptors[154]. Secreted Wise binds to LRP4[160] and competes with WNT8 for binding to LRP6[161]. Wise is also able to reduce cell surface translocation of LRP6, when it is retained in the endoplasmic reticulum[162]. Interestingly, only *Xenopus* Cerberus sequesters Wnt proteins[163], but not its murine homolog Cerl-1[164]. The last member of the secreted inhibitors, IGFBP-4, is

controversially discussed. Some studies report that IGFBP-4 competitively blocks WNT3A from binding to LRP6 and Frizzled8[165], while others describe IGFBP-4 as an Wnt signaling agonist[166] promoting cell proliferation and invasion.

Proteins of the transmembrane family Shisa[167] are expressed in the ER, where they cell-autonomously trap Fzd and the fibroblast growth factor (FGF) receptor, preventing their maturation[168]. Waif1a acts as a feedback inhibitor of WNT8-mediated signaling during vertebrate gastrulation. It inhibits Wnt signaling and concomitantly activates non-canonical Wnt pathways by binding to LRP6, thereby inhibiting WNT3A and Dkk-1-induced LRP6 internalization[169]. The Wnt target gene *APCDD1*[170] is expressed as membrane-bound glycoprotein. It binds to WNT3A and prevents the formation of the Wnt receptor complex[171]. Tiki1 belongs to the family of transmembrane metalloproteases and inhibits Wnt signaling by removing eight amino-terminal residues from Wnt itself, resulting in the formation of oxidized Wnt oligomers with impaired receptor binding capability[172].

2.5.3 Wnt signaling in colorectal cancer

Given the important role of Wnt/β-catenin signaling in embryonic development and adult tissue homeostasis, it is obvious that disruptions of the Wnt pathway are associated with many diseases such as hereditary disorders or cancer. Common known disruptions of the Wnt pathway are activating or silencing mutations of Wnt ligands[173], Fzd/LRP5/6[174] receptor complexes, APC[52,175], axin[176], β–catenin[177] regulation or TCF[178]/LEF[179] complexes. However, the most striking link between Wnt signaling and cancer has been the discovery of genetic mutations in the midstream signaling components (APC, β-catenin), resulting in stabilization of β-catenin and constitutive activation of the canonical Wnt signaling[177]. As mentioned before, the majority of colorectal tumors have inactivating mutations or loss of APC. Up to now over 600 mutations of the *APC* gene in form of frameshift insertions (30 %), deletions (35 %) or missense (19 %) mutations have been documented[65]. Truncation of APC, for instance, leads to loss of repetitive elements within the protein, which are responsible for binding to β-catenin and axin, resulting in severely impaired phosphorylation of GSK3β and subsequent stabilization of β-catenin[180]. Furthermore, some APC mutations are known to disrupt its ability to regulate β-catenin function in the nucleus[181] as APC acts as a nuclear-cytoplasmic shuttle protein. After translocation of APC into the nucleus it promotes the export of β-catenin for proteasomal degradation resulting in deactivation of TCF mediated transcription[182]. Loss of this property leads to constitutive TCF/LEF transcription. In approximately 10 % of CRCs cases with wild-type *APC*, mutations in the gene *CTNNB1* encoding the protein β-catenin are frequently found. These mutations mostly affect one of the four regulatory NH_2-terminal Ser/Thr residues, which constitute the GSK3β phosphorylation domain of β-catenin[177]. Such

mutations also lead to stabilization of β-catenin and inappropriate formation of β-catenin/TCF complexes in the nucleus, resulting in constitutive TCF/LEF transcriptional activity. Consequently, expression of TCF/LEF target genes is drastically stimulated in mutated Wnt signaling. Among the typical β-catenin/TCF effector genes, there are genes regulating cell cycle (c-myc)[183], facilitating cell migration (MMPs)[184], inhibiting apoptosis (Survivin)[185], and inducing cell growth[186,187] as well as components of the Wnt pathway (e.g. LEF)[179] itself. Overexpression of β-catenin/TCF effector genes disrupts the fine-tuned regulation of the Wnt pathway, which is essential for the maintenance of the pool of proliferating cells within the intestinal crypts. However, not only gene mutations in key proteins of the Wnt pathway result in a constitutively active TCF/LEF transcriptional activity. Moreover, it is known that members of the Wnt pathway cross talk with diverse proteins acting as co-activators (Pygo)[188] and co-repressors (Groucho[189], CtBP[190]) and thereby influence Wnt-mediated gene transcription. Disruption of these cross talks were also found to disturb normal intestinal homeostasis leading to abnormal growth of colorectal epithelium[191].

2.5.4 Origin of colorectal cancer

The existence of intestinal stem cells (ISC) has been based on *in vivo* studies showing that intestinal crypts were monoclonal in nature[192-194]. Intestinal stem cells are responsible for the renewal of the epithelium. They are defined as cells giving rise to all type of differentiated intestinal epithelial cells and at the same time replenish themselves. Stem cells fulfill these two tasks by dividing asymmetrically into one daughter stem cell and one committed daughter cell, which can further differentiate towards one of the mature epithelial linages. Moreover, after intestinal injury, such as irradiation, ISCs undergo symmetric division to compensate each other for replacing damaged ISCs, a process called 'neutral drift'[195,196]. For a long time, the exact location of ISCs has been discussed: the crypt base columnar cells (CBC)[197-201] and the +4 label retaining cells (LRC)[202-204]. The first marker for CBC cells, Leu-rich repeat-containing G protein-coupled receptor 5 (*Lgr5)*, was identified as a Wnt target gene selectively expressed at the base of adult intestinal crypts. Depletion of *Lgr5* in mice showed that CBCs are the main pool of active ISCs[205]. To maintain intestinal homeostasis high Wnt activity combined with BMP, PI3K, and Notch signaling is crucial. However, intestinal cancer is initiated by Wnt pathway-activating mutations, such as *APC* and *CTNNB1.* Several studies investigated in which compartment of the intestinal crypt mutations have to occur to be able to provoke adenoma formation. Two models of tumor cell origin have been discussed: mutations in non-stem cells and mutations in stem cells. Cells of the transient amplifying (TA) zone are more prone to acquire mutations, because of the high proliferation activity, compared to cells of the intestinal stem cell zone. However, TA cells are shed from the intestine within 3-4 days,

as long as the cell migration is not perturbed. In contrast, ISCs with oncogenic mutations can be replaced by other ISCs in the crypt, minimizing the fixation of the mutation[195,206]. The discovery of ISC expression markers, such as *Lgr5*[205], *Sox9*[207,208], Achaete–Scute homologue 2 (*Ascl2*)[196], *EphB2*[209], and olfactomedin 4 (*Olfm4*)[210], facilitated the search for the cell of origin (**Figure 9**). An *in vivo* study with depleted *Apc* in either intestinal stem cells (ISC) or non-stem cells showed that *Apc* deletion in Lrg5$^+$ cells specifically provoked rapid adenoma formation[211], whereas only small non-tumorigenic lesion were formed when *Apc* was depleted in non-stem cells[212]. Another study showed that deletion of the stem cell marker *Rnf43,* which recently has been identified[213], was also able to form small intestinal adenomas when its homologue *Znrf3* was deleted at the same time[214]. Thus, the activation of Wnt signaling due to mutagenesis of genes in ISC is sufficient for adenoma formation, defining the ISC as the most likely cell of origin for intestinal tumorigenesis in mice.

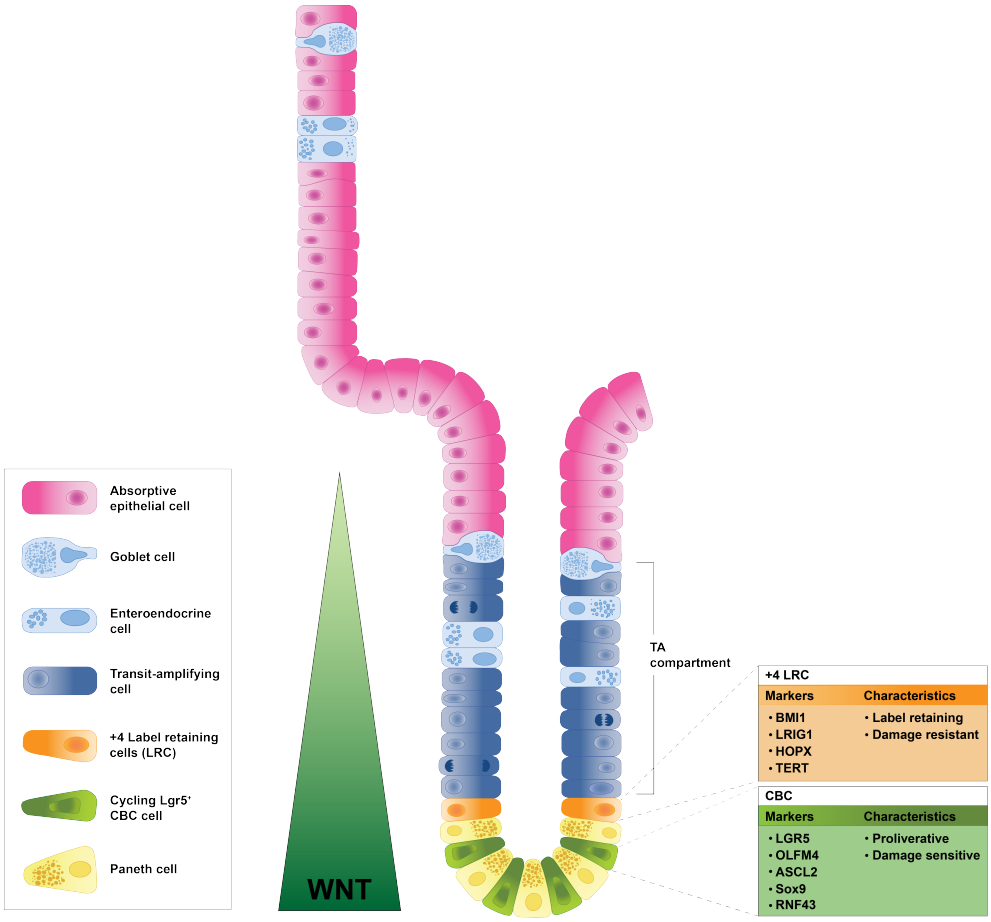

Figure 9:Schematic representation of intestinal crypt.
Cellular architecture of the intestinal crypt. LGR5$^+$ CBC and Paneth cells occupy the bottom of the crypt followed by +4 LRCs. Proliferative transit amplifying cells reside at the walls of the crypts differentiating into absorptive, goblet, and enteroendocrine cells while migrating upwards to the intestinal lumen. Strong Wnt activity is observed in the lower part of the crypts and decreases toward the intestinal lumen. Adapted from: The EMBO Journal Jun 13;31(12):2685-96 (2012).

2.6 RING Finger Proteins

2.6.1 The RING finger protein family

Members of the RING finger (RNF) protein family contain a characteristic RING finger domain. This motif was first identified in the early 1990's and is apostrophized as **R**eally **I**nteresting **N**ew **G**ene[215]. Until now, approximately 300 functionally different human proteins have been identified containing this domain. Among them, 49 RNF proteins have hydrophobic regions predicted to be transmembrane domains[216]. The RING finger motif is described as a cysteine-rich sequence with the general formula C-x_2-C-$x_{(9-39)}$-C-$x_{(1-3)}$-C-H-$x_{(2-3)}$-C-x_2-C-$x_{(4-48)}$-C-x_2-C, where x can be any amino acid (**Figure 10**). The domain is classified into at least three subgroups: C_3HC_4 (RING-HC), $C_3H_2C_3$ (RING-H2), and C_4HC_3 (RINGv) fingers. This sequence suggests a classical zinc finger motif. Indeed, RING finger motifs coordinate two zinc ions in an cross-braced arrangement with either four cysteines, or three cysteines and a histidine: The first and the third pair of metal ligation residues bind the first zinc (site I) and the second and fourth pair bind the second zinc (site II) ion[217]. This arrangement endows the RING domain with a globular conformation, characterized by a central alpha-helix and variable-length loops separated by several small beta-strands[217].

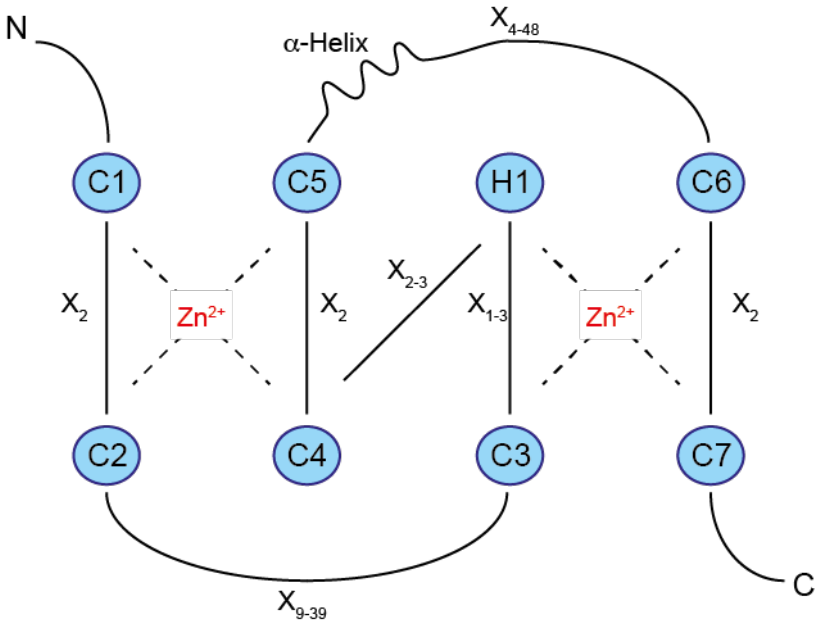

Figure 10: Schematic representation of RING finger domain.
Sequence shows the RING-HC domain organization. C1, first cysteine: H, histidine; X_n, number of amino acid residues in the spacer regions.

Up to date, no reports describe proteins containing two or more RING finger domains. However, proteins were found harboring other zinc-finger-like domains adjacent to the RING domain. For example, besides the RING finger motif, tumor necrosis factor (TNF) receptor-

associated factor 5 (TRAF5) contains two TRAF-type zink finger domains and a meprin and TRAF homology (MATH) domain[218-220]. In contrast to classical zinc fingers proteins, which are generally restricted to the nucleus and function in binding nucleic acids, RING domain proteins are present throughout the whole cell mediating diverse protein-protein interactions[221]. Although different functions have been described so far[222,223], it appears that a large number of RING fingers act as E3 ubiquitin ligases[224].

2.6.2 RING E3 ubiquitin ligases

RING E3 ubiquitin ligases play an essential role in the regulation of many biologic processes such as cell cycle, DNA repair[225], cell signaling[226] and responses to hypoxia[227] by catalyzing the ubiquitination of their substrate. Ubiquitination of proteins is achieved through an enzymatic cascade involving ubiquitin-activating (E1), ubiquitin-conjugating (E2), and ubiquitin-ligating (E3) enzymes. In this process, the E3 ligase enzyme binds to both substrate and an E2 thioesterified with ubiquitin (E2-Ub), bringing them in proximity so that the ubiquitin is transferred from the E2 to the substrate, building a covalent E3-ubiquitin thioester intermediate (**Figure 11**). In case of RING containing E3 ubiquitin ligases, the RING domain serves as a scaffold for binding to E2 enzymes to their substrate[228].

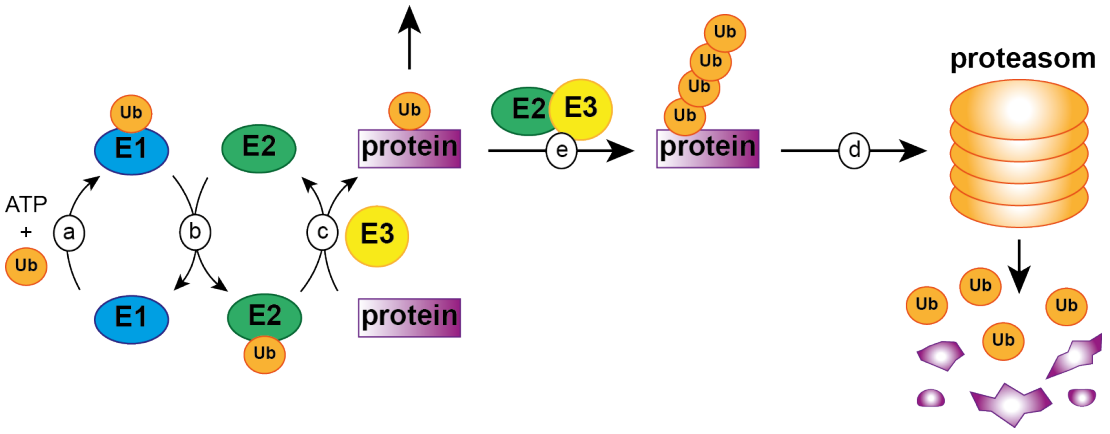

Figure 11: Schematic representation of the ubiquitin system.
(a) Ubiquitin proteins are activated with ATP for the transfer by E1. (b) Activated ubiquitin is transferred in thioester linkage from E1 to E2. (c) The E2-Ub thioester interact with E3 ubiquitin ligase, thereby E3 transfers the Ub form E2-Ub to a lysine residue of a substrate. Monoubiquitinated protein can either dissociate from E3 or can be ubiquitinated again in form of a chain (e). (d) Polyubiquitinated protein is degraded by the proteasome.

However, there are some reports describing a non-ubiquinitation activity of the RING domain in E3 ubiquitin ligases. For example, the RING domains of Bard1[229], Bmi1[230], and MdmX[231] do not exhibit E3 activity by themselves. But in each of these cases the RING domain interacts with another RING domain-containing protein forming heterodimers, where the second E3

performs ubiquitination[229-231]. In addition, in some cases of well-studied RING domain proteins ubiquitin ligase activity has never been conclusively demonstrated. Examples include the Cdk-activating kinase assembly factor Mat1 [232] and the Ste5[233]. Given the important role of RING E3 ubiquitin ligases in cellular homeostasis, it is not surprising that E3s are implicated in malignancy as oncogenes (Cbl[234], Mdm2[235,236]) or inactivated tumor suppressors (BRCA1[229,237], VHL[238,239]). Interestingly, the role of E3 ubiquitin ligase β–TrCP, which tightly regulates the Wnt/β-catenin signaling[240], is controversial. Different studies correlate high levels of β-TrCP to tumorigenesis, including colon cancer[241], hepatoblastoma[203], pancreatic cancer[242], and melanoma[243]. In contrast, mutations in β-TrCP have been observed in various cancers[244,245] implying a tumor suppressive role. Recently, the RING E3 ubiquitin ligase 43 has been linked to Wnt signaling.

2.6.3 RING finger protein 43

RING finger protein 43 (RNF43), an E3 ubiquitin ligase[76] consists of 783 amino acids and has a molecular weight of 85 kDa (**Figure 12A**). Three additional isoforms of RNF43 are predicted (**Figure 12B**). The RNF43 gene is localized at the minus strand on chromosome 17q22[246]. Sequential analysis revealed that RNF43 contains a N-terminal signal peptide, a putative 5-prime transmembrane domain, a RING finger motif and two C-terminal nuclear localization signals.

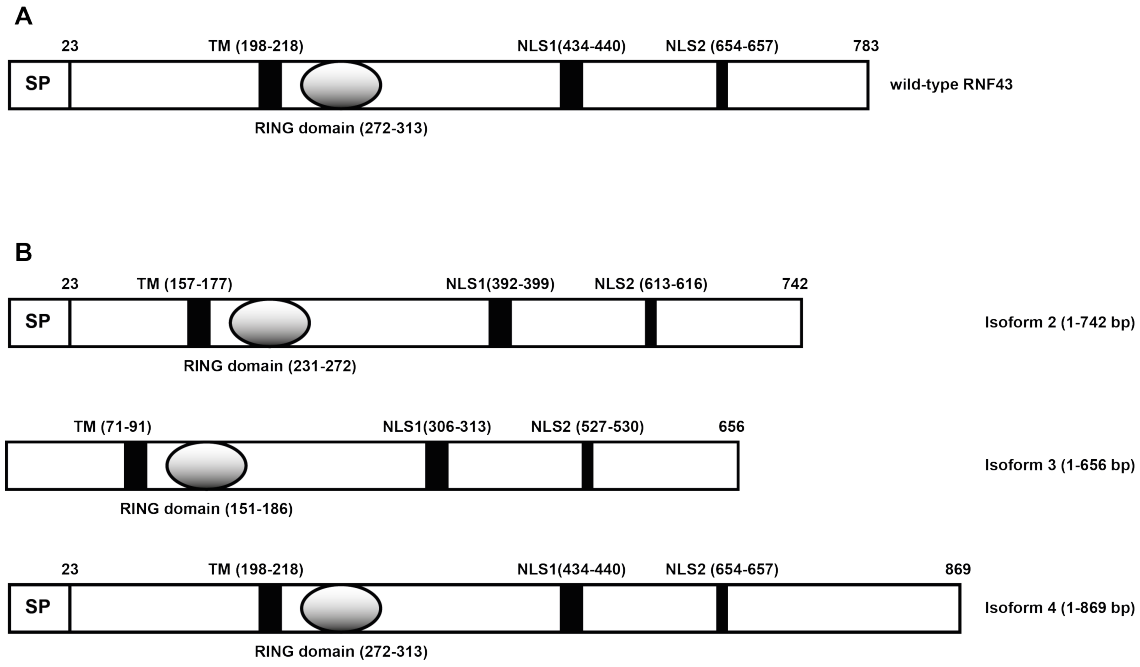

Figure 12: Schematic representation of RNF43 and its isoforms.

(A) Schematic model of wild-type RNF43, isoform 1. (B) Different predicted isoforms of wild-type RNF43. SP, signal peptide; TM, transmembrane domain; NLS, nuclear leading sequence; numbers indicate amino acid position.

Early findings suggested that RNF43 might be implicated in colon cancer pathogenesis due to high expression in colorectal tumors and growth-promoting effects in colon cancer cell lines[247-249]. However, more recent reports support the hypothesis of RNF43 as a tumor suppressor. Mutations in the *RNF43* gene in different types of tumors have been reported in pancreatic cancer[250,251], mucinous tumors of ovary[252], liver fluke-associated cholangiocarcinoma[253], and in gastric[254,255] as well as in colon cancer[254,256].

Furthermore, there are conflicting data regarding the function of RNF43 depending on its subcellular localization. Different publications claimed that RNF43 and its homolog ZNRF3 inhibit Wnt signaling by reducing frizzled receptor abundance at the plasma membrane[148,214,257], which are supported by different structural analyses of the LGR5/ZNRF3/R-spondin complex based on crystallographic data[258-260]. In contrast to these data, previous reports showed RNF43 to be localized to the nuclear envelope, the endoplasmic reticulum, and the nucleoplasm[247,261,262]. In line with this observation, RNF43 has been described to be involved in DNA damage response (DDR), supporting the nuclear localization and function of RNF43[263].

2.7 Objectives

RNF43 mRNA is highly expressed in human colorectal cancer tissue, yet commercial antibodies have limitations, especially when trying to detect endogenous RNF43 protein.

The **first objective** of this study was to screen several hybridoma supernatants for antibodies recognizing specifically endogenous RNF43, which can be used to study the function of endogenous RNF43.

The subcellular localization of RNF43 has remained controversial, since under overexpression conditions, RNF43 has been detected in the nucleus as well as in the cytoplasm of cells.

The **second objective** of this study was to elucidate the subcellular localization of overexpressed RNF43 and most importantly of endogenous RNF43.

RNF43 has been described as an oncogene as well as a tumor suppressor after overexpression in different types of cancer.

The **third objective** of this study was to investigate the endogenous function of RNF43 in colorectal cancer *in vitro* and *in vivo*.

RNF43 was found being frequently mutated in human gastrointestinal tumors, suggesting an altered activity of RNF43.

The **fourth objective** of this study was to characterize the impact of mutations in RNF43 function, found in human cancer tissue, *in vivo* and *in vitro.*

3 Materials and Methods

3.1 Materials

3.1.1 Consumables

BD Falcon tubes, 15 ml, 50 ml	BD Bioscience, Heidelberg, Germany
BD Falcon cell culture flasks, sterile 25 cm^2, 75 cm^2	BD Bioscience, Heidelberg, Germany
Blotting Paper	Whatman, Dassel, Germany
Cell scrapers, 30 cm	SPL Life science, South Korea
Coverslips	Menzel-Gläser, Braunschweig, Germany
Cryotubes (Nalgene)	Thermo Scientific, Karlsruhe, Germany
CultureSlides (4-well)	BD Bioscience, Heidelberg, Germany
TipOne Graduated Filter Tips, 1-200 µl	Starlab, Ahrensburg, Germany
TipOne Bevelled Filter Tips, 20 µl	Starlab, Ahrensburg, Germany
MultiGuards Barrier Tips, 1000 µl	BD Bioscience, Heidelberg, Germany
Corning transwells, 8 µm pore	Sigma GmbH, Deisenhofen, Germany
Safe Seal Tips professional, 10µl	Biozym Scientific GmbH, Hessisch Oldendorf, Germany
Serological pipette, 2 ml, 5ml, 10ml, 25 ml	Greiner Bio-one GmbH, Solingen, Germany
Superfrost plus microscope slides	Menzel GmbH, Braunschweig, Germany
Tips	VWR International GmbH, Darmstadt, Germany
Tissue culture plate, 6, 12, 24 and 96 well	BD Bioscience, Heidelberg, Germany
Tissue culture plate, 10 cm^2	BD Bioscience, Heidelberg, Germany
Polypropylene Round-bottom Tube	BD Bioscience, Heidelberg, Germany
Protran Nitrocellulose Transfer Membran	Whatman, Dassel, Germany
Novax®Gel cassettes	Invitrogen, Karlsruhe, Germany
Novex® Gel Combs	Invitrogen, Karlsruhe, Germany
Novex® Gel loading tips	Invitrogen, Karlsruhe, Germany
X-ray films	Kodak, Stuttgart, Germany

3.1.2 Equipment

Agarose Running chambers	BioRad

AxioVert 40 microscope	Zeiss
ÄKTA™ avant 25	GE Healthcare
Biofuge Primo Centrifuge	ThermoScience
BioRad CFX384 systems	BioRad
Cell culture incubator, HeraCell 240	Heraeus, ThermoScience
Cell strainer 70 µm	BD Bioscience
Centrifuge 5424	Eppendorf
Centrifuge Micro 200R	Hettich
Confocal microscope, Leica SP5	Leica
Developing machine (Durex60)	AGFA
Electrophoresis power supply	BioRad
Eppendorf tubes, 1.5 mL, 2 mL	Eppendorf
Fluorescence Microscope, DMRB	Leica
Freezer -20 °C	Liebherr
Freezer -80 °C	GFL
Heatable magnetic stirrer	IKA
HiTrap Protein G HP, 1ml	GE Healthcare
Ice machine	Scotsman
Laboratory precision scale	Sartorius Analytic
Laboratory scale	Kern
Laminar airflow cabinet, HeraSafe	Heraeus, ThermoScience
4D-Nucleofector™ X Unit	Lonza Cologne
Orion Microplate Luminometer	Berthold
pH-Electrode	WTW inoLab
pH-Meter	WTW inoLab
Pipettboy, Easypet	Eppendorf
Power Supply Power	BioRad
Refrigerator 4-8 °C	Liebherr
Shaker, Titramax 100	Heidolph
Single Channel Pipettor, 0.5-10µl	Corning
Single Channel Pipettor, 2-20 µl	Corning

Single Channel Pipettor, 20-200 µl	Corning
Single Channel Pipettor, 200-1000 µl	Corning
Spectrophotometer NanoDrop 1000	ThermoScientific
SP5 confocal microscope	Leica
Thermomixer compact	Eppendorf
UV Transilluminator, Eagle Eye	BioRad
Vortex Genie 2	Schultheiss
Waterbath	GFL
ChemoCam Imager 3.2	Intas Science Imaging
XCell II™ Blot Module	Invitrogen
XCell *SureLock*® Mini-Cell	Invitrogen
Thermal Cycler C1000 Touch	BioRad
Sunrise™ Mikroplate Reader	Tecan

3.1.3 Software

Axio Vision Rel.4.8	Zeiss
CFX384 Touch™ Real-Time PCR	BioRad
CLC Workbench 6	CLC Bio
Illustrator CS6	Adobe Software
LAF-AS	Leica
Molecular Imager Gel Doc XR+System	BioRad
Prism 5	GraphPad Softwar
Photoshop CS6	Adobe Software

3.1.4 Chemicals

Acetic acid	Merck GmbH, Schwalbach, Germany
Aceton	Merck GmbH, Schwalbach, Germany
Acrylamid	AppliChem, Darmstadt, Germany
Agar	Carl Roth GmbH, Karlsruhe, Germany
Agarose peqGOLD Universal	PeqLab, Erlangen, Germany
Albumin	AppliChem, Darmstadt, Germany
Ammoniumpersulfat, APS	AppliChem, Darmstadt, Germany

Ampicillin	AppliChem, Darmstadt, Germany
Anti-Digoxigenin-POD Fab fragments	Roche GmbH, Penzberg, Germany
β-Mercaptoethanol (50 mM)	Sigma GmbH, Deisenhofen, Germany
DAB Reagent	Cell Signaling, Leiden, Netherlands
Difco™ Noble Agar	BD Science, Heidelberg, Germany
Disodium hydrophosphate ($Na_2HPO_4x2H_2O$)	Merck GmbH, Schwalbach, Germany
Dithiothreitol, DTT	AppliChem, Darmstadt, Germany
DPX Mountant for hisotogy	Sigma GmbH, Deisenhofen, Germany
DNA-Ladder Bench Top, 1kb	Promega, Mannheim, Germany
Dual Luciferase Reporter Assay	Promega, Mannheim, Germany
Eosin 1 %	Morphisto, GmbH, Frankfurt Germany
Ethanol, absolute	AppliChem, Darmstadt, Germany
Ethylenediaminetetraacetic acid, EDTA	AppliChem, Darmstadt, Germany
Fat-free powder milk	Carl Roth GmbH, Karlsruhe, Germany
Fetal Calf Serum	Invitrogen, Karlsruhe, Germany
Glycerin	AppliChem, Darmstadt, Germany
Glycin	Merck GmbH, Schwalbach, Germany
Hämatoxylin 5 %	Morphisto, GmbH, Frankfurt Germany
Hexadimethrine bromide	Sigma GmbH, Deisenhofen, Germany
Hydrochloric acid (HCl)	Merck GmbH, Schwalbach, Germany
Hydrogen peroxide 30 %	Merck GmbH, Schwalbach, Germany
Isopropanol	AppliChem, Darmstadt, Germany
Lipofectamine 2000	Invitrogen, Karlsruhe, Germany
Methanol, absolute	Carl Roth GmbH, Karlsruhe, Germany
Monopotassium phosphate (KH_2PO_4)	Merck GmbH, Schwalbach, Germany
Natriumchloride (NaCl)	Merck GmbH, Schwalbach, Germany
Natriumhydroxide (NaOH)	AppliChem, Darmstadt, Germany
peqGOLD Protein-MarkerV	PeqLab, Erlangen, Germany
Potassiumchloride (KCL)	Merck GmbH, Schwalbach, Germany
Protease Inhibitor Cocktail Tablets, (complete EDTA free)	Roche GmbH, Penzberg, Germany

Protein agarose A beads	Roche GmbH, Penzberg, Germany
Protein agarose G beads	Roche GmbH, Penzberg, Germany
ProtoGel 40 % Acrylamide/Bis Solution	AppliChem, Darmstadt, Germany
Restore Western Blot Stripping Buffer	Thermo Scientific, Karlsruhe Germany
RNase Away®	MBP, San Diego, USA
RNasin	Promega Corp, Mannheim, Germany
RohtiClear®	Carl Roth GmbH, Karlsruhe,
Germany	
Rothi®-Safe	Carl Roth GmbH, Karlsruhe, Germany
Sample Buffer XT 4x	BioRad Laboratories, Munich, Germany
Saponin	Carl Roth GmbH, Karlsruhe, Germany
SignalStain Antibody Diluent	Cell Signaling, Leiden, Netherlands
Sodium Citrate	Carl Roth GmbH, Karlsruhe, Germany
Sodium dodecyl sulfate (SDS)	ICN Labsolutions GmbH, Northeim, Germany
Super Signal West Pico chemiluminescent Substrate	Thermo Scientific, Karlsruhe, Germany
Tetramethylethylenediamine (TEMED)	AppliChem, Darmstadt, Germany
Tris	Carl Roth GmbH, Karlsruhe, Germany
Tris Base	AppliChem, Darmstadt, Germany
Triton-X 100	AppliChem, Darmstadt, Germany
Tryptone	AppliChem, Darmstadt, Germany
Tween 20	AppliChem, Darmstadt, Germany
Vectashield mounting medium	Vector Laboratories, Eching, Germany
Yeast extract	Fluka GmbH, Buchs, Schweiz

3.1.5 Standards and Kits

Cell Counting Kit-8	Sigma GmbH, Deisenhofen, Germany

DNA-free™ Kit	Ambion GmbH, Kassel, Germany
Dual-Luciferase Reporter Assay System	Promega, Mannheim, Germany
Illustra™ GFX™ PCR DNA and Gel Band Purification Kit	GE Healthcare, Freiburg, Germany
KAPA SYBR® FAST Univrsal 2X qPCR Master Mix	Kapa Biosystems, Woburn, USA Germany
Pierce® ECL Western Blotting Substrate	Thermo Scientific, Rockford, USA
PureYield™ RNA Midiprep System	Promega, Mannheim, Germany
PurLink™ Genomic DNA Mini Kit	Invitrogen, Karlsruhe, Germany
QuikChange Lightning Site-Directed Mutagenesis Kit	Agilent Technologies, Frankfurt, Germany
RNeasy Kit	Qiagen GmbH, Hilden Germany
Wizard® Plus SV Minipreps DNA Purification Systems	Promega, Mannheim, Germany

3.1.6 Cell culture

Trypsin/EDTA	Promo Cell, Heidelberg, Germany
Corning Matrigel Basement Membrane Matrix	VWR, Darmstadt, Germany
Fetal Calf Serum	Sigma GmbH, Deisenhofen, Germany
Gibco® Collagen Type I, rat tail	Invitrogen, Karlsruhe, Germany
Gibco® DMEM	Invitrogen, Karlsruhe, Germany
Gibco® DMEM/F12	Invitrogen, Karlsruhe, Germany
Gibco® Optimem	Invitrogen, Karlsruhe, Germany
Gibco® IMDM	Invitrogen, Karlsruhe, Germany
Gibco® Penicillin/Streptomycin	Invitrogen, Karlsruhe, Germany
Gibco® PBS, sterile	Invitrogen, Karlsruhe, Germany
Gibco® Trypan Blue	Invitrogen, Karlsruhe, Germany
Gibco® GlutaMAX	Invitrogen, Karlsruhe, Germany
Gibco® Hepes 1 M	Invitrogen, Karlsruhe, Germany
Gibco® 50x B-27 Supplement	Invitrogen, Karlsruhe, Germany
Gibco® 100x N-2 Supplement	Invitrogen, Karlsruhe, Germany
N-Acetyl-L-cysteine	Sigma GmbH, Deisenhofen, Germany
Recombinant Murine EGF	Pepro Tech, Hamburg, Germany

Recombinant Murine Noggin	Pepro Tech, Hamburg, Germany
Recombinant Human R-Spondin 1	Pepro Tech, Hamburg, Germany

3.1.7 Standard size ladders

BenchTop 1 kb DNA Ladder	Promega, Mannheim, Germany
BenchTop 100 kb DNA Ladder	Promega, Mannheim, Germany
peqGOLD Protein-MarkerV	PeqLab, Erlangen, Germany
Precision Plus Protein™ Dual Color Standard	Biorad, München, Germany

3.1.8 Enzymes

DpnI	Agilent Technologies, Frankfurt, Germany
FideliTaq™ PCR Master Mix (2x)	Affimetrix USB, Cleveland, USA
GoTaq® Green Mster Mix (2x)	Promega Corp, Mannheim, Germany
M-MLV-RT	Promega Corp, Mannheim, Germany
PNK	New England Biolabs, Frankfurt, Germany
Q5® High-Fidelity DNA Polymerase	New England Biolabs, Frankfurt, Germany
T4 DNA Ligase	Promega Corp, Mannheim, Germany
T7 RNA Polymerase	Promega Corp, Mannheim, Germany
TSAP	Promega Corp, Mannheim, Germany

3.1.9 Antibodies

Name	implemented concentration	Source
Primary antibodies:		
Monoclonal Anti-Flag M2	WB: 1:1000	Sigma GmbH, Deisenhofen, Germany
Monoclonal Anti-HA	WB: 1:1000	Sigma GmbH, Deisenhofen, Germany
Anti-α-tubulin (B-7)	WB: 1:1000	Santa Cruz, Heidelberg, Germany
Anti-β-actin (mouse)	WB: 1:5000	New England Biolabs, Frankfurt, Germany
Anti-β-catenin	WB: 1:1000 IF:1:300	BD Bioscience, Heidelberg, Germany
Anti-non-phosphorylated -β-catenin	WB: 1:1000	New England Biolabs, Frankfurt, Germany
Anti-calnexin (H-20)	WB: 1:1000 IF: 1:300	Santa Cruz, Heidelberg, Germany
Anti-CDC5L	WB:1:1000	Sigma GmbH, Deisenhofen, Germany
Anti-CtBP(mouse)	WB: 1:1000	Santa Cruz, Heidelberg, Germany
Anti-EGFR	WB: 1:1000	New England Biolabs, Frankfurt, Germany
Anti-Ki67	IHC: 1:400	New England Biolabs, Frankfurt, Germany
Anti-lamin A/C	WB:1:1000 IF: 1:300	Sigma GmbH, Deisenhofen, Germany
Anti-RNF43	WB: 1:500	LifeSpan Bioscience, Seattle, USA
Anti-RNF43	IHC: 1:500	Atlas Antibodies, Stockholm, Sweden
Anti-TCF4	WB: 1:1000 IP: 1:170	New England Biolabs, Frankfurt, Germany
Anti-TCF4 cl 6H5-3	IF: 1:300	Merck Millipore, Darmstadt, Germany
Anti rabbit-IgG	IP: 1:170	Santa Cruz, Heidelberg, Germany
Anti mouse-IgG	IP: 1:170	Santa Cruz, Heidelberg, Germany
Anti rat-IgG	IP: 1:170	Santa Cruz, Heidelberg, Germany
Secondary antibodies:		
Anti-mouse IgG HRP	1:3000	Promega, Mannheim, Germany
Anti-rat IgG HRP	1:3000	Dako, Hamburg, Germany
Anti-rabbit IgG HRP	1:300	Promega, Mannheim, Germany
Conjugates used for Immunofluorescence:		
AlexaFluor^{488} goat anti mouse IgG	1:300	Invitrogen, Karlsruhe, Germany

AlexaFluor^{594} donkey anti rat IgG	1:300	Invitrogen, Karlsruhe, Germany
AlexaFluor^{594} chicken anti rabbit IgG	1:300	Invitrogen, Karlsruhe, Germany

Table 1: Antibodies used in this study

3.1.10 Bacterial strains

*E.*coli DH5α, (Invitrogen, Karlsruhe, Germany).

Escherichia coli DH5α is a strain commonly used for DNA manipulation. The chromosomal genotype is defined as huA2 Δ(argF-lacZ)U169 phoA glnV44 Φ80 Δ(lacZ)M15 gyrA96 recA1 relA1 endA1 thi-1 hsdR1. In addition, DH5α is highly transformable, and allows for selection by α-complementation.

One Shot® Stbl3™ Chemically Competent *E. coli*: (Provided from G. Dössinger)

This strain is designed especially for cloning unstable inserts such as lentiviral DNA containing direct repeats. The genotype is defined as F$^-$*mcr*B *mrrhsd*S20(r_B^-, m_B^-) *rec*A13 *sup*E44 *ara*-14 *gal*K2 *lac*Y1 *pro*A2 *rps*L20(Str^R) *xyl*-5 λ$^-$*leumtl*-1

3.1.11 Cell lines

Name	Description	Source
HEK293	Human embryonic kidney cells	ATCC no.: CRL-1573
293T	Human embryonic kidney cells	ATCC no.: CRL-3216
DLD1	Human colon adenocarcinoma	ATCC no.: CCL-221
HT29	Human colon adenocarcinoma	ATCC no.: HTB-38
LS174T	Human colon adenocarcinoma	ATCC no.: CL-188
SW480	Human colon adenocarcinoma	ATCC no.: CCL-228
HCT116	Human colon adenocarcinoma	ATCC no.: CCL-247
Caco2	Human colon adenocarcinoma	ATCC no.: HTB-37
MCF7	Human breast adenocarcinoma	ATCC no.: HTB-22

Table 2: Cell lines used in this study

3.1.12 Plasmids

Name	Description	Source
Cloning:		
pcDNA4^{TM}/TO	For RNF43 constructs; CMV promoter; $TetO_2$ sites; Zeocin resistance; cloning site Not1-EcoR1	Invitrogen
pCMV-SPORT6	For *in-situ* fragment cloning; CMV promoter; ampicillin resistance	Invitrogen
pLVTHM	plasmid 12247; second generation; cloning sites MLU1-Cla1	Addgene; Trono Lab
psPAX2	plasmid 12260; packaging plasmid	Addgene
pMD2.g	plasmid 12259; envelope plasmid	Addgene
pX335	U6-Chimeric_BB-CBh-hSpCas9n(D10A); cloning site Bbs1	Addgene
Luciferase reporter		
TOPFlash	10 TCF binding sites; ampicillin resistance	Provided by M. van de Wetering
FOPFlash	10 mutated TCF binding sites; ampicillin resistance	Provided by M. van de Wetering
Renilla	CMV promoter; ampicillin resistance	Promega
Dishevelled	dominant-active form; ampicillin resistance	Provided by W. de Lau
Dn-axin2	dominant-active form; ampicillin resistance	Provided by W. de Lau
ΔN-β-TrCP	dominant-active form; ampicillin resistance	Provided by W. de Lau
S33Y-β-catenin	dominant-active form; ampicillin resistance	Provided by W. de Lau
TCF4-HA	ampicillin resistance	Provided by C.W. Wu
pCR3.1-PSF(HA)	ampicillin resistance	Provided fby P.Tucker
M67	ampicillin resistance	Addgene
NFκB	3 binding sites	Provided by F. Greten
12xcsl	12 csl binding sites; ampicillin resistance	Provided by A. Groot
N1ICD	Intracellular domain of Notch1	Provided by A. Groot
N2ICD	Intracellular domain of Notch2	Provided by A. Groot

Table 3: Plasmids used in this study

All full-length and truncated RNF43 as well as RING domain mutated (H202R/H295R) constructs were generated by PCR subcloning using EcoRV – Not1 restriction sites of pcDNA4/TO vector.

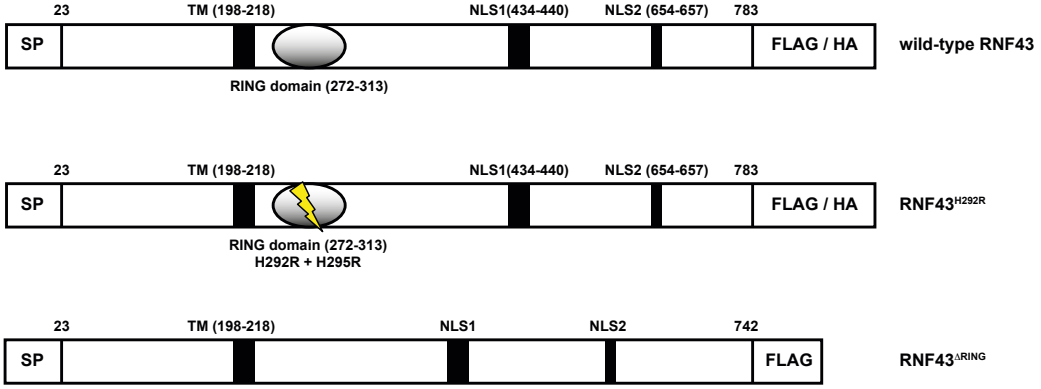

Figure 13: Schematic representation of RNF43 constructs.
SP, signal peptide; TM, putative transmembrane domain; FLAG, Flag-tag; HA, HA (human influenza hemagglutinin) –tag; NLS, nuclear leading sequence; yellow lightning indicates position of mutation; numbers indicate amino acid position

3.1.13 Restriction enzymes

Name	Restriction site	Description
EcoRV (10U/µl):	GAT▾ATC CTA▴TAG	*Escherichia coli* J62 pLG74
NotI1(10U/µl):	GC▾GGCCGC CGCCGG▴CG	*Norcardia otitidis-carviarum*
Xho1(10U/µl):	C▾TCGAG GAGCT▴C	*Xanthomonas holcicola*
Mlu1(10U/µl):	A▾CGCGT TGCGC▴A	*Micrococcus luteus*
Cla1(10U/µl):	AT▾CGAT GATC▴TA	*Caryophanon latum L*
Bbs1(10U/µl):	GAAGAC$(N)_2$▾… CTTCTG$(N)_6$▴…	*Bacillus laterosporus*
BsmA1(10U/µl):	CGTCTC$(N)_1$▾… GCAGAG$(N)_5$▴…	*Bacillus stearothermophilus B61*

Table 4: Restrictions endonucleases used in this study

The listed restriction enzymes were purchased from New England Biolabs (Frankfurt, Germany) and stored at -20 °C. Bbs1 was stored at -80 °C.

3.1.14 Oligonucleotides

3.1.14.1 Oligonucleotides for shRNA

shcontrol fw 5'- CGCGTCCCCGTACAGCCGCCTCAATTCTTTCAAGAGAAGAATTGAG GCGGCTGTACTTTTTGGAAAT-3'

shcontrol rev 5'- CGATTTCCAAAAAGTACAGCCGCCTCAATTCTTCTCTTGAAAGAATT GAGGCGGCTGTACGGGGA

shRNF43 fw 5'-CGCGTCCCCTTCTTGGTAAGATCGAGAGTTCAAGAGACTCTCGATC TTACCAAGAATTTTTGGAAAT-3'

shRNF43 rev 5'- CGATTTCCAAAAATTCTTGGTAAGATCGAGAGTCTCTTGAACTCTCG ATCTTACCAAGAAGGGGA-3'

3.1.14.2 Oligonucleotides for CRISPR/Cas9

Cloning guide RNA

nickRNFA_f 5'-CACCGCGTGGAGGCACGAAATGACC-3'

nickRNFA_r 5'-CAAACGGTCATTTCGTGCCTCCACG-3'

nickRNFB_f 5'-CACCGATCGAACGTGTGTGGACCCC-3'

nickRNFB_r 5'-CAAACGGGGTCCACACACGTTCGAT-3'

Template Oligos

RNFEx8mut_f: 5'-GGGAGCTAGGGAGGTCCTTGTAACCTTTGGTTGGGGCACTCTTGT CTGCTTCAGGAGCTCCGGGTCATTTCGTGTCTCCGCGAGTTTCGTCG CGAACGTGTGTGGACCCCTGGCTATACCAGCATCGGACTTGCCCC CTCTGCATGTTCAACATCGTAGG-3'

RNFEx8mut_r: 5'-CCTACGATGTTGAACATGCAGAGGGGGCAAGTCCGATGCTGGTAT AGCCAGGGGTCCACACACGTTCGACGAAACTCGCGGAGACACGAAA TGACCCGGAGCTCCTGAAGCAGACAAGAGTGCCCCAACCAAAGGTTA CAAGGACCTCCCTAGCTCCC

Screening Primer

RNFmutSC_f	5’-CCAAACTTGCCCAGAGTCAG-3’
RNFmutSC_r	5’-CATCCATCTGTACGCACACAG-3’

3.1.14.3 PCR Primers

Esther 1	5'-GCAGATATCGCCATGAGTGGTGGCCACCAGC-3'
S321X rev	5’-GCAGCGGCCGCTCACTTATCGTCGTCATCCTTGTAATCTGAATCTCCCTCT GTGATGTTGA-3’
G477X rev	5’-GCAGCGGCCGCTCACTTATCGTCGTCATCCTTGTAATCGTCACTGGAAGA GCCATGAC-3’
G566X rev	5’-GCAGCGGCCGCTCACTTATCGTCGTCATCCTTGTAATCGCCATGCCACTG GAACCG-3’
E713X rev	5’-GCAGCGGCCGCTCACTTATCGTCGTCATCCTTGTAATCTTCTGGTAGCAG CCTCTTGTC-3’

3.1.14.4 QuikChange Primers

A33T4fw	5'-CAGGACTGGTACTGACAGCAGCGGTGGAG-3'
A33T rev	5'-CTCCACCGCTGCTGTCAGTACCAGTCCTG-3'
I48T fw	5'-GATCAGCAGAACAGAAAGCTATTACCAGAGTGATCCCC-3'
I48T rev	5'-GGGGATCACTCTGGTAATAGCTTTCTGTTCTGCTGATC-3'
G102fs fw	5'-CGACAATCTGGAGCCTGATTCATCAGCATCGTCA-3'
G102fs rev	5'-TGACGATGCTGATGAATCAGGCTCCAGATTGTCG-3'
G102flag	5'-CGCGGCCGCTCACTTATCGTCGTCATCCTTGTAATCAGCCCCAG CGGCTG-3’
G133X fw	5'-GCGGGTGAGCGATGAGCCAGTGCTG-3’
G133X rev	5'-CAGCACTGGCTCATCGCTCACCCGC-3’
G133flag	5'-CGCGGCCGCTCACTTATCGTCGTCATCCTTGTAATCTCGCTCAC CCGCCATCC-3’
G282fs fw	5’-GAGTTCTCTGAGGGCAGGAGCTACGGGT-3’
G282fs rev	5’-ACCCGTAGCTCCTGCCCTCAGAGAACTC-3'
G282flag	5’-TCACGCGGCCGCCTTATCGTCGTCATCCTTGTAATCGTCCCCAG CCTTGTGCATAGG-3’

R219H fw	5'-CTTCGGTGCTGCACATCCGGTGCCG-3'
R219H rev	5'-CGGCACCGGATGTGCAGCACCGAAG-3'
H306fs fw	5’-CTGGTTACATCAGCCATCGGACTTGCCCC-3’
H306fs rev	5’-GGGGCAAGTCCGATGGCTGATGTAACCAG-3’
H306flag	5'-CGCGGCCGCTCACTTATCGTCGTCATCCTTGTAATCGGGGGCCT GGCCCGGCGTAG-3’
R343H fw	5'-CTCCACCTCATTCACCAGCATCCCGGC-3’
R343H rev	5’-GCCGGGATGCTGGTGAATGAGGTGGAG-3’
K559fs fw	5’-CGGCACCACCACTACAAAAGCGGTTCCAGT-3’
K559fs rev	5'-ACTGGAACCGCTTTTGTAGTGGTGGTGCCG-3'
K559flag	5'-CGCGGCCGCTCACTTATCGTCGTCATCCTTGTAATCAGGGGTG TGCCTCTGGGGACC-3’
R437A fw	5-TGCCCCTACGCGCGGCCAGGCCCC-3’
R437A rev	5'-GGGGCCTGGCCGCGCGTAGGGGCA-3'
K655A fw	5'-GACACCCACAGAGGGCAAGGCGGGGGGGTC-3'
K655A rev	5'-GACCCCCCCGCCTTGCCCTCTGTGGGTGTC-3'

3.1.14.5 Primers for qRT-PCR

hRNF43 fw	5’-CCTGTGTGTGCCATCTGTCT-3’
hRNF43 rev	5’-GCAAGTCCGATGCTGATGTA-3’
Axin2 fw	5’-ATGGGATGATCTGTTGCAGAGGGA-3’
Axin2 rev	5’-TGTCATTTCCACGAAAGCACAGCG-3’
Twist1 fw	5′-CATGTCCGCGTCCCACTAG-3′
Twist1 rev	5′-TGTCCATTTTCTCCTTCTCTGG-3′
MMP7 fw	5'-AAACTCCCGCGTCATAGAAAT-3'
MMP7 rev	5'-TCCCTAGACTGCTACCATCCG-3'
LGR5 fw	5’-TGATGACCATTGCCTACAC-3’
LGR5 rev	5’-GTAAGGTTTATTAAAGAGGAGAAG-3’
hGAPDH fw	5’-GAAGGTGAAGGTCGGAGT-3’
hGAPDH rev	5’-GAAGATGGTGATGGGATTTC-3’

3.1.14.6 Screening Primers

CMV fw	5’-CGCAAATGGGCGGTAGGCGTG-3’
BGH rev	5’-TAGAAGGCACAGTCGAGG-3’
T7	5’-TAATACGACTCACTATAGGG-3’
SP6	5’-ATTTAAGGTGACACTATAG-3’
U6	5’-ACTATCATATGCTTACCGTAAC-3’
RNF43 400 se	5’-CTGTCCTCTTTGACATCACTG-3’
RNF43 700 se	5’-GAGAACAGCCTGGGCCATC-3’

3.1.15 Buffers and solutions

10xPBS	137 mM NaCl 2.7 mM KCl 100 mM $Na_2HPO_4 * 2H_2O$ 2 mM KH_2PO_4 pH 7.4;
TAE	40 mM Tris 20 mM Acetic acid 1 mM EDTA
10x TBS	500 mM Tris 1.5 M NaCl pH 7.6
1x TBS-T	1/10 of 10x TBS 1/10 diluted in ddH2O 0.1 % Tween20
6x Loading dye	10 mM Tris-HCl (pH 7.6) 60 mM EDTA 60 % (v/v) glycerol 0.03 % (w/v) Bromphenol blue filled up to 50 mL with ddH_2O
Citrate Buffer	10 mM Sodium Citrate pH 6.0

Buffers for lentivirus production

2x HBS	280 mM NaCl 50 mM Hepes 1.42 mM Na_2HPO_4 x7 H_2O pH 7.05

Buffers for HPLC purification

Buffer A	20 mM Na_2HPO_4 140 mM NaCl pH 7.2
Buffer B	100 mM Citric acid pH 3.2

Solutions for Immunofluorescence

Fixation solution	Methanol/Aceton 1:1, storage at -20 °C

IF blocking buffer	3 % (w/v) BSA 1 % (v/v) Triton X-100 1 % (w/v) Saponine in PBS
Wash solution 1	3 % (w/v) BSA 1 % (w/v) Saponine in PBS
Wash solution 2	1 % (w/v) Saponine in PBS

Buffers for Western Blot Analysis

Running buffer	25 mM Tris 0.2 M Glycin 0.1 % (w/v) SDS
Transfer buffer	39 mM Glycin 48 mM Tris Ultra 0.04% SDS 20 % Methanol
SDS lysis buffer	62.4 mM Tris pH 6,8 2 % SDS 10 % Glycerol 50 mM DTT 0.01 % Bromophenol blue
NP40 lysis buffer	50 mM Tris-HCl 150 mM NaCl 1 %NP40 1 protease inhibitor tablet to 50ml pH 8.0
CST lysis buffer	20 mM Tris Ultra 150 mM NaCl 1 mM EDTA 1 mM EGTA 2.5 mM $Na_4P_2O_7$ 1 % Trion x-100

Solutions for Dual-Luciferase Assay

Lysis buffer	1 % (v/v) Triton X-100 25 mM Glycylglycin pH 7.8 15 mM $MgSO_4$ 4 mM EGTA 1 mM DTT, added directly before use store at 4 °C

Solutions for subcellular fractionation

RIPA buffer	50 mM Tris-HCl, pH 7.4 150 mM NaCl 1 %Triton x-100 1 % Sodium deoxycholate 0.1 % SDS 1 protease inhibitor tablet to 50ml
CLB buffer	10 mM Hepes 10 mM NaCl 5 mM $NaHCO_3$ 1 mM $CaCl_2$ 0.5 mM $MgCl_2$ 5 mM EDTA pH 7.4
TSE buffer	10 mM Tris, pH 7.5 300 mM Succrose 1 mM EDTA 0.1 % NP40

Solutions for in-situ hybridization

DEPC-ddH_2O:	0.1 % Diethylpyrocarbonat solved in ddH_2O, Incubated overnight under the hood with open lid autoclaved
DEPC-PBS (PBSo):	1/10 of 10x PBS in 1l DEPC-ddH_2O
20x SSC:	3 M NaCl 300 mM $C_6H_5Na_3O_7$ pH 7,0
Hybridization buffer:	50 % Formamid 5x SSC 2 % Blocking Reagenz 5 mM EDTA 0.05 % Chaps 50 µg/mL Heparin 50 µg/mL Yeast t-RNA
Blocking Buffer:	0.5 % Blocking Reagenz 0.1 % Goat serum in TBS-T
NTM Buffer:	0.1 M Tris pH 9,5 0.05 M $MgCl_2$ 0.1 M NaCl

NBT/BCIP staining:
10 mL NTM-Puffer
0.8 M Levamisol
1 tablet NBT/BCIP

3.1.16 Bacterial media

Luria-Bertani (LB)-Agar + Ampicillin
0.5 % (w/v) NaCl
0.5 % (w/v) Yeast extract
1.0 % (w/v) Tryptone
1.5 % (w/v) Agar
pH 7.4 (NaOH)

Medium was autoclaved, cooled to 50-60 °C before addition of antibiotics (100 µg/mL Ampicillin) and transferred to culture plates. After cooling down to room temperature the plates were stored at 4 °C.

LB-Medium (liquid)
1.0 % (w/v) NaCl
0.5 % (w/v) Yeast extract
1.0 % Tryptone
pH 7.4 (NaOH)

Medium was autoclaved, cooled to 50-60 °C before addition of antibiotics (100 µg/mL Ampicillin). After cooling down to room temperature LB-Medium was stored at 4 °C.

3.1.17 Cell culture media

Complete growth medium
500 mL DMEM
50 mL FCS
5 mL Penicillin (10000 U/ml) /Streptomycin (10000 µg/ml)

Soft agar media

IMDM
50 mL IMDM
0.5 ml Penicillin (10000 U/ml) /Streptomycin (10000 µg/ml

IMDM 10 % FCS
45 mL IMDM
5 mL FCS
0.5 ml Penicillin (10000 U/ml) /Streptomycin (10000 µg/ml)

IMDM 20 % FCS
40 mL IMDM
10 mL FCS
0.5 ml Penicillin (10000 U/ml)/Streptomycin (10000 µg/ml)

Agar (2 %)
2 g Difco agar solved in 100 mL IMDM
heated up to 95 °C
aliqouted in 2 ml volumes
stored at 4 °C.

Bottom agar (0.6 %)	450 µL agar (2 %), pre-warmed 1050 µL IMDM
2x concentrated Top agar (0.6 %)	300 µl agar (2 %), pre-warmed 700 µL IMDM

Organoid culture media

Single crypt medium	50 mL DMEM/F12 0.5 mL GlutaMax 0.5 mL P/S 0.5 mL Hepes
SCM + GF (growth factors)	20 mL SCM 400 µL **B27** (50xstock) 200 µL **N2** (100 x stock) 50 µL n-Acetylcystein (500 mM stock)
ENR (SCM + GF, EGF, Noggin)	85 µL SCM + GF 5 µl EGF 10 µL Noggin
Culture	5 µL R-spondin-1 5 µl ENR 500 µl SCM+GF

3.2 Microbiological methods

3.2.1 Preparation of consumables, media and solutions

Heat stable consumables, media and solutions were autoclaved at 121 °C and 2 bar for 20 min. Non-heat stable media and solutions were sterilized using mechanical filters either with the pore size of 0.45 µm to remove bacteria or with the pore size of 0.20 µm to remove viruses.

3.2.2 Culture and storage of *Escherichia coli* strains DH5α and One shot® Stbl3

The *E. coli* DH5α strain, which contains a plasmid coding Ampicillin resistance, was cultured at 37 °C on LB- agar or in LB broth containing Ampicillin (100 µg/mL). For long time storage glycerol stocks of *E. coli* DH5α were prepared by mixing an aliquot (800 µl) of bacteria suspension, grown overnight in LB broth with 100 µg/mL Ampicillin, with 200 µL of 80 % glycerol. Subsequently the glycerol stocks were rapidly frozen using liquid nitrogen or dry ice and stored at -80 °C.

3.2.3 Transformation of chemical competent DH5α or One shot® Stbl3 *E.coli* cells

100 ng of the repective plasmid-DNA was added to 50 µL of chemical competent *E. coli* cells thawed on ice. The transformation was accomplished by using the heat shock procedure. After incubating on ice for 10 min, cells were subjected to 42 °C for 45 s and rapidly cooled down on ice for 5 min. Subsequently, 900 µL of pre-heated (37 °C) LB-medium were added and the cells were centrifuged at 4500 rpm for 10 min at room temperature. After discarding the supernatant, cells were plated on agar plates containing Ampicillin (100 µg/ml) using a Drygalski spatula under sterile conditions and incubated overnight at 37 °C.

3.2.4 Culture and storage of transformed *E.coli*

After transformation of the respective plasmid into *E. coli* cells, one single clone was picked and transferred to either 5 mL or 100 mL of LB broth containing 5 µL or 100 µL ampicillin (stock: 1mg/mL), respectively. The bacteria culture was incubated on a shaker at 37 °C overnight. For long time storage at -80 °C, 800 µL of the cell suspension were mixed with 200 µL of 80 % glycerol and subsequently frozen on dry ice or liquid nitrogen.

3.3 Molecular biological methods

3.3.1 Plasmid DNA isolation from overnight culture

DNA isolation was performed from 5 mL *E.coli* overnight cultures using the SV Miniprep Wizard Plus System from Promega, Mannheim, Germany following manufacturer's instructions.

For high amounts of plasmid DNA isolation was performed from 100 mL bacteria overnight cultures with PureYield™ Plasmid Midiprep Kit from Promega Corp, Mannheim, Germany, according to manufacturer's protocol.

Both systems provide high-speed purification of plasmid DNA, based on alkaline lysis of transformed bacteria. After lysis, lysate clearing was accomplished using silica-membrane-based columns followed by few washing steps including endotoxin decontamination. The elution is performed in small volumes of either 30 µL nuclease-free water for Minipreps or 500 µL pre-heated (65 °C) nuclease-free water for Midipreps. The isolated plasmid DNA was stored at 4 °C for short time or at -20 °C for permanent storage.

3.3.2 RNA isolation from mammalian cells and human tissue

The isolation of RNA from mammalian cells and human tissue were performed with *GenElute™ Mammalian total RNA Miniprep Kit* (Sigma GmbH) after manufactures protocol. Briefly, cells cultivated in *6-well* plates tissue were washed with PBS and lysed with Guanidinthiocyanat and 2-mercaptoethanol. Afterwards, lysates were filtered to remove cellular residues before RNA was bound to silica gel membranes by using specific columns provided by manufacturer. Then, RNA was washed several times and eluted with 30 µL RNase-free water. RNA was stored at -80 °C.

3.3.3 DNaseI-treatment of RNA samples

To remove genomic DNA from RNA samples the *DNAfree™ kit* (Ambion) was used after manufacturer's instructions. For this, RNA samples were adjusted to a concentration of 250 ng/µL in a total volume of 250 µl. Afterwards, 2.5 µL DNase buffer (10X) and 1 µL DNaseI enzyme were added and incubated at 37 °C for 25 min. To stop the reaction 2.5 µL Inactivation buffer was added and incubated for 2 min at RT. After centrifuging at 10000 rpm of 2 min the supernatant fraction was removed and delivered in a fresh reaction tube.

3.3.4 Determination of DNA and RNA concentration

In this study the quantification of DNA concentrations was performed with the spectrophotometer NanoDrop ND-1000 (Thermo Scientific, Karlsruhe, Germany) at 260 nm (A_{260}) using 1.5 µL of the plasmid DNA or RNA. The purity of the DNA or RNA was analyzed by performing a second measurement at 280 nm (A_{280}) assessed by the ratio A_{260}/A_{280}. For pure DNA or RNA without any protein contamination the standard range is 1.8 – 2.0.

3.3.5 Amplification of DNA using polymerase chain reaction (PCR)

Polymerase chain reaction (PCR) was used to generate RNF43 C-terminal deletion constructs. For each construct two specific primers binding complementary to the target sequence were designed. The PCR was carried out either with Fidelitaq DNA polymerase (Affimetrix) or Q5® High-Fidelity DNA Polymerase (New England Biolabs). The annealing temperature for Fidelitaq DNA polymerase (Affimetrix) was calculated according to following formula:

T= 4 x (number of G or C) + 2 x (number of A or T) – 5

Whereas the annealing temperature of Q5® High-Fidelity DNA Polymerase (New England Biolabs) was calculated using NEB T_M Calculator Software (http://tmcalculator.neb.com)

Compound	**25 µL volume**	**Final concentration**
Fidelitaq™ PCR MasterMix (2X)	12.5 µL	1X
10 µM Forward Primer	1 µL	0.4 µM
10 µM Reverse Primer	1 µL	0.4 µM
Template DNA	3 µL	30 ng
Nuclease-free water	7.5 µL	-

Table 5: Optimized composition for Fidelitaq reaction

PCR step	**Temperature**	**Time**	
Initial denaturation	95 °C	4 min	
Denaturation	95 °C	30 s	36 cycles
Anneling	56 °C	30 s	
Elongation	68 °C	1 min	
Repeat from step 2: 36 times			
Final elongation	68 °C	5 min	
Final Hold	12 °C	∞	

Table 6: Optimized Cycler parameter for Fidelitaq reaction

Compound	**50 µL volume**	**Final concentration**
Q5® High-Fidelity (2X) master mix	25 µL	1X
10 µM Forward Primer	2.5 µL	0.5 µM
10 µM Reverse Primer	2.5 µL	0.5 µM
Template DNA	5 µL	50 ng
Nuclease-free water	15 µL	-

Table 7: Optimized composition for Q5 High-Fidelity reaction

PCR step	Temperature	Time	
Initial denaturation	98 °C	30 s	
Denaturation	98 °C	10 s	36 cycles
Anneling	50°-72 °C	30 s	
Elongation	72 °C	20-30 s/kb	
Repeat from step 2: 36 times			
Final elongation	72 °C	2 min	
Final hold	12 °C	∞	

Table 8: Optimized Cycler parameter for Q5 High-Fidelity reaction

To check the purity and the correct size of the generated amplicons agarose gel electrophoresis was employed.

3.3.6 Site-directed mutagenesis

The RNF43 frameshift and point mutations were introduced in the RNF43 plasmid by site-directed mutagenesis using *QuikChange Lightning Site-Directed Mutagenesis Kit* (Agilent Technologies) after manufacturer's protocol. The internal primers were designed using the *QuikChange Primer Design Program* Software from Agilent (*www.agilent.com/genomics/qcpd).*

Compounds	50 µL volume	Final concentration
10x Reaction buffer	5 µL	1x
Forward Primer	1.25 µL	125 ng
Reverse Primer	1.25 µL	125 ng
dNTP	1 µL	
QuikSolution reagent	1.5 µL	
Template plasmid	5 µL	25 ng
QuikChange Lightning Enzyme	1 µL	
Nuclease-free water	35 µL	

Table 9: Optimized composition for *QuikChange Lightning Site-Directed Mutagenesis*

PCR step	Temperature	Time	
Initial denaturation	95 °C	2 min	
Denaturation	95 °C	20 s	18 cycles
Annealing	60 °C	10 s	
Elongation	68 °C	30 s/kb	
Repeat from step 2: 18 times			
Final elongation	68 °C	5 min	
Final hold	12 °C	∞	

Table 10: Optimized Cycler parameter for *QuikChange Lightning Site-Directed Mutagenesis*

After the cycler reaction DpnI treatment was performed to digest the parental plasmid. Therefore, 2 µL of DpnI enzyme was directly added to each reaction mix and incubated for 10 min at 37 °C. Then, XL-Gold ultracompetent cells were transformed with 2 µL of each mutated plasmid after manufacturer's protocol. Briefly, 2 µL of β-mercaptoethanol was mixed with 45 µL thawed cells and incubated on ice for 2 min. Next, 2 µL of DpnI-treated sample was transferred to ultracompetent cell aliquots and incubated for 30 min on ice. A heat-pulse treatment followed at 42 °C for 30 s before samples were again replaced on ice for 2 min. Afterwards, 500 µL of preheated LB-medium was added to the cell samples and incubated for 1 h at 37 °C with shaking at 250 rpm. After centrifuging at 4500 rpm the supernatant was discarded and cells resuspended in 50 µL LB-medium for plating cells on LB-ampicillin agar plates overnight at 37 °C.

3.3.7 Reverse Transcription

Total RNA was isolated from cultured cells or human tissue and reverse-transcribed with Moloney Murine Leukemia Virus Reverse Transcriptase RNase H- Point Mutant (M-MLV-RT (H-) (Promega) according to manufacturer's instructions. For this, 1 µg RNA was mixed with 1 µL *Random Primer* [150 ng/µl] and filled up with ddH_2O to a total volume of 14 µL. The RNA mix was first incubated at 70 °C for 5 min and then at 4 °C for 5 min. Next, a mix of 5 µL M-MLV *5x Reaction buffer,* 1.25 µL dNTP's*,* 4.75 µL ddH_2O and 1 µL M-MLV-RT (H-) enzyme was added per sample. cDNA synthesis was performed at RT for 10 min and at 50 °C for 50 min. Enzyme inactivation was achieved at 70 °C for 15 min. For negative control the respective RNA mix was used without M-MLV-RT (H-) enzyme.

3.3.8 Quantitative *Real-time* PCR (qRT-PCR)

The KAPA SYBR® FAST qPCR Universal Master Mix (Peqlab) was used to analyze mRNA expression according to manufacturer's instructions. The transcript abundance was assessed using the BioRad CFX384 system (BioRad). For each reaction a mastermix of the following reaction components was prepared:

Compound	10 µL volume	Final concentration
KAPA SYBR® FAST Universal 2X qPCR Master Mix	5 µL	1x
10 µM Forward Primer	0.5 µL	200 nM
10 µM Reverse Primer	0.5 µL	200 nM
Template cDNA [50 ng/µl]	4 µL	200 ng

Table 11: Optimized composition for KAPA SYBR® FAST qPCR

Each sample was performed in triplicates. In addition, template-free and reverse transcriptase-free negative controls were included in each experiment.

The PCR conditions used are shown in table 11:

PCR step	Temperature	Time	
Enzyme activation	95 °C	3 min	
Denaturation	95 °C	15 s	40 cycles
Annealing	60 °C	10 s	
Melting Curve	60–95 °C	Increment of 0.5 °C /s	
Final Hold	12 °C	∞	

Table 12: Optimized PCR protocol for KAPA SYBR® FAST qPCR

Gene expression analysis was performed using the comparative $\Delta\Delta C_T$ method with the housekeeping gene GAPDH for normalization.

$$ratio = \frac{2^{\Delta CP_{target}\ (control-sample)}}{2^{\Delta CP_{ref}\ (control-sample)}}$$

CP= Crossing Point

target = gene of interest

3.3.9 Agarose gel electrophoresis

The size of the DNA fragments was determined by agarose gel electrophoresis. Agarose gels were prepared by dissolving 1-2 % (w/v) agarose in 1xTAE buffer while heating in a microwave. Afterwards, the solution was cooled and 7.5 µL Rothi®−Safe were added to 150 mL of agarose solution. Subsequently, the solution was transferred into a gel chamber. A comb was placed to form pockets for the samples. After hardening, the comb was removed and the gel was placed into an electrophoresis chamber, which was filled with 1xTAE buffer. Then, the samples mixed with the appropriate amount of the 6x loading Dye, were filled into the pockets and the electrophoresis was performed at 90 V for 60-70 min. Afterwards, the separated DNA fragments were visualized by UV illumination (λ=302 nm) and documented by taking a picture with Molecular Imager Gel Doc XR+System from BioRad Laboratories, Munich, Germany.

3.3.10 Purification of DNA fragments

The *illustra™ GFX™ PCR DNA and Gel Band Purification Kit* (GE Healthcare) was used to obtain pure and salt-free DNA fragments of enzymatic reactions or DNA-containing agarose gel slices. The procedure was performed according to manufacturer's protocol. The enzymatic mix or the melted gel slice was applied to columns with silica gel membranes. The DNA selectively bound to the membranes in presence of high concentrated salt. After several washing steps the DNA was eluted with 30 µL ddH_2O.

3.3.11 Analytical DNA hydrolysis using restriction endonucleases

The digestion of plasmid DNA with restriction enzymes was performed for analytical and preparative purposes. Therefore, the plasmid DNA was digested with restriction enzymes purchased from Promega or NEB. The digestion was performed as a double digestion in a total volume of 20 µL. Table 12 shows the optimized protocol.

Compound	**20 µL volume**
DNA	500 – 1000 ng
10x Buffer	2 µL
Restriction enzyme I (10 U/µL)	1 µL
Restriction enzyme II (10 U/µL)	1 µL
ddH_2O	filled up to a total volume of 20 µL

Table 12: Optimized protocol for DNA digestion

All digests were confirmed by agarose gel electrophoresis and UV illumination. Eventually, digest products were isolated from agarose gel slices and purified with *illustra™ GFX™ PCR DNA and Gel Band Purification Kit* (GE Healthcare) for further applications.

3.3.12 Annealing of oligonucleotides

The annealing of synthesized complementary shRNA oligonucleotides was performed in PCR tubes using Thermal Cycler C1000 (BioRad) according to following protocols:

Compound	10 µL volume
Oligo 1 [100 µM]	1 µL
Oligo 2 [100 µM]	1 µL
ATP	1 µL
10X T4 ligation buffer (NEB)	1 µL
ddH_2O	6 µL

Table 13: Optimized protocol for sample preparation of oligonucleotide annealing

Temperature	Time	
37 °C	30 min	
95 °C	5 min	Ramp down
25 °C	At 1.5 °C per min	

Table 14: Optimized Cycler protocol for annealing oligonucleotides

For storage samples were frozen at -20 °C until usage.

3.3.13 Ligation of oligonucleotides into expression vectors

3.3.13.1 De-phosphorylation of vectors

Before the ligation was carried out the PCR fragments and the vectors were digested with respective restriction enzymes. To minimize re-ligation, the expression vectors pcDNA™4/TO and pLVTHM were de-phosphorylated with the Thermosensitive Alkaline Phosphatase (TSAP; Promega). De-phosphorylation was performed with 1 µg vector DNA mixed with 5 µL Multi-Core™ 10X buffer and 1 µL TSAP in a total reaction volume of 50 µL at 37 °C for 15 min. Afterwards, the enzyme was heat-inactivated at 74 °C for 15 min. Finally, the vectors were purified using *illustra™ GFX™ PCR DNA and Gel Band Purification Kit* (GE Healthcare) and stored at -20 °C.

3.3.13.2 Phosphorylation of oligonucleotides

To facilitate the ligation of DNA fragments into the de-phosphorylated vectors the inserts were phosphorylated using T4 Polynucleotide Kinase (PNK; NEB). The reaction was set up by using 300 pmol insert DNA mixed with 5 µL 10X T4 PNK Reaction Buffer, 5 µL ATP [10 mM] and 1 µL T4 PNK in a total volume of 50 µL. Eventually, the reaction buffer was substituted with 1X T4 DNA Ligase Buffer containing 1 mM ATP. Then, samples were incubated at 37 °C for 30 min followed by 65 °C for 20 min. Finally, the PCR fragments were purified using *illustra™ GFX™ PCR DNA and Gel Band Purification Kit* (GE Healthcare) and stored at -20 °C.

3.3.13.3 Ligation of inserts into vectors

The ligation of phosphorylated PCR fragments and synthesized oligonucleotides into de-phosphorylated vectors were performed using T4 DNA-Ligase (NEB).

To obtain a high ligation efficacy the amount of insert and vector for the reaction were calculated with the NEBioCalculator (http://nebiocalculator.neb.com/#!/ligation). The best results were obtained by using a molar ratio of 1:3 vector to insert. The ligation was performed using T4 DNA Ligase (NEB) according to manufacturer's instructions:

Compound	**20 µL volume**
10X T4 DNA Ligase buffer	2 µL
Vector DNA	50 ng
Insert DNA	37 ng
ddH_2O	Up to 20 µL
T4 DNA Ligase	1 µL

Table 14: Optimized ligation protocol with T4 DNA ligase

The reaction was incubated 3 hours at RT or overnight at 4 °C and inactivated at 65 °C for 10 min. Samples were cooled down on ice before 5 µL of the approach was transformed in 50 µL competent DH5α cells.

3.3.14 Colony-PCR

Colony-PCR (GoTaq® Green Master Mix, Promega) was used to screen transformed bacteria for the presence of the correct insert DNA after cloning. Individual *E. coli* transformants were picked with pipet tips and delivered in 20 µL dH_2O. 5 µL of the bacterial suspension was

added to the PCR reaction and lysed during the initial heating step. This initial heating step causes the release of the plasmid DNA from the cell to serve as template for the amplification reaction. Primers designed to specifically target the insert DNA, were used to determine the correct DNA fragment of interest. For each PCR reaction a mastermix of the following reaction components was prepared:

Compound	**25 µL volume**	**Final concentration**
GoTaq® Green Master Mix (2x)	12.5 µL	1x
10 µM Forward Primer	1 µL	0.4 µM
10 µM Reverse Primer	1 µL	0.4 µM
Bacterial suspension	5 µL	-
ddH_2O	5.5 µL	-

Table 15: Optimized colony-PCR composition

According to manufacturer's instructions the PCR reaction was performed as follows:

PCR step	**Temperature**	**Time**	
Initial Denaturation	95 °C	5 min	
Denaturation	95 °C	30 s	
Annealing	56 °C	30 s	36 cycles
Elongation	72 °C	2 min	
Final elongation	72 °C	5 min	
Final Hold	12 °C	∞	

Table 16: Optimized Cycler protocol for GoTaq colony-PCR.

The correct size of the PCR-products was confirmed by agarose gel electrophoresis.

3.3.15 DNA-Sequencing

To verify the correct sequence of the cloned constructs, the plasmids were sent for sequencing to MWG Eurofins. Each sample was diluted to 50 ng/µL in a total volume of 15 µL including 10 µM specific primers. Eventually, common sequencing primers offered from the company were used.

3.4 Cell culture methods

3.4.1 Culturing of cell lines

All cell lines used in this study are listed in Table 2. Cell lines were cultured in 25 cm^2 or 75 cm^2 culture flasks in 7 or 13 mL of Dulbecco's Modified Eagle's Medium (Gibco®, Invitrogen, The Netherlands). All media were supplemented with 10 % Fetal Calf Serum (FCS) and cells were maintained at 37 °C with 5 % CO_2. Cells were subcultured by removing medium, washing cells with 5 mL DPBS (Gibco®, Invitrogen, The Netherlands) and incubating them with 1.0 mL of 0.05 % Trypsin-EDTA (Promo Cell, Heidelberg, Germany) at 37 °C and 5 % CO_2 for approximately 10 min. Trypsinization was stopped by the addition of 6 mL DMEM supplemented with 10 % FCS (DMEM/10 % FCS) and detached cells were transferred to 15 mL falcon tube for centrifugation at 1000 rpm for 5 min. After the supernatant was discarded, the cell pellet was resuspended in 5 mL DMEM/10 % FCS and seeded at an adequate cell density.

3.4.2 Determination of cell number

The Neubauer hemacytometer cell counting chamber was used to determine the number of living cells. One corner quarter represent the area of 1 mm^2 and the height of 0.1 mm. Thus, the cell number of one quarter represents 0.1 µL cell suspension. A volume of 10 µL cell suspension was diluted 1:10 in trypan blue. Trypan blue is a vital dye used to selectively stain dead cells blue since it penetrates the cell membrane of dead cells, whereas in viable cells trypan blue is not absorbed. 10 µL of the trypan blue cell dilution were filled into a Neubauer hemacytometer chamber. The total cell number was calculated as follows: first, the cells in each of the four corner quarters were counted, then the mean of the cell number was calculated dividing the counted cells by the four quarters. Finally, the mean was multiplied by 10 to respect the cell dilution and then multiplied by 10^4 to include the volume of the chamber.

3.4.3 Freezing and thawing of cell lines

For long term storage cells were frozen. After trypsinizing cells, the cell pellet was resuspended in 900 µL culture medium and transferred to an ice-cold cryotube containing 100 µL DMSO. Cryotubes were frozen stepwise: first, incubated on ice for a few minutes, then put into -80 °C freezer for 24 – 72 hours before transferred to liquid nitrogen and stored at -190 °C.

Thawing of cells: 10 mL of pre-heated medium (DMEM/10 % FCS) were prepared in 15 mL falcon tubes. Then, cells were thawed by incubating the cryotube for a short periode in a 37 °C water bath. Afterwards, the cells were transferred to the pre-heated medium and applied to centrifugation (1000 rpm, 5 min, RT). Cells were resuspended in 1 mL medium and transferred to 25 cm^2 culture flask containing 6 mL medium.

3.4.4 Cell transfection

3.4.4.1 Transfection with Lipofectamine 2000

Cell transfection was performed in 24-wells for TOPFlash/FOPFlash assays, in 12-wells for immunofluorescence, in 6-wells for RNA and protein lysate preparation, and in 10 cm^2 dishes for immunoprecipitation and subcellular fractionation.

Every time cells were transfected with the respective plasmid DNA using Lipofectamine 2000 (Invitrogen, Karlsruhe, Germany) approximately 24 h after seeding. Procedure was performed according to manufacturer's protocol. Detailed information is listed at the respective experiment.

3.4.4.2 Transfection with 4D-Nucleofector™

To enhance the transfection efficacy for cell lines the 4D-Nucleofector™ X Unit System from Lonza Cologne GmbH was used. The cell line HT-29 was transfected with the optimized protocol for the 4D-Nucleofector™ X unit device of Lonza according to manufacturer's protocol. Also, the transfection of HCT116 for WNT target gene expression analysis was carried out with the optimized protocol for the 4D-Nucleofector™ X unit device of Lonza according to manufacturer's protocol.

3.4.5 Lentiviral shRNA knock-down

3.4.5.1 Lentiviral production

For safety reasons, the components necessary for virus production are split across multiple plasmids. In this study, a second generation lentiviral system consisting of three plasmids was used. The packaging plasmid (psPAX2) encodes the HIV gag, pol, rev, and tat genes. The envelope protein VSV-G is encoded on a second plasmid (pMD2.g). The third plasmid (pLVTHM) is used as a transfer plasmid containing the viral LTRs, psi packaging signal and the shRNA of interest (shRNF43).

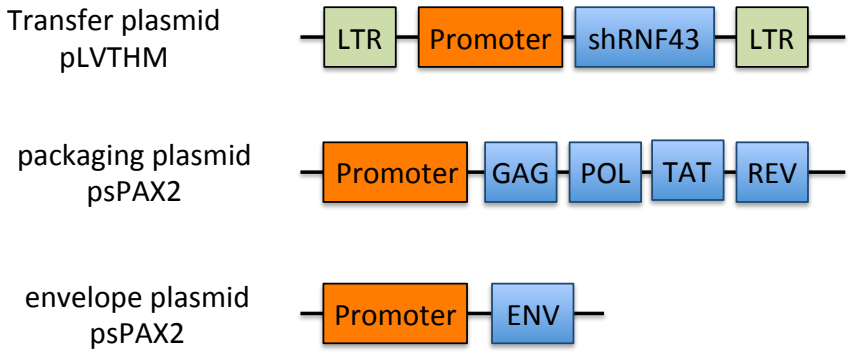

Figure 14: Schematic representation of second generation lentivirus vectors.
LTR, Long terminal repeat; GAG, POL, TAT, REV, and ENV viral genes coding for structural proteins.

For lentivirus production 293T cells were seeded in 75 cm^2 cell culture flasks with 10 mL culture medium DMEM supplemented with 10 % FCS. Cells were grown at 37 °C for 24 h. Next day, culture medium was renewed 2 hours before cells were co-transfected with the plasmids using $CaPO_4$ co-precipitation. Briefly, 20 µg pLVTHM-shcontrol or 20 µg pLVTHM-shRNF43, 15 µg psPAX2 and 6 µg pMD2.g were mixed in a 1.5 mL reaction tube and filled up with dH_2O to a total volume of 439 µL. 61 µL $CaCl_2$ [2 M] was added to the plasmid mix. In parallel, a 15 mL polystyrene tube was prepared containing 500 µL 2x HBS. The Ca-DNA solution was added to the HBS solution in a dropwise manner while bubbling and incubated at RT for 20 min. Afterwards, the Ca-DNA complex solution was added to the 293T cells and incubated at 37 °C. 18 h post transfection the medium was changed to 6 mL fresh DMEM 10 % FCS containing 40 mM caffeine and incubated again at 37 °C. After 24 h the lentiviral supernatant was collected and filtered using 0.45 µm filter units. For short term storage the supernatant was aliquoted in 1 mL volumes and frozen at -80 °C.

3.4.5.2 Lentiviral cell transduction

For lentiviral tumor cell transduction tumor cells were seeded in 3 mL culture medium supplemented with 10 % FCS in 6-well cavities and grown for 24 h. The next day, growth medium was removed from cells and replaced by 1 mL lentiviral supernatant containing 8 µg/mL hexadimethrine bromide (polybrene, Sigma). Cells were incubated at 37 °C for 2 h while gently swirling every 30 min. After the incubation time 4 mL cell culture medium with 10 % FCS was added. 24 h post transduction cells were checked for GFP expression and lentiviral medium was replaced by fresh growth medium supplemented with 10 % FCS and 1 % P/S.

3.4.6 Small-interfering knockdown

The human *RNF43*-targeting small-interfering RNA kit SR310324 from OriGene was used to knockdown endogenous RNF43 in colon cancer cells. Three siRNA sequences were introduced in HT-29 using optimized standard protocol for 4D-Nucleofection™X unit transfection (Lonza).

3.5 Organoid culture

3.5.1 Isolation of murine intestinal crypts

Before starting the isolation of murine crypts matrigel was put on ice in order to thaw it. For harvesting crypt cells the small intestine was taken from a 12-week old mouse. The intestine was placed in a Petri dish on ice containing ice-cold washing solution for opening it lengthwise and clearing the luminal contents. The villi of an intestine were scraped off using a cover glass.

Next, the intestine was washed with washing solution and then cut with sharp scissors into 2-4 mm pieces, before the material was transferred into a 50 mL falcon tube contain 10 – 20 mL of washing solution. The intestinal pieces were pipetted up and down a few times with a 25 mL pipette. After sedimentation of tissue fragments, the supernatant was removed. For removing single cells, a strong washing was performed. 10 mL of washing solution was added to the tissue fragments, pipetted up and down and let for sedimentation. Next, the supernatant was removed. This was repeated until the supernatant was clear (approximately 20 times). Afterwards, 25 mL of 2 mM EDTA was added to the tissue fragments and placed on a shaker for 15 min incubation at 4 °C. Tissue fragments were sedimented followed by the removal of the supernatant and washed two times with 10 mL of washing solution. Then, 10 mL of washing solution was added and passed through a 70 µm cell strainer to isolate crypts from tissue fragments. The flow-through (fraction I) was stored on ice, whereas the remaining tissue fragments were used for further proceedings. They were transferred with a pipette tip into a 50 mL falcon tube containing 25 mL of 2 mM EDTA and incubated for 30 min on a shaker at 4 °C. After tissue sedimentation, the supernatant was discarded, washing solution was added and the fragments were gently pipetted up and down before passed again through a 70 µm cell strainer (fraction II). Crypts form both fractions were observed for finger-like structures under the microscope and eventually pooled. Afterwards, crypts were spinned down at 600 rpm for 5 min at 4 °C. The pellet was resuspended in 10 mL of ice-cold Basal Medium 2 and crypts were counted. The crypts were centrifuged at 800 rpm for 5 min at 4 °C and resuspended in matrigel with a concentration of 100 crypts per 50 µL matrigel. 45 µL of the suspension were pipetted as a drop into one well of a pre-warmed 24-well plate and

incubated for 3 min at RT. The plate was then incubated at 37 °C for 10 min until the matrigel solidified completely. 500 µL of crypt culture medium was added per well.

3.5.2 Culture of organoids

For cultivating isolated crypts the medium was changed 2 - 3 times per week. Growing organoids were splitted in a 1:4 ratio once a week. For this the medium is replaced by 500 µL ice-cold Basal medium 1 per well and incubated on ice for 10 min. Next, organoids were pipetted up and down using cooled pipette tips. All organoids were then transferred into one ice-cold 15 mL falcon tube and filled up with Basal Medium 1 to final volume of 15 mL. Organoids were next centrifuged for 600 rpm for 5 min at 4 °C. The supernatant was carefully removed, the pellet was resuspended in 10 mL of ice-cold Base Medium 1 and centrifuged at 800 rpm for 5 min at 4 °C. The supernatant was removed completely and the organoids were mixed with 4x volumes of matrigel. 45 µL suspension per well was pipetted in drop shape. The plate was left for 3 min at RT before it was incubated for10 min at 37 °C. Afterwards, 500 µL of crypt culture medium was added per well.

3.6 Protein biochemical methods

3.6.1 Protein A affinity chromatography of IgG from serum

For affinity purification of IgG from rat sera, the HiTrap Protein G HP 1 mL column was used. The serum samples were diluted in Buffer A to a final volume of 10 mL and loaded onto the pre-equilibrated column. After washing with 10 CV Buffer A, the antibodies were eluted with Buffer B taking 1 mL fractions into 50 µL Elution Neutralization Buffer. The fractions were pooled according to the 280 nm absorbance chromatogram and dialyzed to 1×PBS. The sample was concentrated and stored at –20 °C.

3.6.2 Co-Immunoprecipitation

For each Co-IP, cells were seeded in a 10 cm^2 dish in an appropriate density and transfected with Lipofectamine 2000 using 6 µg plasmid DNA. 48 h after transfection, cells were washed with 1x PBS and placed on ice before lysis, which was performed with 900 µL NP40 lysis buffer. Cell lysates were pre-cleared by incubation with 50 µL protein agarose A beads (for anti-rabbit antibody) for 2 h at 4 °C on a rotating wheel. Afterwards, cell lysates were centrifuged at max. speed at 4 °C for 2 min and the pre-clearing was repeated once. Then 10 % of the raw lysate were added to 3x SDS lysis buffer and frozen at -20 °C. The remaining lysates were transferred into fresh reaction tubes (Eppendorf) before a specific antibody (see

Table 1: Antibodies used in this study) was added and lysates were incubated overnight at 4 °C on a rotating wheel. The next day lysates were mixed with 50 µL of protein agarose A and incubated on a rotating wheel for at least 4 h at 4 °C. Afterwards, lysates were centrifuged at 6000 rpm for 3 min at 4 °C, supernatants were discarded and beads were washed 3 times with lysis buffer and 2 times with sterile PBS. Then, 100 µL of 1x SDS buffer were added beads and lysates were heated up to 95 °C for 5 min before freezing at -20 °C. Analysis of Co-IP was performed by Western bot analysis.

3.6.3 Subcellular fractionation

For subcellular fractionation cells were seeded in 10 cm^2 culture plates in 10 mL DMEM supplemented with 10 % FCS and incubated overnight at 37 °C. Next day, cells were harvested, counted and divided in 1x 10^6 cells per 100 µL in CLB-buffer containing protease inhibitors for each condition. Then, cells were incubated on ice for 5 min before they were dounced 50 times. Afterwards, cells were centrifuged at 3000 rpm for 5 min at 4 °C. The supernatant (S1) was transferred to a fresh reaction tube and placed on ice for later treatment.

The cell pellet (P1) was resuspended in 800 µL TSE-buffer and 30 times dounced. Next, the pellet suspension was centrifuged at 3000 rpm for 5 min at 4 °C. The supernatant was discarded and the pellet was washed in 800 µL TSE-buffer before centrifuged again. Then, the supernatant was removed and the pellet was resuspended in 100 µL RIPA buffer containing protease inhibitors and 0.1 % SDS. 50 µL of 3x SDS lysis buffer were added and samples were cooked at 95 °C for 5 min. The P1 fraction containing nuclear proteins and chromatin was frozen at -20 °C.

The S1 fraction containing membranes and cytosolic proteins, which was stored on ice, was then centrifuged at 39 000g for 15 min at 4 °C. The supernatant (S2) was transferred to a fresh reaction tubes and stored on ice for later use.

The pellet fraction (P2) containing membrane proteins was resuspended in 50 µL 1x SDS, cooked at 95 °C for 5 min and stored at -20 °C until usage.

100 µL of the S2 fraction containing cytosolic proteins was mixed with 50 µL 3x SDS lysis buffer, cooked at 95 °C for 5 min and stored at -20 °C.

3.6.4 Western blot

3.6.4.1 Cell lysis

Lysates for Western blot were obtained from cells transfected with the plasmid of interest using Lipofectamine 2000. Cells were seeded in 6-wells in an appropriate density. Per 6-well, 0.5 µg plasmid DNA were transient transfected using Lipofectamine 2000 (Invitrogen) for 24 h. For cell lysis medium was removed, cells were washed with 1x PBS and lysed with 100 µL 1x SDS lysis buffer. Then, lysates were transferred to 1.5 mL reaction tubes (Eppendorf) and put on ice and sonicated for 10 sec with amplitude of 30. Afterwards, lysates were heated to 95 °C for 5 min and either directly implemented for Western blotting or frozen at -20 °C for storage.

3.6.4.2 SDS-Polyacrylamide electrophoresis (SDS-Page)

The molecular weights of proteins were analyzed using 8 % polyacrylamide (PAA) gels. Gels were prepared as shown in Table 13 and transferred into gel cassettes (Invitrogen). Afterwards, the gel solution was covered with 1 mL of isopropanol to prevent drying-out and incubated for one hour at RT to polymerize. Then, the water was removed, and replaced by the loading gel. The stacking gel was prepared as shown in Table 13. Before polymerization, a comb with 12 wells was placed into the stacking gel to create pockets for the samples. After 45 – 60 min polymerizing at RT gels were used either directly or wrapped in wet paper towels and stored at 4 °C.

For electrophoresis, gels were fixed in XCell *SureLock*® Mini-Cell chambers (Invitrogen) and filled with 1x SDS running buffer. Same amounts of protein extracts were loaded into gel pockets. Electrophoresis was applied to 150 V for 1 h, unless otherwise indicated.

Separating gel		**Stacking gel**	
Components	**Volumes**	**Components**	**Volumes**
Tris (2.5 M; pH 8.8)	7.5 mL	Tris (0.5 M; pH 6.5)	0.5 mL
PAA (40 %)	2.0 mL	PAA (40 %)	0.2 mL
ddH_2O	5.44 mL	ddH_2O	1.30 mL
APS (10 % (w/v))	0.05 mL	APS (10 % (w/v))	10 µL
TEMED	10 µL	TEMED	2 µL

Table 13: Composition of reagents used for preparing SDS gels

3.6.4.3 Semi-Dry blot and development

Separated proteins were blotted onto nitrocellulose membranes (Whatman GmbH, Germany) using Semi-Dry Transblot system (BioRad, Munich, Germany) at 90 mA / cm^2 for 100 min in transfer buffer. Afterwards, membranes were blocked for 1 h at RT in TBS containing 0.1 % Tween20 (TBS-T) and 5 % fat-free milk powder (BioRad Laboratories, Munich, Germany). After blocking, the membranes were incubated with primary antibodies according to Table 1 in 5 % BSA TBS-T solution at 4 °C overnight. After washing 3 times for 10 min with TBS-T, membranes were incubated with secondary anti-mouse IgG or anti-rabbit HRP-conjugated antibody (Promega, Germany) (for concentration see Table 1) in 5 % milk-TBS-T at RT for 1 h. Membranes were washed again with TBS-T (5 to 6 times, changing every 10 min) and detected with either Pierce® ECL-detection Kit (Thermo Scientific, Karlsruhe, Germany) or SuperSignal West Pico Chemoluminescent Substrate (Thermo Scientific, Karlsruhe, Germany) by using x-ray films (Kodak) and developing machine Curix60 or Intas Science Imaging.

3.7 Histological methods

3.7.1 In-situ hybridization

3.7.1.1 In-vitro transcription

Digoxigenin-labeled (Roche) antisense and appropriate sense control RNA probes for human RNF43 (NM_017763.4, nucleotides 3824 to 4402) and murine Rnf43 (NM_172448) were generated from cDNA-containing vectors by *in vitro* transcription as follows:

Compounds	Volume
Linearized DNA	1 – 2 µg
Transcription buffer	4 µL
DTT (0.1 M)	2 µL
Dig RNA labeling mix	2 µL
RNAse inhibitor	1 µL
T7 or SP6 RNA polymerase	1.5 µL
ddH_2O	Fill up to 20 µL

Table 14: Composition of in vitro transcription reaction

In vitro transcription was performed at 37 °C for 2-4 h. Afterwards, 1 µL of (RNAse-free) DNAase enzyme was incubated for 10 min at 37 °C to digest the template DNA. Digoxigeninlabeled RNA was purified using RNeasy kit (Qiagen).

3.7.1.2 RNA Hybridization

Paraffin-embedded human and murine tissue were cut in 9 µm sections, mounted on Super Frost Slides and dried at 50 °C overnight. Samples were dewaxed following these steps: 3 times in RotiClear (AppliChem) for 5 min, 2 times in absolute EtOH for 5 min, in 75 % EtOH for 5 min, in 50 % EtOH for 5 min, in 25 % EtOH for 5 min, and finally 2 times rinsed with DEPC treated H_2O. Next, samples were incubated in 0.2 N HCl for 15 min before proteinase K treatment was applied:

Tissue	Prot K concentration	Time
Embryo E 15 / E 16	20 µg/mL in PBS	10 min at RT
Adult intestine and colon	30 µg/mL in PBS	20 min at 37 °C

Table 15: Proteinase K treatment

Afterwards, samples were rinsed with 0.2 % glycine-PBS and two times with PBS. Postfixation was performed for 10 min with 4 % paraformaldehyde and samples were subsequently rinsed 2 times with PBS before acetic anhydride treatment with 0.1 M triethanolamine (pH 8) mixed with 0.25 % acetic anhydride in DEPC-treated H_2O was carried out for 5 min. Anhydride treatment was repeated once. Then, samples were washed 2 times with PBS and 2 times with 5x SSC (pH 4.5). For prehybridization, slides were placed in humidified box (5x SSC/50 % formamide) and covered with 500 µL hybridization solution at 70 °C for 1 h. For the hybridization reaction, the prehybridization solution was replaced by 50 µL hybridization solution containing 1 µg/µL digoxigenin-labeled RNA probe per slide, which had been denatured at 95 °C for 5 min and stored on ice until use. Samples were incubated at 68 °C for 72 h. After hybridization, slides were rinsed in 2x SSC (pH 4.5) and washed three times with 2x SSC (pH 4.5) at 65 °C for 30 min. Next, samples were washed 5 times with TBS-0.1 % Tween. For immunological detection, slides were blocked with 400 µL goat serum for at least 30 min before they were incubated overnight with digoxigenin-Fab (Roche, 1:2000). The next day, slides were washed five times with TBS-0.1 % Tween and 3 times wit NTM buffer. For detection, the NBT/BCIP staining solution was prepared and added to the samples overnight. Afterwards, reaction was stopped by rinsing samples with ddH_2O, before slides

were covered with Kaiser's Glyceringelatine (Merck GmbH). Pictures were taken with Keyence microscope BZ-9000.

3.7.2 H&E staining

Murine intestinal tissue was isolated from mice, fixed in 4 % paraformaldehyde, dehydrated and embedded in paraffin before usage. For deparaffinization and rehydration, samples were incubated at 60 °C for 20 min before incubated three times in RothiClear for 10 min, two times in absolute ethanol for 10 min, and two times in 90 %, 70 %, and 50 % ethanol for 5 min each. Afterwards, samples were washed once in dH_2O for 5 minutes. Next slides were stainined with hematoxylin 5 % (Morphisto) for 6 min at RT, rinsed in tapwater and incubated for 6 min in eosin 1 % (Morphisto). Afterwards, slides were washed with tap water and dehydrated with 50 %, 70 %, and 90 % ethanol for 1 min. Sections were incubated two times in absolute ethanol for 5 min and and three times in RothiClear for 3 min. Finally, samples were mounted with DPX Mountant (Sigma Aldrich).

3.7.3 Immunohistochemistry

Paraffin-embedded human tissue samples were obtained from the tissue bank of the Institut für Pathologie, Klinikum Bayreuth, Germany. Murine intestinal tissue was isolated from mice, fixed in 4 % paraformaldehyde, dehydrated and embedded in paraffin before usage. For deparaffinization and rehydration, samples were incubated three times in RothiClear for 10 min, two times in absolute ethanol for 10 min, and two times in 95 %, 70 %, and 50 % ethanol for 5 min each. Afterwards, samples were washed twice in dH_2O for 5 minutes. Heat induced antigen retrieval was performed using 10 mM sodium citrate (pH 6) for 10 min. Then, slides were cooled down for 30 min at RT, and washed once with dH_2O for 5 min each. For staining, samples were incubated in 3 % hydrogen peroxide for 10 min and washed twice with dH_2O for 5 min and once with TBS/0.1 % Tween-20 for 5 min. Afterwards, sections were blocked with 150 µL 5% goat serum for 1 h at RT. Blocking solution was then replaced by 150 µL antibody solution (RNF43, 1:1000, Atlas Antibodies AB; Ki67, 1:400, Cell Signaling Technology) and incubated overnight at 4 °C. The next day, samples were washed with TBS/0.1 % Tween-20 three times for 5 min, before 150 µL secondary antibody (anti-rabbit-HRP, Promega), diluted 1:200 in TBS/0.1 % Tween-20 were applied. Sections were incubated 30 min at RT and washed three times with TBS/0.1 % Tween-20 for 5 min. For detection, 150 µL DAB substrate (Cell Signaling Technology) was added and staining was closely monitored. After development, slides were immersed in dH_2O and counterstaining was performed with hematoxylin. Next, slides were rinsed two times in dH_2O for 5 min.

Dehydration was performed by incubating sections two times in 95 % ethanol for 5 min, two times in absolute ethanol for 5 min, and two times in RothiClear for 5 min. Finally, samples were mounted with DPX Mountant (Sigma Aldrich).

3.8 Immunofluorescence

For immunofluorescence, 500 ng plasmid DNA were transient transfected in 12-well plates seeded with cancer cells in appropriate cell density using Lipofectamine 2000 (Invitrogen, Karlsruhe, Germany) according to manufactures protocol.

After incubation, the medium and the chamber walls were removed, cells were washed with 1x PBS and fixed with ice-cold methanol/aceton in same amounts for 15 min. Following 3 washing steps with 1x PBS the cells were permeabilized and blocked with IF blocking buffer for 15 min at RT and then incubated with primary antibody diluted in Wash solution 1 (applied concentration see Table 1) overnight in a humidified chamber at 4 °C. The next day, 3 washing steps with wash solution 1 were performed and cells were incubated with secondary antibody diluted in wash solution 1 (applied concentration see Table 1) for 1 h at RT in the dark. Afterwards, cells on chamber slides were washed 3 times with wash Solution 2, mounted with Vectorshield mounting medium containing DAPI (Vector Laboratories, Eching, Germany) and covered with glass coverslips (Menzel-Gläser, Braunschweig, Germany). Subsequently, confocal microscopy (Leica SP5 or FluoView) was performed. Chamber slides could be stored for max. 3 days at -20 °C before fluorescence intensity decreased.

3.9 Proliferation

To compare the proliferative capacity of tumor cells *in vitro*, cells were seeded in quadruplicates of 500, 1000 and 1500 cells per 96-well cavity in 100 µL culture medium. In addition, four 96-well cavities without cells were included as background control (blank). 24 h after seeding culture medium was replaced with serum-free medium for cell cycle synchronization. After 24 h of starving cells were released by replacing serum-free medium with complete culture medium supplemented with 10 % FCS. 48 h later cells were adjusted to room temperature for 30 min and 10 µL Cell counting kit-8 solution (CCK8, Sigma) was added to each well. Cells were then incubated at 37 °C for 1h and measured at 450 nm / 650 nm using Sunrise Elisa Reader (Tecan).

3.10 Invasion

The Boyden-Chamber system was used to analyze the invasiveness of tumor cells *in vitro*. Therefore, tumor cells were seeded in 6-well cavities in 3 mL culture medium in appropriate cell density. After 24 h culture medium was replaced by serum-free medium for starving conditions. In parallel, the lower site of 8 µm pore size transwell inserts for 24-well cavities (Corning) were coated with 10 µg rat collagen I (Gibco, Invitrogen) for 4 h at RT under sterile conditions. Afterwards, inserts were washed 3 times with 1x PBS and dried for 2 – 3 h at RT. Meanwhile, matrigel (Sigma Aldrich) was thawed on ice for several hours. Then, matrigel was adjusted to 10 µg/mL in 0.02 N acetic acid and 100 µL of the dilution was added into each insert chamber. Matrigel was dried overnight under sterile conditions. 1 h before cell invasion started the matrigel was rehydrated with 200 µL serum-free culture medium. Meanwhile, the cells were trypsinized, adjusted to $20x10^4$ cell / mL in serum-free medium and 500 µL of the cell suspension was added to the dehydrated matrigel. In addition, the lower chamber was filled up with 750 µL culture medium supplemented with 10 % FCS. Cells were incubated at 37 °C for 24 h. Removing the inserts from the 24-well cavities stopped the invasion assay. The inserts were washed with 1x PBS and the upper chamber membrane was carefully cleaned of non-migrated cells using cotton wool-tips. For quantitative analysis migrated cells on the lower site of the insert membrane were fixed with 4 % PFA, stained with DAPI and cell nuclei were counted microscopically.

3.11 Colony formation assay

Colony formation assay was carried out using the soft agar method in a 96-well format to measure the anchor-independent tumorigenicity of tumor cells *in vitro*. Each condition was performed in quadruplicates.

First, 50 µL of pre-warmed (42 °C) 0.6 % bottom agar was plated in 96-well cavities to serve as a prelayer and incubated at RT to solidify. Meanwhile, cells were trypsinized, counted and adjusted to 500, 1000 or 15000 cells per well in IMDM supplemented with 20 % FCS and 1 % P/S in a total volume of 25 µL per 96-well. 0.3 % semisolid top agar was prepared by mixing the cells with 25 µL of pre-warmed (42 °C) double concentrated top agar (0.6 % agar). Subsequently, 50 µL of the cell agar solution was layered on top of the solidified bottom agar avoiding air bubbles. After solidification 50 µL of IMDM supplemented with 10 % FCS was added as feeding layer to each well. The 96-well plates were sealed with paraffin foil to prevent dehydration and incubated for one week at 37 °C with 5 % CO_2. Afterwards, pictures were taken microscopically from the cell colonies. Cell proliferation and viability were scored

adding 40 µL MTT [5mg/ml] per well and incubated for 3 h at RT. Cell growth was measured using plate reader with excitation of 570 nm.

3.12 Luciferase reporter assay

Transient transfections were carried out in 24-well cavities seeded with colon cancer cells in an appropriate cell density with Lipofectamine 2000 (Invitrogen). 100 ng of pTOPFlash and pFOPFlash plasmids containing ten binding sites for TCF/LEF, m67 containing four binding sites for Stat3, 12xcsl plasmid containing 12 binding sites for Notch, or NFκB plasmid containing 3 binding sites were used as reporter plasmids, respectively. Cells were cotransfected with 10 ng of simian virus 40 Renilla luciferase plasmid (Promega) to account for differences in transfection efficiency. The expression of firefly and renilla luciferases was measured using the Dual Luciferase Reporter Assay System (Promega, Mannheim, Germany) with the Orion Microplate Luminometer (EG & Berthold) after 48 h treatment, according to the manufacturer's instructions. The experiment was performed in duplicates and the relative luciferase activity was defined as luciferase reporter plasmid activity normalized to renilla luciferase values.

3.13 Statistical analysis

Results are presented as mean ± SD of three independent experiments, unless otherwise indicated. Statistical analysis of normally distributed data was performed using *t* test or ANOVA with Dunnett's multiple comparison posttest. Statistical significance was established when $p \leq 0.05$.

4 Results

Part of the results presented here are published:

Loregger A*, Grandl M*, Mejías-Luque R, Allgäuer M, Degenhart K, Haselmann V, Oikonomou C, Hatzis P, Janssen KP, Nitsche U, Gradl D, van den Broek O, Destree O, Ulm K, Neumaier M, Kalali B, Jung A, Varela I, Schmid RM, Rad R, Busch DH, Gerhard M.; **The E3 ligase RNF43 inhibits Wnt signaling downstream of mutated β-catenin by sequestering TCF4 to the nuclear membrane**. *Sci Signal.* Sep 8;8(393):ra90. (2015)

4.1 Screening for antibodies against human RNF43.

4.1.1 Screening of RNF43 hybridoma supernatants by Western blot analysis

To investigate the endogenous function and subcellular localization of RNF43, a monoclonal antibody to detect RNF43 in different applications was required. Some commercially available antibodies claimed to recognize endogenous RNF43, but none of them have been proven to work reliable for Western blot, immunofluorescence, and immunoprecipitation analysis to investigate the expression and localization of the endogenous protein. Therefore, rats were immunized with an *in-silico* predicted immunogenic peptide of RNF43 – SRSYQEPGRRLHLIRQHPGH (**Figure 15**) in order to generate a monoclonal antibody.

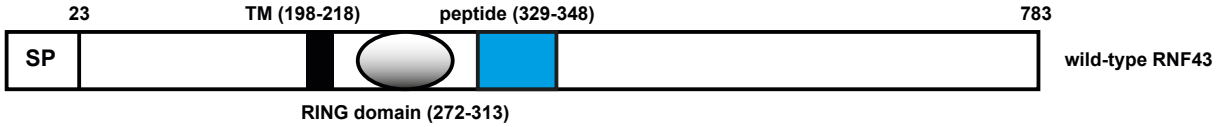

Figure 15: Schematic representation of RNF43 showing localization of the peptide used for immunization
SP, signal peptide; TM, putative transmembrane domain; blue box indicates *in-silico* predicted peptide sequence (329-348) of RNF43 for immunization - SRSYQEPGRRLHLIRQHPGH; numbers indicate amino acid position

Immunization and generation of antibody producing hybridoma cells were performed in collaboration with Dr. Elisabeth Kremmer, Institut für Molekulare Immunologie at the Helmholtz Zentrum München. The hybridoma supernatants obtained were screened by Western blot analysis for positive recognition of RNF43, firstly in HCT116 lysates overexpressing RNF43 and secondly in MCF7 lysates for detecting endogenous wild-type RNF43. Three hybridoma supernatants 8D6, 10F8, and 15B12 (of 156 investigated) recognized bands in HCT116 cells with a strong signal at the molecular weight of overexpressed FLAG-tagged RNF43 (**Figure 16A**). Furthermore, they detected one band in

MCF7 lysates at the molecular weight of endogenous RNF43, which was recognized with a commercial RNF43 antibody (**Figure 16B**). All other supernatants detected either many unspecific bands or no protein at all. Therefore, 8D6, 10F8, and 15B12 were selected for further analyses.

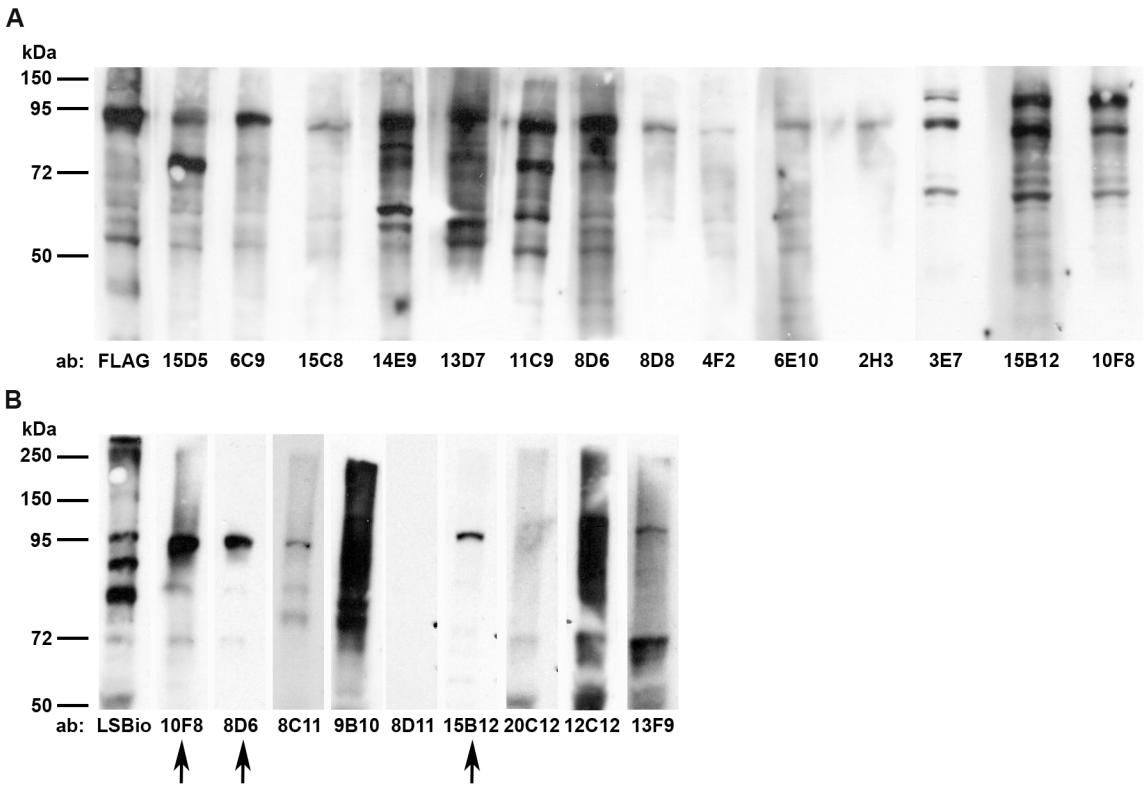

Figure 16: RNF43 is recognized by different antibodies secreted by hybridoma cells.
(A) Western blot analysis of some hybridoma supernatants using lysates of HCT116 cells overexpressing RNF43-FLAG. (B) Analysis of some hybridoma supernatants with MCF7 cell lysates expressing endogenous RNF43 by Western blot. Black arrows indicate hybridoma supernatants used for further analysis; ab, antibody; LSBio, commercial antibody for RNF43 Western Blot analysis; kDa, kilo Dalton

4.1.2 Screening of RNF43 hybridoma supernatants by immunofluorescence analysis

For functional analysis of endogenous RNF43 it is necessary to obtain antibodies suitable for different techniques. Therefore, the supernatants of 8D6, 10F8, and 15B12 were tested for immunofluorescence analysis. Only 8D6 and 10F8 recognized RNF43 in HCT116 cells overexpressing RNF43 (**Figure 17A**). Interestingly, when applying 8D6 or 10F8 for detection of endogenous RNF43 in HT29, DLD1 and MCF7 cells 8D6 showed a localization of RNF43 in the nuclear compartment with different intensities, whereas the 10F8 detected a protein in a punctuated pattern in the cytoplasm of HT29 cells but no protein in MCF7 cells (**Figure 17B**).

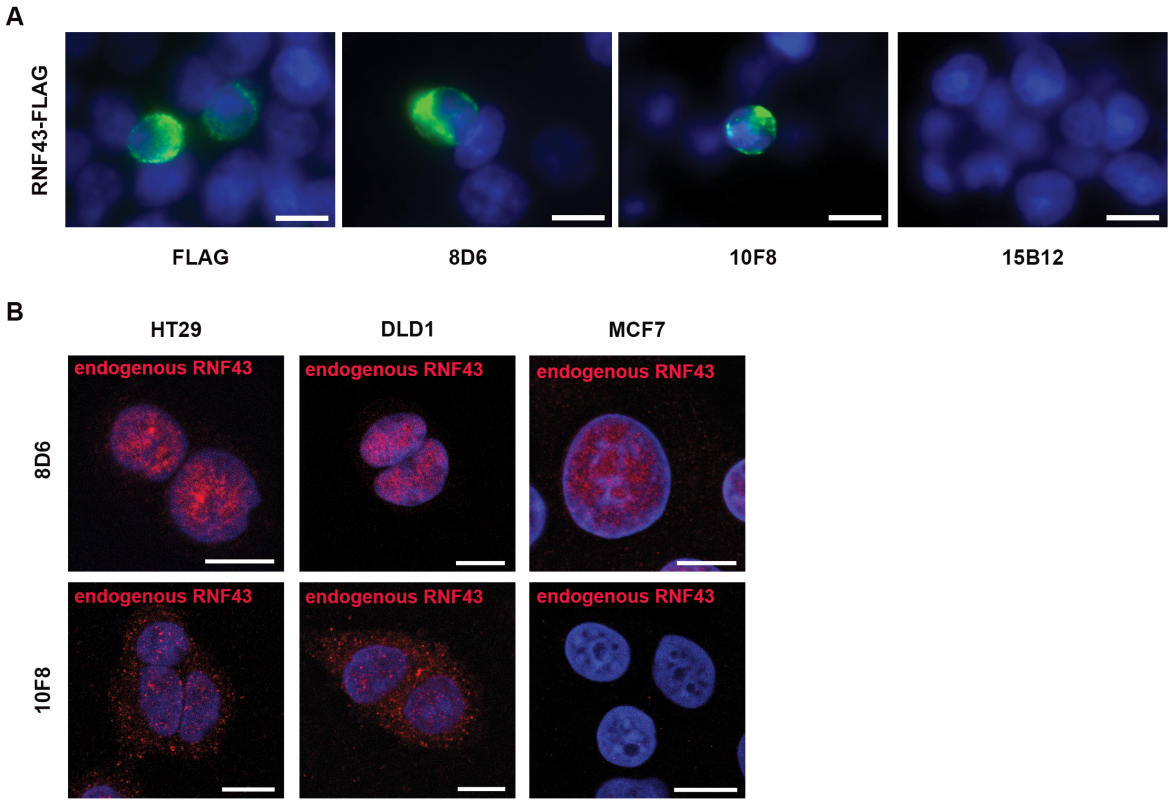

Figure 17: 8D6 detects endogenous RNF43 in the nuclear compartment.
(A) Immunofluorescence staining of HCT116 cells overexpressing RNF43-FLAG using the hybridoma supernatants 8D6, 10F8, and 15B12. Scale bars, 10 µm. (B) Confocal immunofluorescence imaging of endogenous RNF43 in HT29, DLD1, and MCF7 cells with 8D6 and 10F8. Scale bars, 10 µm

4.1.3 Purification of RNF43 antibodies

Since 8D6 and 10F8 supernatants recognized overexpressed as well as endogenous RNF43 in Western blot and immunofluorescence analysis, the antibodies of both supernatants were purified using high performance liquid chromatography (HPLC) (**Figure 18A**). Coomassie staining shows only specific bands for the heavy and light chains of the IgG proteins, showing that both antibodies were successfully purified (**Figure 18B**). To test the specificity of both purified antibodies, they were used to detect endogenous RNF43 in MCF7 cells transiently transfected with siRNA to knockdown RNF43. The 8D6 antibody detected almost no protein in lysates with knocked down RNF43, whereas the 10F8 showed comparable bands in sicontrol and siRNF43 lysates, suggesting that 10F8 detected a protein at the same molecular weight as RNF43 (Figure 17C). Taken together, these results identify the monoclonal antibody 8D6 as a specific antibody to detect endogenous RNF43.

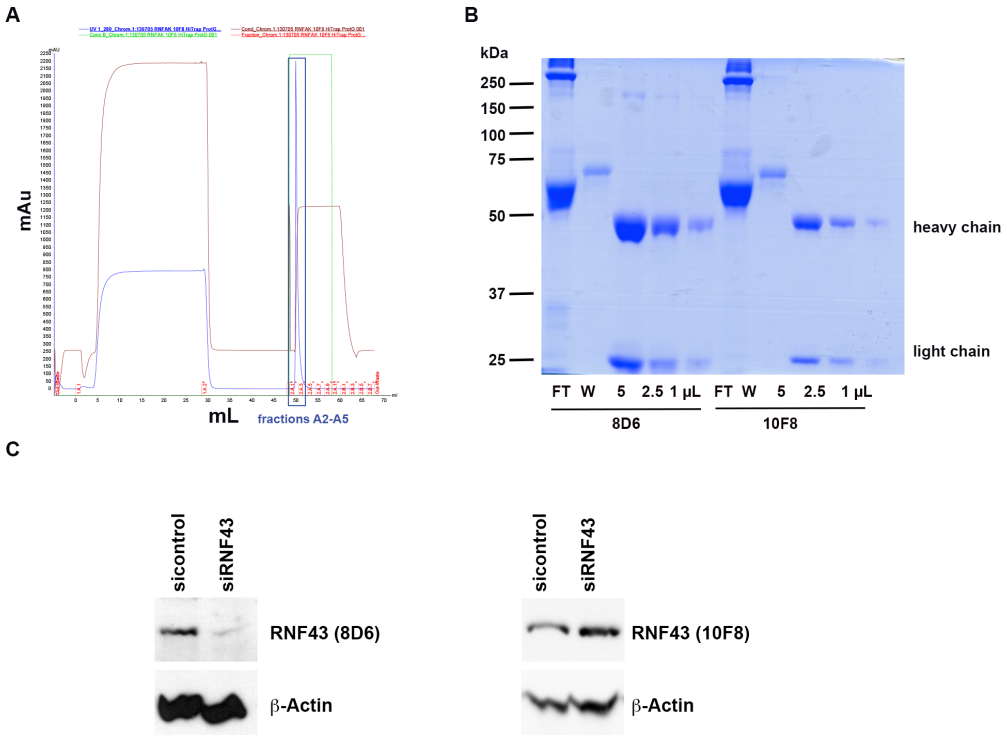

Figure 18: Monoclonal 8D6 antibody is specific for endogenous RNF43.
(A) HPLC purification of monoclonal 8D6 from hybridoma supernatant using HiTrap ProteinG column. (B) SDS-gel electrophoresis with Coomassie staining of flow-through (FT), wash (W), and pooled A2 – A5 fractions (5 µl, 2.5 µL, and 1 µL sample loading) after HPLC purification of 8D6 (left) and 10F8 (right). (C) Western blot analysis of purified 8D6 (left) and 10F8 (right) of MCF7 lysates after siRNA knockdown of RNF43.

4.1.4 Analysis of purified 8D6 for immunoprecipitation application

Only the purified 8D6 antibody specifically detected RNF43 by Western blot analysis. In a next step, 8D6 was tested for immunoprecipitation analysis. 8D6 precipitated overexpressed RNF43-HA (85 kDa) in MCF7 cells (**Figure 19**). In addition, a band of 95 kDa was detected, which could correspond to a splice variant.

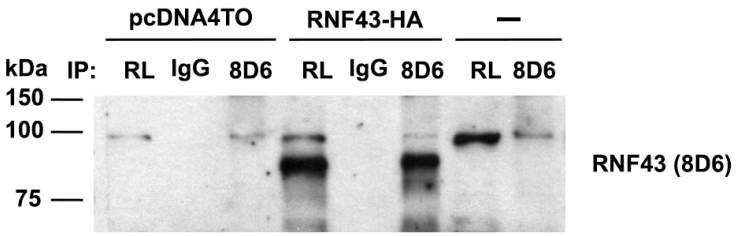

Figure 19: 8D6 precipitates overexpressed RNF43.
Western blot analysis of immunoprecipitated overexpressed empty vector pcDNA4TO, RNF43-HA, and endogenous RNF43 in MCF7 cells using the purified 8D6 antibody or immunoglobublin G (IgG) control. bar, not transfected; IP, immunoprecipitation, RL, raw lysate; kDa, kilo Dalton.

4.2 Subcellular expression of RNF43

4.2.1 Subcellular localization of RNF43 in cancer cells

One of the main aspects unclear about RNF43 was its subcellular localization. Some studies described a nuclear localization of RNF43[247,261,264], whereas other reports showed a cytoplasmic[248], cellular membrane or ER expression of RNF43[214,265]. To explore the expression and localization of RNF43, subcellular fractionation experiments were performed after overexpression of RNF43 and the mutant RNF43^{H292R}, having two point mutations H292R and H295R in the RING domain, in HCT116 cells. HCT116 cells were used because they express no endogenous RNF43. RNF43 was unambiguously detected in the nuclear fraction (**Figure 20A**). To exclude a mislocalization of the protein due to overexpression, subcellular fractionation was also performed in MCF7 cells, which express wild-type *RNF43* (**Figure 20B**). Also in these cells, the localization of endogenous RNF43 was detected in the nuclear fraction.

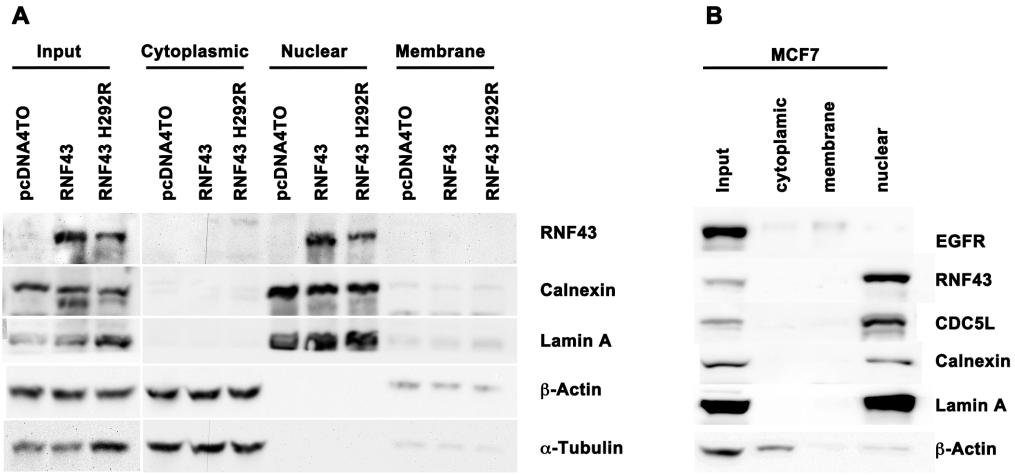

Figure 20: RNF43 is detected in nuclear fractions of human cancer cell lysates.
(A) Subcellular fractionation of HCT116 cells after transfection of overexpressed wild-type RNF43 or RNF43^{H292R}. (B) Subcellular fractionation of MCF7 cell lysates and detection of endogenous RNF43. EGFR, calnexin, lamin A, CDC5L, or β-actin and α-tubulin were used as markers for membrane fraction, ER, nuclear fraction, or cytoplasmic fraction, respectively. From Loregger and Grandl *et al*. The E3 ligase RNF43 inhibits Wnt signaling downstream of mutated β-catenin by sequestering TCF4 to the nuclear membrane. *Sci. Signal.* 8, ra90 (2015). Reprinted with permission from AAAS

For further analysis of the subcellular localization of RNF43 confocal immunofluorescence experiments were carried out. Staining of overexpressed FLAG- or HA-tagged RNF43 and RNF43^{H292R} in HCT116 and SW480 cells revealed a subcellular localization at the nuclear envelope and, partially in the nucleoplasm and endoplasmic reticulum (ER) (**Figure 21A**). Colocalization was observed with the marker for the inner nuclear membrane, lamin B

receptor, and the nuclear RNA binding protein polypyrimidine tract-binding protein-associated splicing factor (PSF). In addition, RNF43 was found to colocalize with calnexin, a marker for the endoplasmic reticulum) (**Figure 21B**). Together, these results show a nuclear localization of RNF43 in colon tumors and colorectal cancer cells, indicating that RNF43 might have diverse functions depending on its subcellular localization.

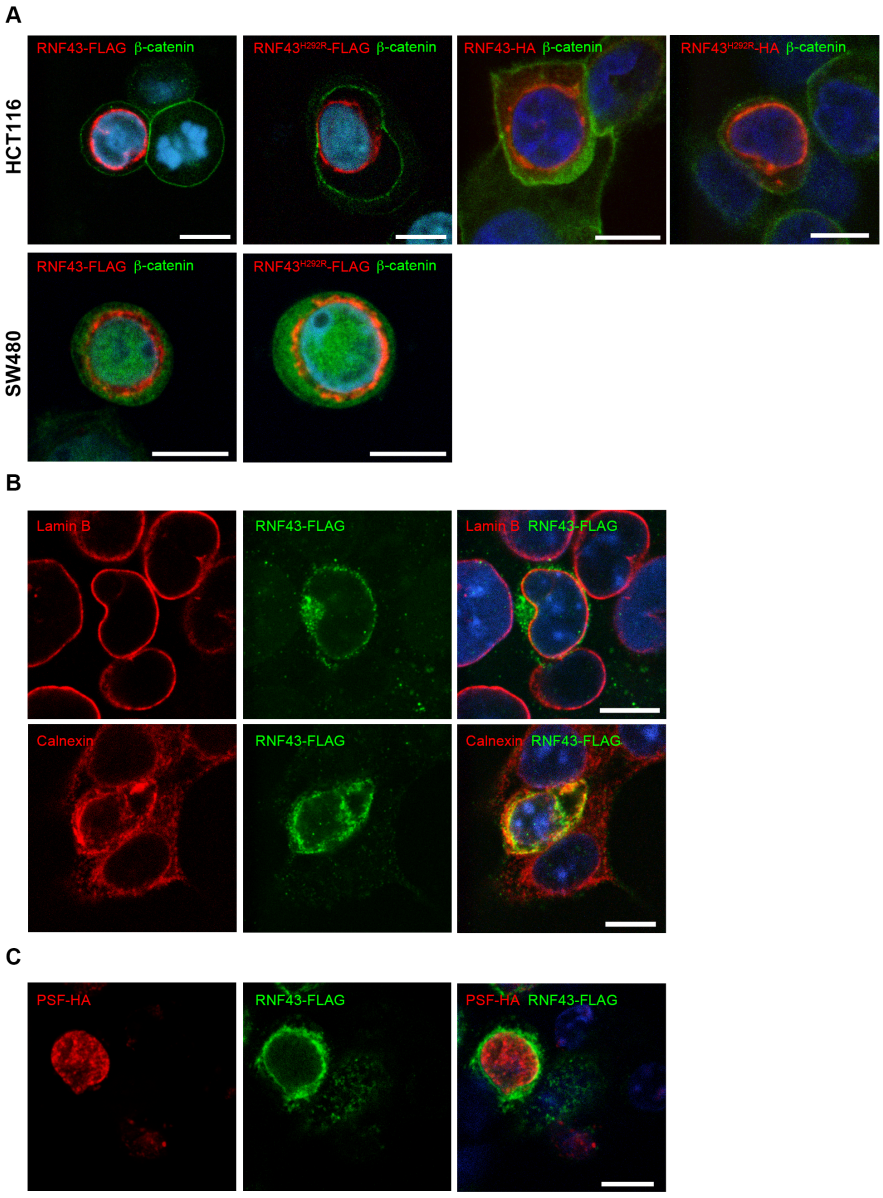

Figure 21: Overexpressed RNF43 is localized at the nuclear membrane in human cancer cells.
(A) Subcellular localization of overexpressed wild-type RNF43 or mutant RNF43^{H292R} (red) in HCT116 and SW480 cells detected by confocal immunofluorescence imaging. Scale bars, 10 μm. (B) RNF43 (green) colocalizes with lamin B receptor and calnexin at the nuclear envelope in HCT116 cells transiently transfected with RNF43. (C) RNF43 (green) colocalizes with PSF at the nuclear membrane in HCT116 cells transfected with RNF43-FLAG and PSF-HA constructs. Scale bar, 10 μm. From Loregger and Grandl *et al*. The E3 ligase RNF43 inhibits Wnt signaling downstream of mutated β-catenin by sequestering TCF4 to the nuclear membrane. *Sci. Signal.* 8, ra90 (2015). Reprinted with permission from AAAS

4.2.2 RNF43 protein expression in human intestinal tumors

In addition, immunohistochemical (IHC) staining was performed on human small intestine tissue and tumor samples using the only commercial anti-RNF43 antibody (Atlas Antibodies) suitable for IHC. A specific localization of endogenous RNF43 was detected in the nucleus of intestinal normal tissue and an increased abundance of RNF43 in the tumor samples (**Figure 22**), confirming the nuclear localization *in vivo*.

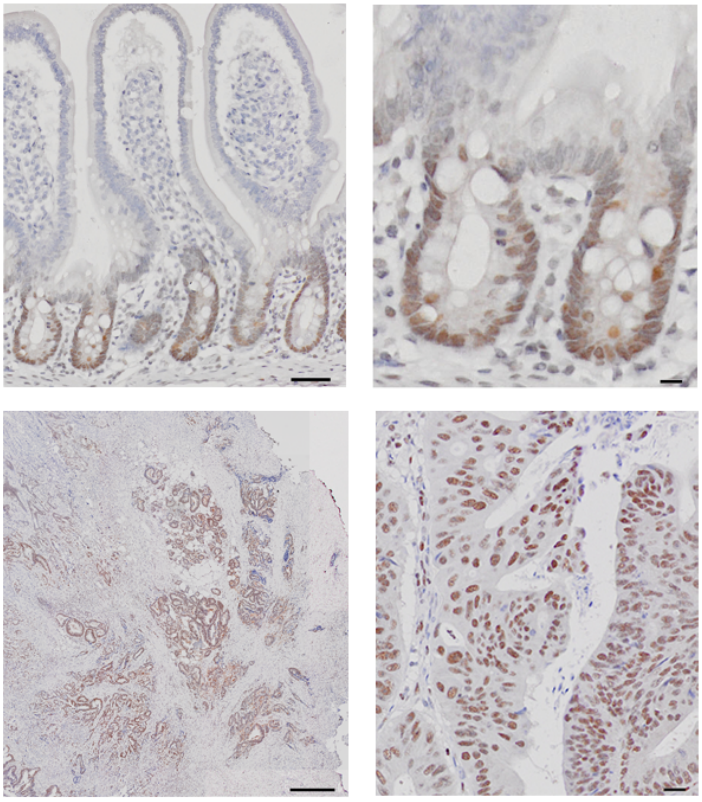

Figure 22: RNF43 is overexpressed in human colon tumors.
RNF43 detected by immunohistochemistry in human small intestine (top images) and human colon tumors (bottom images). Scale bars, 50 µm (left) and 20 µm (right). From Loregger and Grandl *et al*. The E3 ligase RNF43 inhibits Wnt signaling downstream of mutated β-catenin by sequestering TCF4 to the nuclear membrane. *Sci. Signal.* 8, ra90 (2015). Reprinted with permission from AAAS

4.3 Tissue distribution of Rnf43

After confirming that RNF43 is expressed in the nuclear compartment of human intestinal crypts and cancer cells, the distribution of Rnf43 was investigated in samples of murine embryonic tissue at E15 to E16 using *in-situ* hybridization. Murine *Rnf43* mRNA was detected in dermal papillas of hair follicle development, eye, lung, stomach and intestine[266] (**Figure 23A**). Moreover, the mRNA labeling of murine small intestine tissue of adult mice revealed a

restricted expression to few cells at the base of intestinal crypts, being stronger at the '+4 position', as well as in crypt base columnar cells (**Figure 23B**). In correlation to the increased RNF43 levels observed in human colon carcinomas, high levels of *Rnf43* mRNA were detected in aberrant foci and intestinal adenomas and tumors of APC^{min} mice (**Figure 23C**).

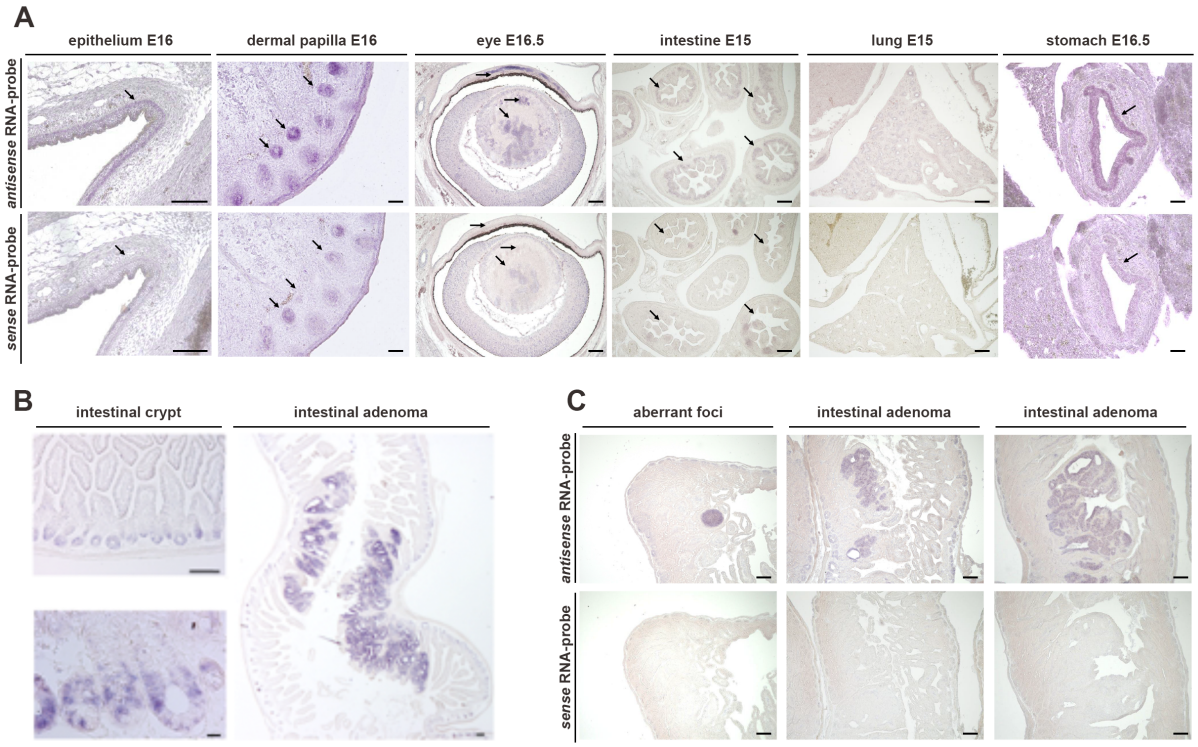

Figure 23: *Rnf43* mRNA is expressed during embryonic development and in the intestine of adult mice.
(A) *In-situ* hybridization of *Rnf43* in murine embryonic tissue of E15, E16 and E16.5. E, embryonic stage. (B) *Rnf 43* expression in murine small intestine and tumor of APCmin mice. (C) High expression of *Rnf43* in aberrant foci and adenomas of APCmin mice. Scale bars, 100 µm. From Loregger and Grandl *et al*. The E3 ligase RNF43 inhibits Wnt signaling downstream of mutated β-catenin by sequestering TCF4 to the nuclear membrane. *Sci. Signal.* 8, ra90 (2015). Reprinted with permission from AAAS.

4.4 Knockdown of RNF43 in cancer cell lines

4.4.1 Mutation status of *RNF43* in cancer cells

In order to investigate the function of endogenous RNF43, the *RNF43* gene was analyzed by next-generation sequencing (NGS) in the human colon cancer cell lines HT29, LS174T, DLD1, SW480, Caco2, HCT116, and breast cancer cell line MCF7 and the mutational status was determined. Wild-type *RNF43* was detected in HT29, Caco2 and MCF7 cells, whereas LS174T cells showed two point mutations (K108E and R389H). One point mutation was found in DLD1 cells at position L241M, and frameshift mutations were detected in HCT116 cells at position G144fs and in SW480 at position G469fs. (**Figure 24A**). Investigating the RNF43

mRNA expression in cancer cells revealed that HT29 and LS174T cells express high levels of mRNA, DLD1, SW480 and MCF7 showed intermediate levels and Caco2 and HCT116 only very low levels. (**Figure 24B**)

A

	Position	Change	Residue Change	AA change
HT29	-	-	-	wild-type
LS174T	322	A→G	K(Lys) → E(Glu)	K108E
	1166	G→A	R(Arg) → H(His)	R389H
DLD1	640	C→A	L(Leu) → M(Met)	L214M
SW480	-	-	-	wild-type
Caco2	-	-	-	wild-type
HCT116	349	C→-		G144fs
MCF7	-	-	-	wild-type

B

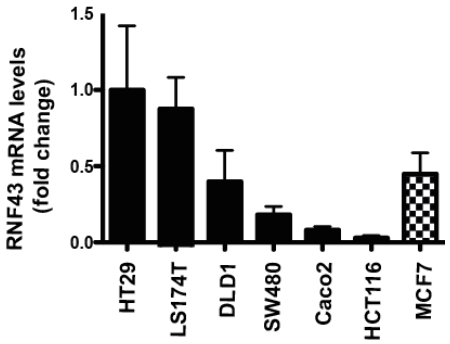

Figure 24: Human cancer cell lines express different levels of mutated and wild-type RNF43.
(A) RNF43 is mutated in different human cancer cell lines. (B) *RNF43* mRNA expression in human cancer cell lines (n=3).

4.4.2 Generation of human RNF43 knockdown cancer cells

To analyze the function of RNF43, the human cancer cell lines HT29, Caco2 and MCF7 were chosen as a wild-type model and LS174T as a mutant model for the lentiviral knockdown of endogenous *RNF43*. After cloning the shcontrol and shRNF43 sequence into the expression vector pLVTHM, lentiviral particles were produced in 293T cells as confirmed by strong green fluorescence protein (GFP) signal in the supernatant and nucleus of the cells (**Figure 25A**). The supernatant was used to transduce the cancer cell lines. The successful transduction was verified by the detection of the GFP signal in the nucleus of the cells. Moreover, no differences in cell morphology between shcontrol and shRNF43 treated cells were noticed (**Figure 25B**).

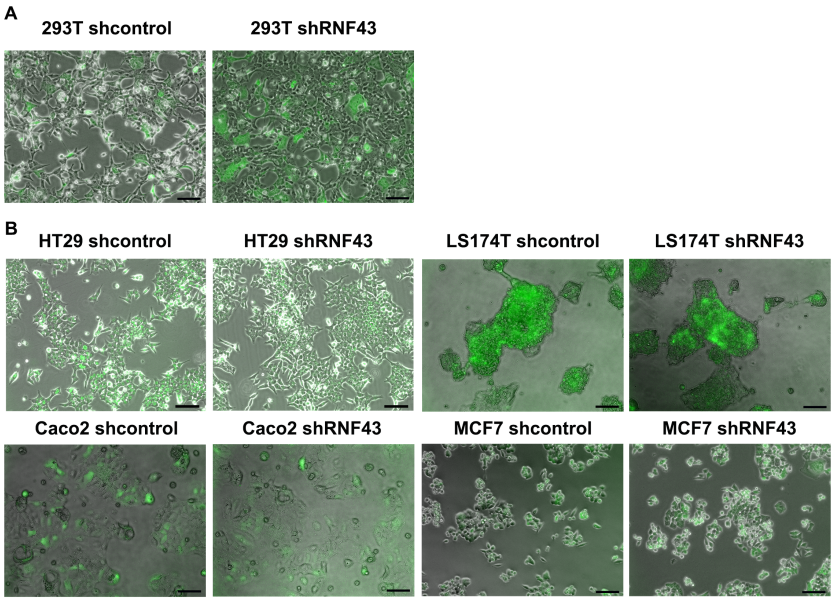

Figure 25: Lentiviral transduction of cancer cells.
Representative microphotographs of (A) 293T cells expressing viral RNF43 and control shRNA particles and (B) human cancer cell lines HT29, LS174T, Caco2, and MCF7 transduced with lentiviral shcontrol or shRNF43 supernatant. Scale bars, 50 µm.

4.4.3 Verification of successful knockdown of endogenous RNF43

To verify the knockdown of endogenous RNF43 in the lentivirally transduced cell lines quantitative real-time PCR (qRT-PCR) was performed. The analysis confirmed a knockdown in Caco2 cells by 92 % and in LS174T cells by 94 %, and an intermediate knockdown in HT29 (75 %) and MCF7 (58 %) cells (**Figure 26A**). The knockdown on protein level was corroborated using Western blot analysis (**Figure 26B**).

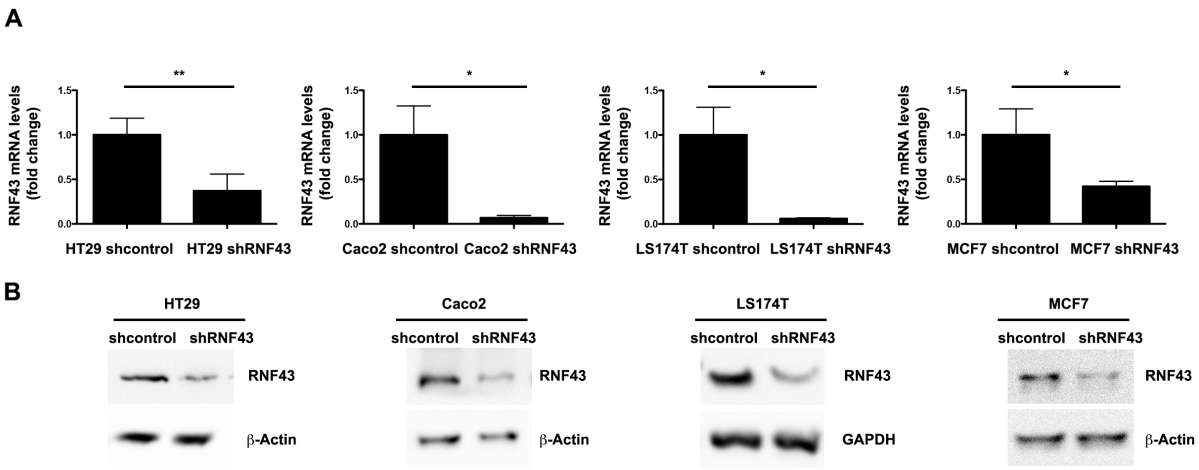

Figure 26: RNF43 expression is impaired in human RNF43 knockdown cancer cell lines.
(A) *RNF43* mRNA levels after shRNA knockdown in HT29, LS174T, Caco2 and MCF7 cancer cells (n=3).
(B) RNF43 protein levels detected with purified 8D6 of HT29, LS174T, Caco2 and MCF7 cancer cells of shcontrol or shRNF43 lysates.

To further confirm the knockdown of endogenous RNF43 in the cancer cell line HT29 immunocytochemistry was performed, using the commercially available RNF43 antibody (HPA008079; Atlas Stockholm, Sweden). In correlation to the Western blot analysis, all RNF43 knockdown cells showed strongly reduced RNF43 protein levels compared to the shcontrol cells (**Figure 27**).

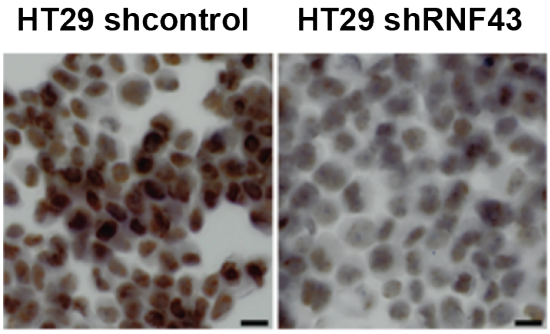

Figure 27: Less RNF43 is expressed in human cancer cell lines after lentiviral RNF43 knockdown.
RNF43 protein expression detected by immunocytochemistry in HT29 cells transduced with either control or RNF43 shRNA. Scale bars, 10 µm. From Loregger and Grandl *et al*. The E3 ligase RNF43 inhibits Wnt signaling downstream of mutated β-catenin by sequestering TCF4 to the nuclear membrane. *Sci. Signal.* **8**, ra90 (2015). Reprinted with permission from AAAS.

Similar results were obtained when endogenous RNF43 was analyzed by confocal immunofluorescence in these cell lines. Endogenous RNF43 was detected in shcontrol cells of HT29, Caco2, and MCF7, whereas a clear reduction of the protein was noted in the corresponding RNF43 knockdown cells. In LS174T shcontrol cells the mutated endogenous $RNF43^{K108E,\ R389H}$ was detected in the nucleus and cytoplasm. After lentiviral treatment, most of the cytoplasmic RNF43 was deleted, whereas nuclear RNF43 expression was still detected, although to a lesser extent (**Figure 28A**). To exclude staining artifacts due to the lentiviral treatment, non-transduced cells were analyzed. Endogenous RNF43 was detected similarly to the shcontrol treated cells (**Figure 28B**). Together, these results confirmed a successful knockdown of endogenous RNF43 in human cancer cells and were used for further experiments.

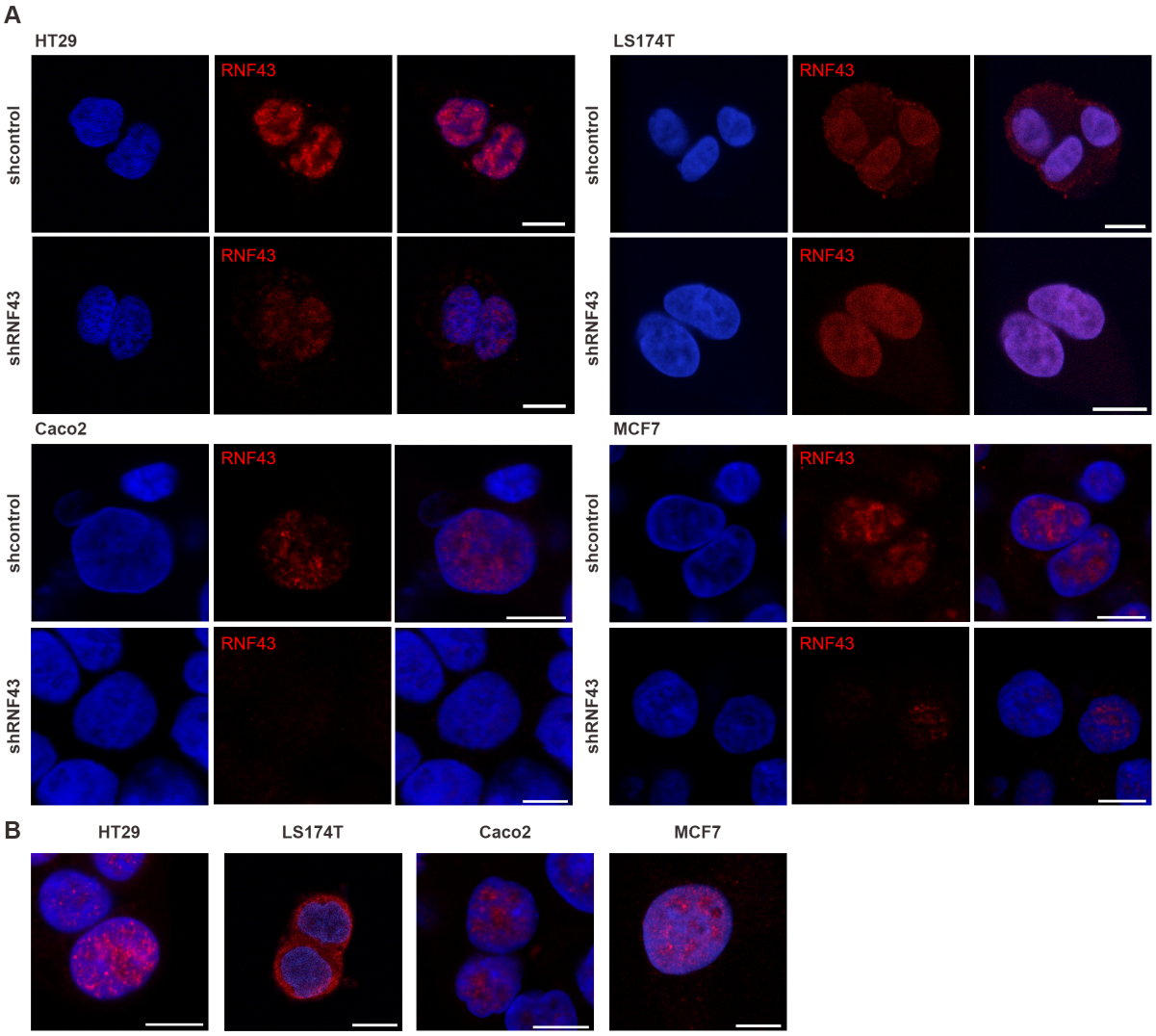

Figure 28: Endogenous wild-type RNF43 is localized at the nuclear compartment of human cancer cells.
(A) Confocal immunofluorescence imaging of endogenous RNF43 in HT29, LS174T, Caco2, and MCF7 cells after lentiviral transduction with shRNA. (B) Endogenous RNF43 in HT29, LS174T, Caco2, and MCF7 cells without any treatment. Scale bars, 10 µm.

4.5 Functional analysis of RNF43

4.5.1 RNF43 regulates Wnt signaling

It was shown that *RNF43* is a direct target gene of the Wnt signaling pathway[267], and an inhibitor of the Wnt signaling pathway[214,265]. To confirm the Wnt inhibitory function of RNF43 and further explore the underlying mechanisms TOPFlash luciferase reporter assays were performed. Therefore, HEK293 cells, which are devoid of constitutive Wnt signaling, were stimulated with WNT3A. In line with the literature, overexpressed RNF43 significantly decreased WNT3A-induced TCF/LEF transcriptional activity in a dose-depended manner. In contrast, introduction of the two point mutations H292R and H295R in the RING domain

(RNF43^{H292R}) enhanced Wnt signaling activity (**Figure 29A**). Depletion of the RING domain (RNF43$^{\Delta RING}$) abolished the inhibitory effect of RNF43 (**Figure 29B**), indicating that the functional wild-type RING domain in RNF43 is crucial for its inhibitory effect on the Wnt signaling pathway.

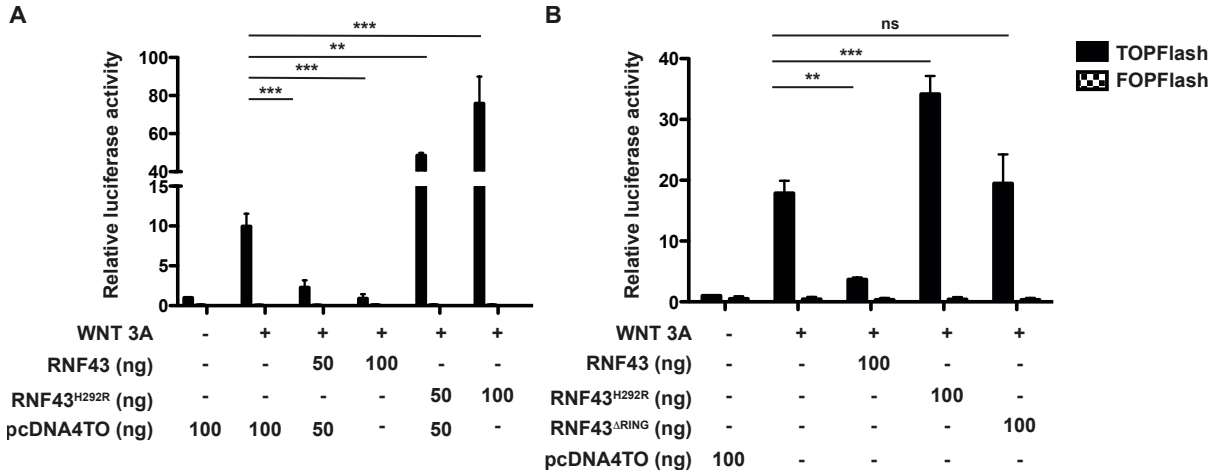

Figure 29: RNF43 inhibits WNT3A induced Wnt signaling.
(A) Dose-depended TCF/LEF transcriptional activity in presence of wild-type RNF43 or RING domain point mutant RNF43^{H292R} after WNT3A stimulation in HEK293 cells (n=3). (B) TCF/LEF transcriptional activity of transiently transfected wild-type RNF43, RNF43^{H292R} or RING domain lacking mutant RNF43 $^{\Delta RING}$ after WNT3A stimulation in HEK293 cells (n=3). *P <0.05, **P≤0.01, ***P<0.0005, ANOVA with Dunnett's multiple comparison posttest. From Loregger and Grandl *et al*. The E3 ligase RNF43 inhibits Wnt signaling downstream of mutated β-catenin by sequestering TCF4 to the nuclear membrane. *Sci. Signal.* **8**, ra90 (2015). Reprinted with permission from AAAS.

To decipher the endogenous function of RNF43 in the Wnt signaling pathway, TCF/LEF transcriptional activity was investigated in absence of RNF43. Therefore, the luciferase activity was measured in the HT29, Caco2, LS174T, and MCF7 RNF43 knockdown cells, which were generated by lentiviral treatment as mentioned before. Significantly increased TCF/LEF transcriptional activity in cells with knocked down wild-type RNF43 and no change in Wnt activity in mutant shRNF43$^{K108E,\ R389H}$ cells were measured (**Figure 30A**). In addition, transient knockdown of wild-type RNF43 in HT29 by siRNA transfection resulted also in an enhanced TCF/LEF transcriptional activity (**Figure 30B**), confirming that wild-type RNF43 is an inhibitor of Wnt signaling under overexpression and endogenous conditions.

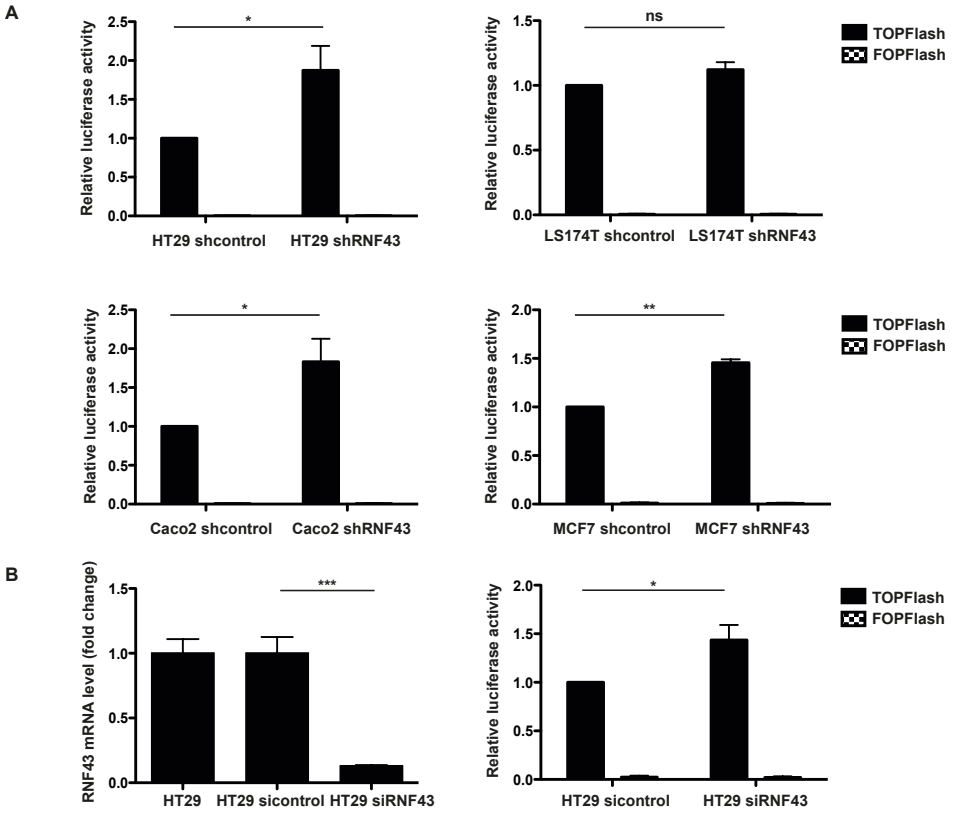

Figure 30: RNF43 knockdown activates Wnt signaling in human cancer cells.
(A) TCF/LEF transcriptional activity in absence of endogenous RNF43 in human cancer cell lines (n=4). (B) *RNF43* mRNA levels after knockdown of RNF43 by siRNA transfection (n=3) (left) and TCF/LEF transcriptional activity after siRNA knockdown in HT29 cells (n=3) (right). *P <0.05, **P≤0.01, ***P<0.0005, Student's *t*-test was performed. From Loregger and Grandl *et al*. The E3 ligase RNF43 inhibits Wnt signaling downstream of mutated β-catenin by sequestering TCF4 to the nuclear membrane. *Sci. Signal.* **8**, ra90 (2015). Reprinted with permission from AAAS.

4.5.2 RNF43 inhibits Wnt signaling downstream of β-catenin

Different studies claimed that RNF43 inhibits Wnt signaling by reducing Fzd receptor abundance at the plasma membrane, showing that overexpressed RNF43 is localized at the cellular membrane[214,265], which is in contrast to the nuclear localization detected in this study. This suggested that the Wnt inhibitory mechanism of RNF43 depends on its subcellular localization. Thus, it was analyzed at which level of the cascade overexpressed RNF43 inhibits Wnt signaling. For this, WNT3A-stimulated HEK293 cells were transfected with different constitutive active proteins of the Wnt signaling pathway, Dvl, dominant-negative (dn) Axin2, dn-β-TrCP, and S33Y-β-catenin, and TCF/LEF transcriptional activity was measured. RNF43 was able to suppress TCF4 activity induced by all constitutive active molecules analyzed (**Figure 31A**). Interestingly, RNF43 inhibited also Wnt activity induced by non-phosphorylated S33Y-β-catenin. This is remarkable since many mutations at position S33 in

β-catenin are frequently found to prevent phosphorylation of β-catenin resulting in activated Wnt signaling in colon tumor patients[65,93]. These findings indicate that RNF43 acts downstream or at the level of β-catenin. In order to validate this observation, RNF43 was investigated in HCT116 and DLD1 colon cancer cell lines since both cell lines have a constitutive active Wnt signaling due to activating mutations in *CTNNB1* (β-catenin) and *APC,* respectively. Overexpression of RNF43 in these cell lines caused also an inhibitory effect on the Wnt signaling pathway, whereas overexpression of the RING mutant RNF43^{H292R} enhanced the signaling in a dominant-negative manner, although both effects were not as strong as in HEK 293 cells (**Figure 31B**).

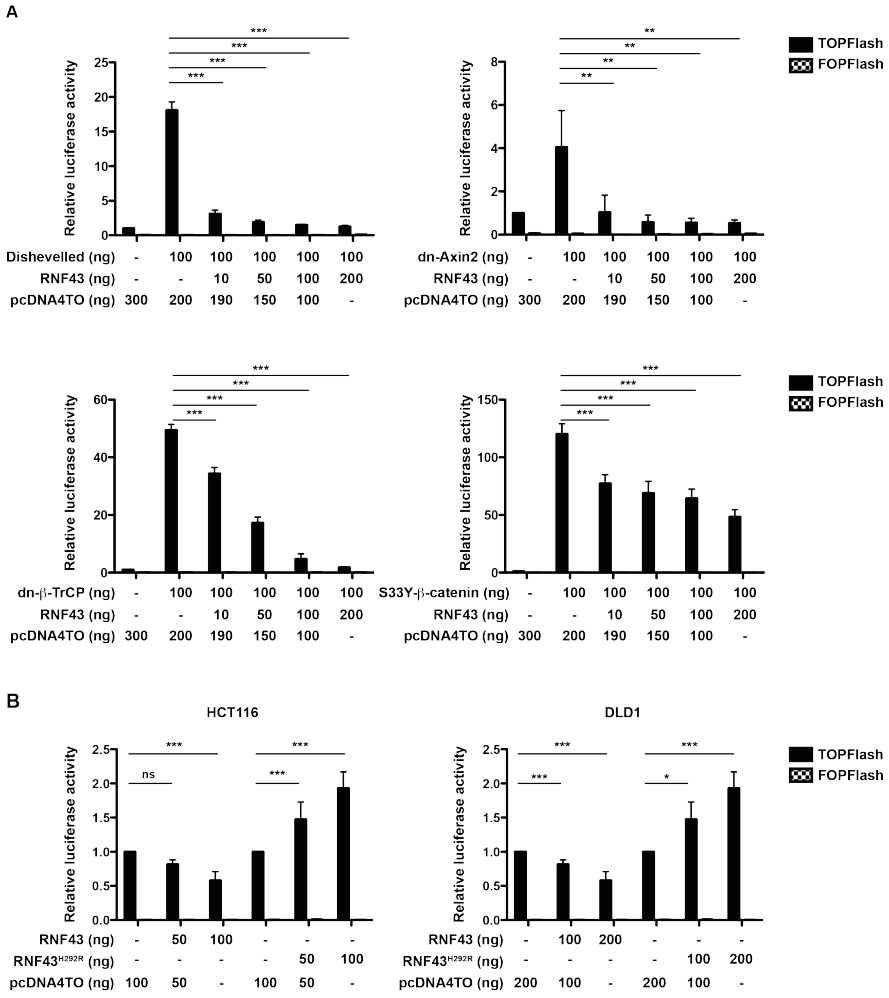

Figure 31: RNF43 inhibits Wnt signaling downstream of β–catenin.

(A) TCF/LEF transcriptional activity induced by constitutive active Dishevelled, dn-Axin2, β-TrCP, and stabilized β-Catenin (S^{33}-β-catenin) after RNF43 overexpression in HEK293 cells (n=3). (B) TCF/LEF transcriptional activity in colon cancer cell lines harboring mutations in β-catenin (HCT116) or APC (DLD-1) after overexpression of wild-type or RNF43^{H292R} RING domain mutant (n=3). *P <0.05, **P≤0.01, ***P<0.0005, ANOVA with Dunnett's multiple comparison posttest was performed. From Loregger and Grandl *et al*. The E3 ligase RNF43 inhibits Wnt signaling downstream of mutated β-catenin by sequestering TCF4 to the nuclear membrane. *Sci. Signal.* 8, ra90 (2015). Reprinted with permission from AAAS

To exclude that the dominant-negative effect of RNF43^{H292R} derives from increased autocrine Wnt signaling luciferase reporter assays were performed in presence of the porcupine inhibitor LGK974. LGK974 did not change the observed activation of RNF43^{H292R} on TCF/LEF transcriptional activity (**Figure 32**). Together these data strongly suggest that RNF43 acts at the level or downstream of β-catenin.

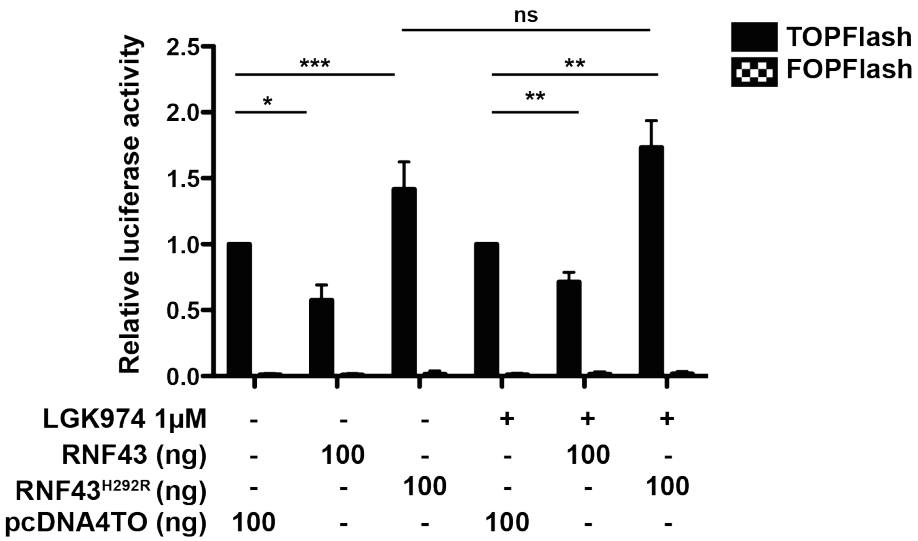

Figure 32: Porcupine inhibitor LGK974 does not influence RNF43 mediated effect on Wnt signaling.
TCF luciferase reporter assay after expression of RNF43 wild-type or mutant RNF43^{H292R} in the presence of the porcupine inhibitor LGK974 (n=4). *P<0.05, **P≤0.01, ***P<0.0005, ANOVA with Dunnett's multiple comparison posttest.

4.5.3. RNF43 does not mark β-catenin for degradation

RNF43 is an E3 ubiquitin ligase. Moreover, it has been shown that wild-type RNF43 exhibited autoubiquitination activity[268]. To identify a possible mechanism by which RNF43 regulates Wnt activity, experiments were carried out to test whether RNF43 is able to ubiquitinate β-catenin for proteasomal degradation. Thus, the protein abundance of endogenous β-catenin was analyzed, but found to be unchanged by overexpressing RNF43 or RNF43^{H292R} in HCT116 cells (**Figure 33A**). In addition, coimmunoprecipitation analysis did not show a direct interaction between RNF43 and β-catenin (**Figure 33B**), indicating that β-catenin is not a substrate of RNF43.

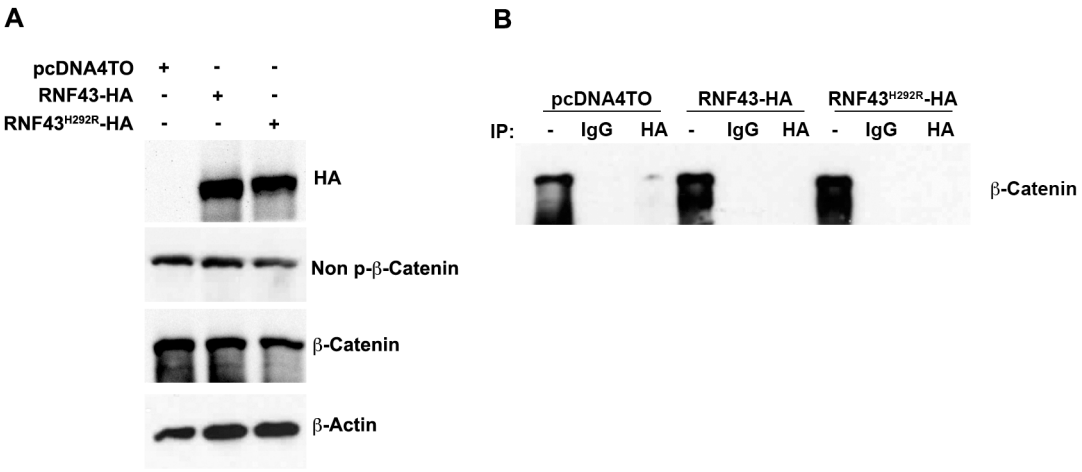

Figure 33: RNF43 does not interact with β-catenin

(A) Effect of ectopic expression of empty vector pcDNA4TO, wild-type RNF43 and mutant RNF43^{H292R} on β-catenin protein abundance in HCT116 cells. (B) Immunoprecipitation (IP) of empty vector pcDNA4TO, RNF43-HA or mutant RNF43^{H292R}–HA with β-catenin or IgG control analyzed by Western blot. From Loregger and Grandl *et al*. The E3 ligase RNF43 inhibits Wnt signaling downstream of mutated β-catenin by sequestering TCF4 to the nuclear membrane. *Sci. Signal.* **8**, ra90 (2015). Reprinted with permission from AAAS.

4.5.4 RNF43 interacts with TCF4

Next, a possible degradation of TCF4 in presence of RNF43 was investigated since TCF4 is the next protein downstream of β-catenin in signaling cascade. Again, the protein abundance did not change upon overexpression of RNF43 or RNF43^{H292R} (**Figure 34A**), suggesting that it is not marked for degradation by RNF43. Interestingly, a robust interaction between overexpressed wild-type RNF43 and endogenous TCF4 in HCT116 cells was found by coimmunoprecipitation. In contrast, only a weak interaction was observed between RNF43^{H292R} and TCF4 (**Figure 34B**). Taken together, these results imply that RNF43 does not regulate Wnt signaling by marking TCF4 for degradation, but rather by interaction with TCF4.

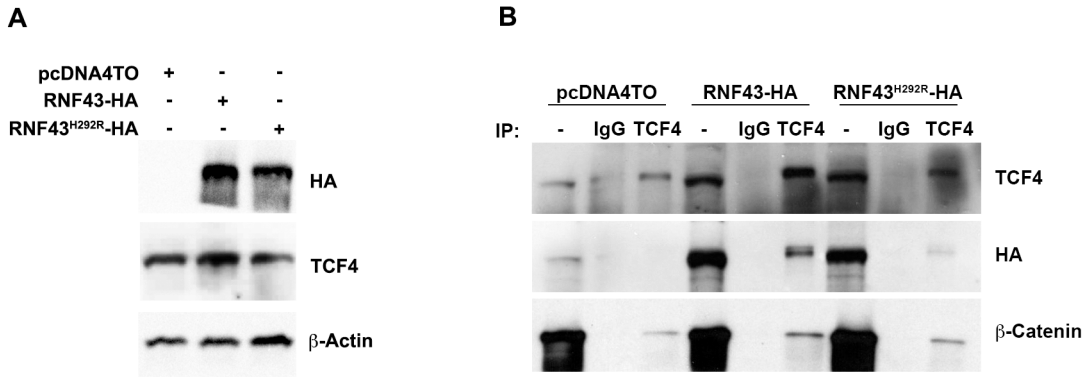

Figure 34: RNF43 interacts with TCF4.
(A) TCF4 protein levels after transient transfection of empty vector pcDNA4TO, RNF43 or mutant RNF43^{H292R}. (B) Immunoprecipitation (IP) of TCF4 or IgG control from HCT116 cells transfected with empty vector pcDNA4TO, HA-tagged wild-type or mutant RNF43^{H292R}, followed by Western blotting. From Loregger and Grandl *et al*. The E3 ligase RNF43 inhibits Wnt signaling downstream of mutated β-catenin by sequestering TCF4 to the nuclear membrane. *Sci. Signal.* **8**, ra90 (2015). Reprinted with permission from AAAS.

4.5.5 RNF43 sequesters TCF4 to the nuclear envelope.

To further explore the interaction between TCF4 and RNF43, coimmunofluorescence staining of RNF43 or RNF43^{H292R} and TCF4 was performed. It is known that TCF4 localizes to the chromatin in a punctate pattern within the nucleus under endogenous conditions[269,270]. Interestingly, overexpression of RNF43 in HCT116 provoked a pronounced relocalization of TCF4 from the nucleoplasm towards the nuclear envelope. There, it colocalized with RNF43. Contrary to this observation, overexpression of RNF43^{H292R} did not change the subcellular localization of TCF4 (**Figure 35A**). To strengthen these results, localization experiments were performed with endogenous RNF43. To analyze whether loss of RNF43 leads to a change in the TCF4 localization, lentiviral transduced HT29 cells were used. Indeed, HT29 shcontrol cells expressing endogenous wild-type RNF43 showed a similar perinuclear pattern of TCF4, although it was not as pronounced as in the overexpressed situation. In RNF43 knocked down HT29 cells, this expression pattern was lost (**Figure 35B**). These results suggest a mechanism by which RNF43 mediates TCF4 activity repression through sequestering the TCF/LEF transcription complex towards the nuclear periphery.

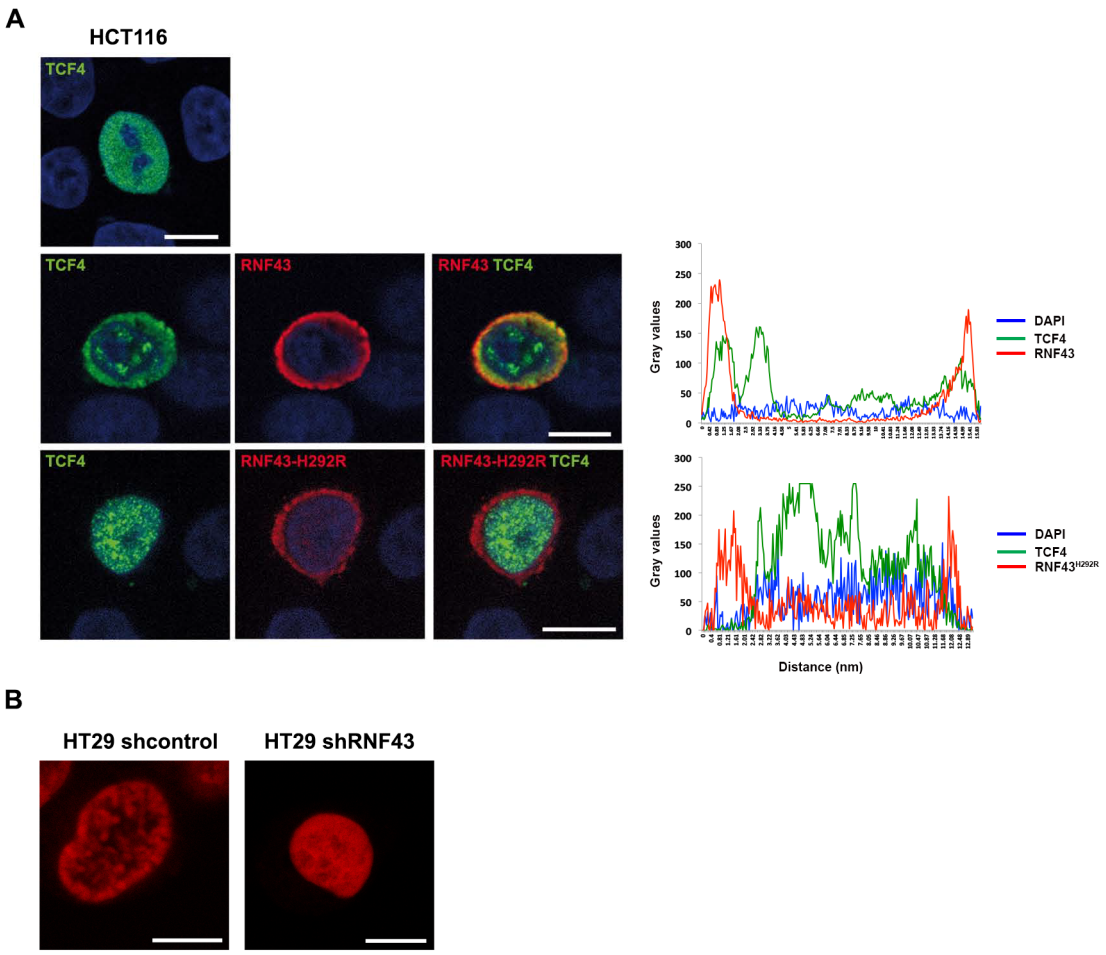

Figure 35: RNF43 binds TCF4 at the nuclear membrane.
(A) Confocal immunofluorescence of TCF4 in HCT116 cells transfected with wild-type or mutant RNF43. Scale bars, 10 µm. Graphs show signal intensities across the transverse axis of the cell. (B) Confocal immunofluorescence of TCF4 in HT29 shcontrol and shRNF43 cells. Scale bars, 10 µm. From Loregger and Grandl *et al*. The E3 ligase RNF43 inhibits Wnt signaling downstream of mutated β-catenin by sequestering TCF4 to the nuclear membrane. *Sci. Signal.* **8**, ra90 (2015). Reprinted with permission from AAAS.

To confirm this hypothesis and to analyze whether the TCF4 transcription complex is disrupted when it is directed toward the nuclear rim, coimmunoprecipitation of C-terminal binding protein 1 (CtBP1) and TCF4 in RNF43 overexpressing HCT116 cells were performed. CtBP1 is a well-known corepressor of the TCF/LEF transcriptional complex[271], where it interacts physically with TCF4. Western blot analysis of the co immunoprecipitation revealed a direct interaction of TCF4 and CtBP1, indicating an intact but silenced transcription complex (**Figure 36**).

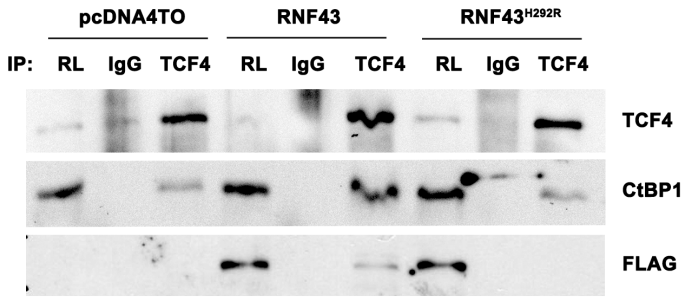

Figure 36: RNF43 does not disrupt TCF/LEF transcription complex.
Immunoprecipitation (IP) of IgG control or TCF4 in HCT116 cells transfected with empty vector pcDNA4TO, FLAG-tagged wild-type or mutant RNF43^{H292R}, followed by Western blot analysis. RL, raw cell lysate. From Loregger and Grandl *et al*. The E3 ligase RNF43 inhibits Wnt signaling downstream of mutated β-catenin by sequestering TCF4 to the nuclear membrane. *Sci. Signal.* 8, ra90 (2015). Reprinted with permission from AAAS

4.5.6 RNF43 binds with its C-terminal region to TCF4

In order to analyze the interaction between RNF43 and TCF4 in more detail, different N-terminally truncated RNF43 mutants were analyzed, showing that they still interacted with TCF4^{268}. This suggests that a region between the RING domain and the C terminus is important for the interaction of RNF43 with TCF4. Therefore, C-terminally truncated RNF43 mutants (ΔC-mutants) were generated, that are RNF43^{S321X}, RNF43^{G447X}, RNF43^{G566X}, and RNF43^{E713X} (**Figure 37**).

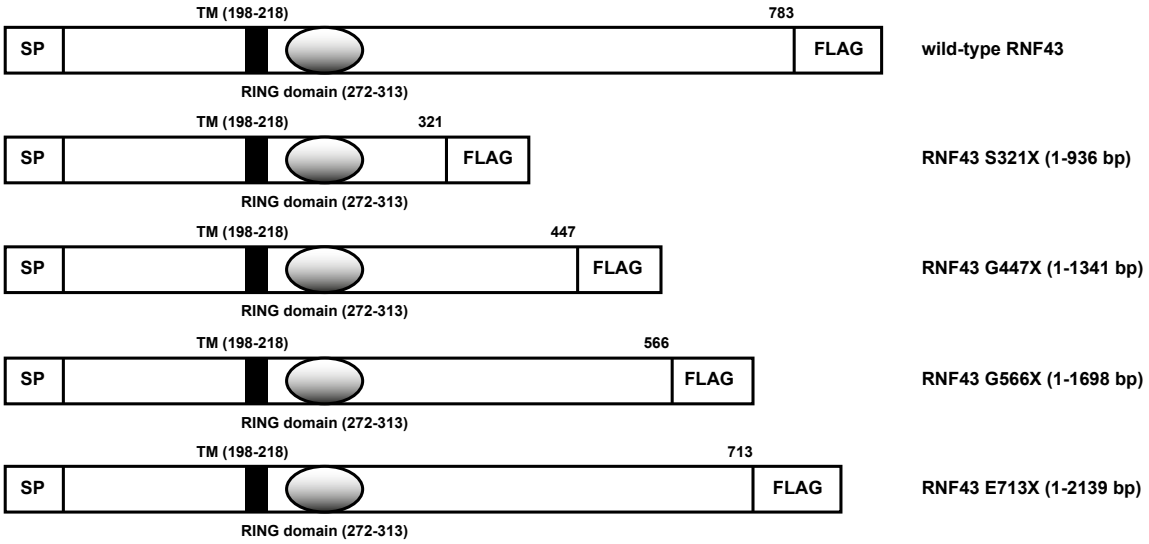

Figure 37: Schematic representation of C-terminally truncated RNF43 constructs.
SP, signal peptide; TM, putative transmembrane domain; bp, base pair; FLAG, Flag-tag; numbers indicate amino acid position

Western blot analysis confirmed the expression of the constructs after cell transfection, except RNF43^{S321X} that was not detected (**Figure 38A**). Analysis of the ΔC-mutants for TCF/LEF transcriptional activity showed an inhibitory capacity of the constructs G566X and E713x, but not of G447X (**Figure 38B**). Interestingly, coimmunoprecipitation analysis detected no interaction between RNF43^{G447X} and TCF4, whereas RNF43^{G566X} and RNF43^{E713X} still bound to TCF4, indicating that the C terminal region from amino acid 566 to 783 is not involved in binding to TCF4 (**Figure 38C**). In addition, immunofluorescence staining of the ΔC-mutants revealed a localization of the mutants RNF43^{G566X} and RNF43^{E713X} at the nuclear membrane and to a lesser extent in the nucleus, whereas RNF43^{G447X} were detected in the cytoplasm upon overexpression in HCT116 cells. Surprisingly, RNF43^{S321X} could be observed in the cell cytoplasm, although no protein was detected by Western blot analyses (**Figure 38D**). These results pinpoint the interaction of RNF43 and TCF4 between RING domain and N-terminal of amino acid 566.

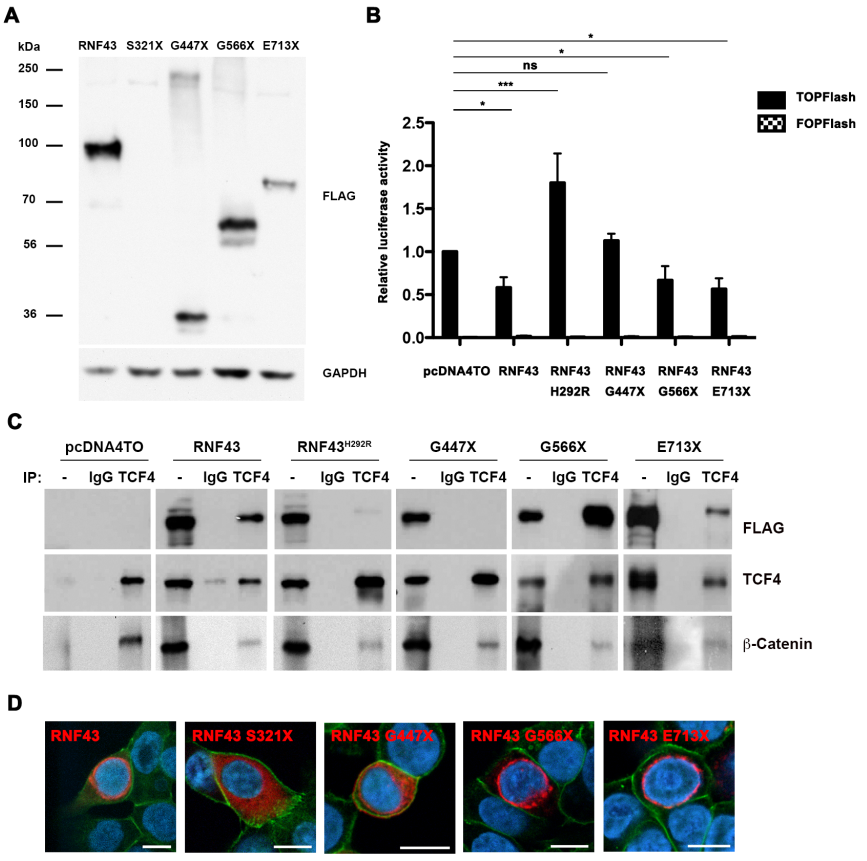

Figure 38: C-terminally truncated RNF43 construct, G447X, abolishes Wnt-inhibitory effect of RNF43.
(A) Expression of C-terminally truncated RNF43 constructs S321X, G447X, G556X, and E713X in HCT116 cells after transient transfection. (B) TCF/LEF transcriptional activity of ΔC-mutants. *P<0.05, **P≤0.01, ***P<0.0005, ANOVA with Dunnett's multiple comparison posttest. (C) Immunoprecipitation (IP) of TCF4 from HCT116 cells transfected with FLAG-tagged C-terminally truncated RNF43 constructs. (D) Subcellular localization of ΔC-mutants (red) and β-catenin (green) in HCT116 cells. Scale bars, 10 μm

4.5.7 RNF43-mediated TCF4 repression reduces Wnt target gene expression

Well-known target genes which are expressed by activated Wnt signaling are Axin2[272], Twist[273], matrix metalloproteinase-7 (MMP7)[274], and LGR5[205]. To corroborate whether the impaired TCF/LEF transcriptional activity leads to changes in transcription of Wnt target genes, mRNA expression of Axin2, Twist, MMP7, and LGR5 were analyzed. A clearly reduced mRNA expression of Axin2 and Twist, and to a lesser extent of MMP7 and LGR5, was detected in RNF43 overexpressing HCT116 cells (**Figure 39A**) while mRNA expression analysis of Wnt target genes in RNF43 depleted HT29 an MCF7 cells showed an enhanced transcription of Axin2 (**Figure 39B**). Together, these data show that the inhibitory effect of RNF43 on TCF/LEF transcriptional activity regulates Wnt target gene expression.

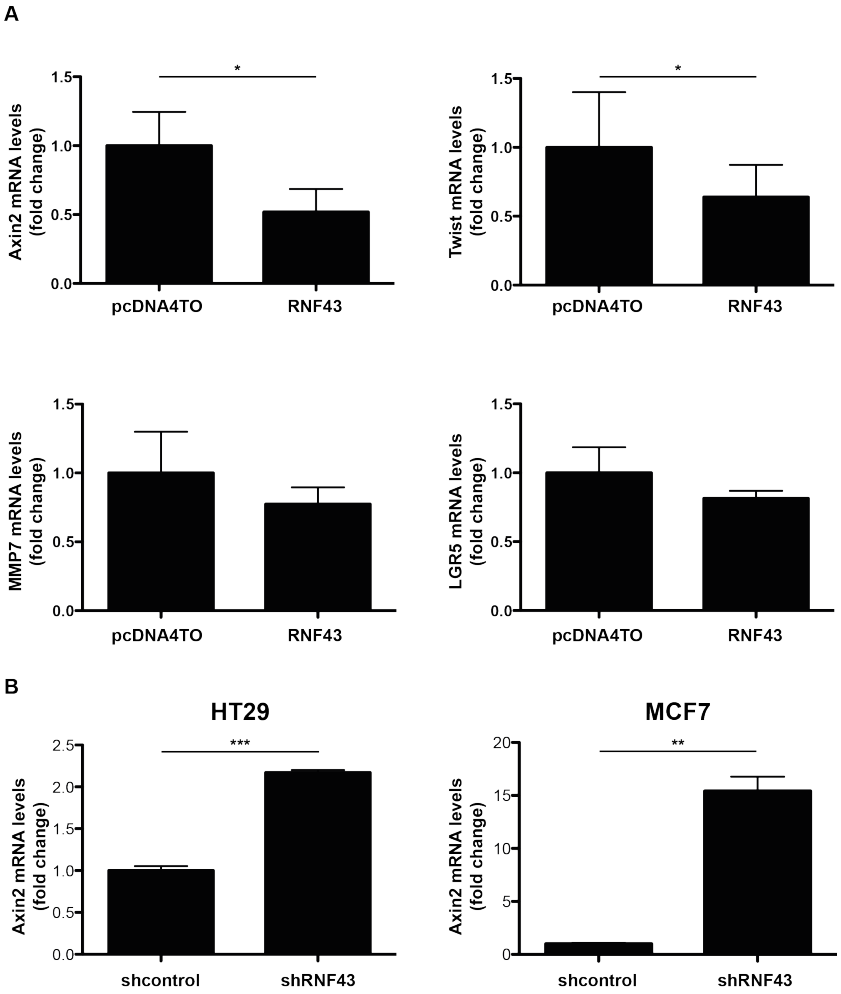

Figure 39: RNF43 inhibits expression of Wnt target genes.
(A) Expression of Wnt target genes Axin2, Twist, MMP7, and LGR5 detected by qPCR after RNF43 overexpression in HCT116 cells (n=3). (B) Quantitative real-time PCR of Axin2 mRNA after knockdown of RNF43 in HT29 and MCF7. *P < 0.05, **P≤0.01, ***P<0.0005, Student's t test. From Loregger and Grandl *et al*. The E3 ligase RNF43 inhibits Wnt signaling downstream of mutated β-catenin by sequestering TCF4 to the nuclear membrane. *Sci. Signal.* 8, ra90 (2015). Reprinted with permission from AAAS

4.5.8 RNF43 activity requires nuclear localization

In silico analysis (PSORTII[275]) of the *RNF43* sequence predicted two putative nuclear localization sites (NLS) at the 3'-prime end. Inhibition of TCF/LEF transcriptional activity by sequestering TCF4 to the nuclear envelope suggested that the subcellular localization of RNF43 is important for its function. To test this, RNF43 mutants of wild-type (**Figure 40A**) or mutated RING domain (**Figure 40B**) were generated with either single (RNF43^{R437A} or RNF43^{K655A}) or double mutated (RNF43$^{R437A, K655A}$) NLS.

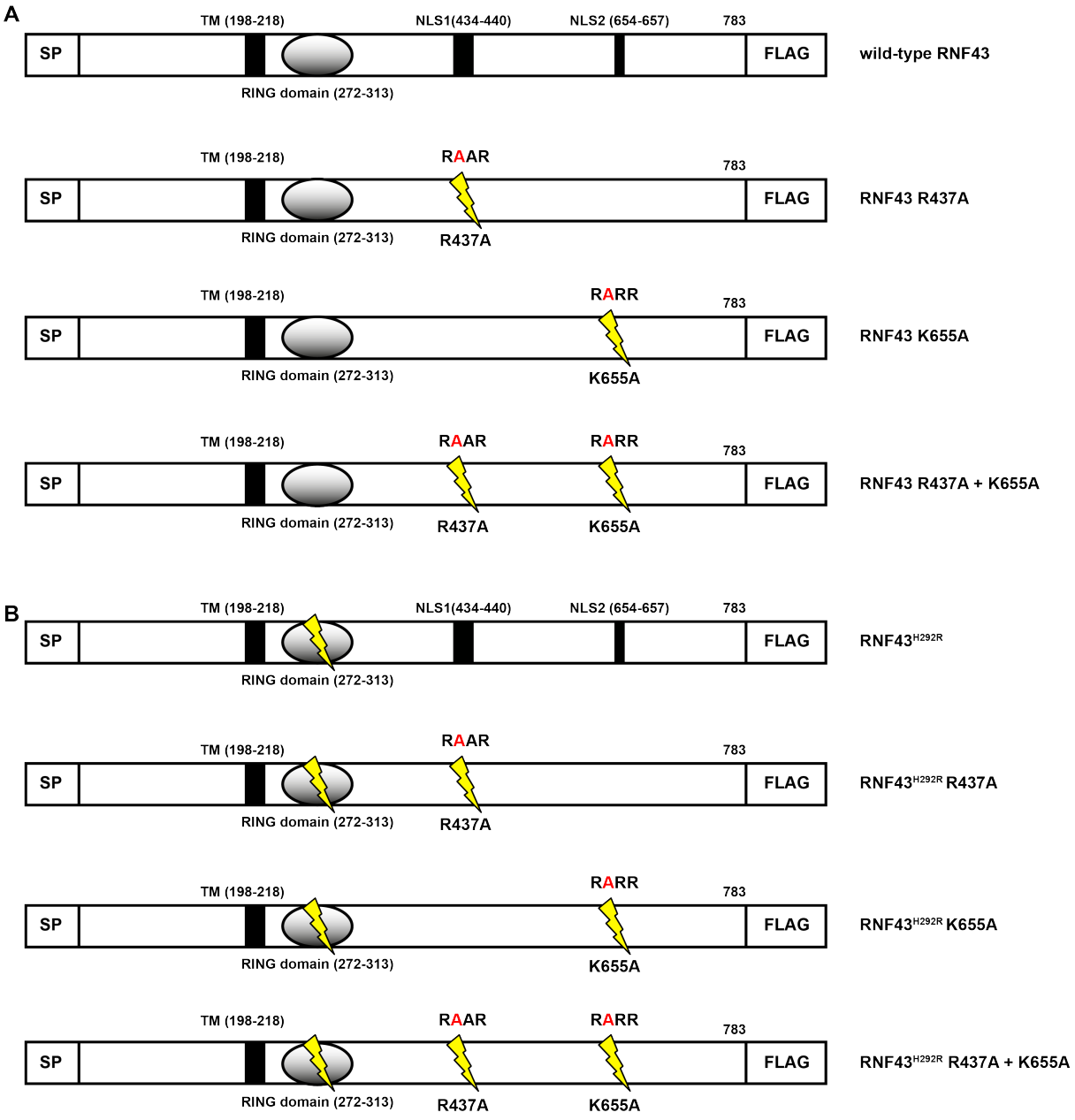

Figure 40: Schematic representation of RNF43 and RNF43^{H292R} constructs with mutated NLS.
SP, signal peptide; TM, putative transmembrane domain; NLS, nuclear leading sequence; FLAG, Flag-tag; yellow lightning indicates position of mutation; red letter indicates mutated amino acid (R to A or K to A) in nuclear leading sequence; numbers indicate amino acid position.

When only one NLS site was mutated in wild-type RNF43, the inhibitory capacity of RNF43 was still observed, whereas two mutated NLS abolished the effect on Wnt signaling. All NLS constructs with mutated RING domain showed a similar enhanced TCF/LEF transcriptional activity as observed in RNF43^{H292R} (**Figure 41A**). Moreover, immunofluorescence staining detected RNF43^{R437A} and RNF43^{K655A} still at the nuclear membrane, whereas RNF43$^{R437A+K655A}$ expression was observed in the cytoplasm. Overexpression of the RNF43^{H292R} NLS variants resulted in a localization at the nuclear rim as observed with RNF43^{H292R} (**Figure 41B**). These data strongly suggest that subcellular localization of RNF43 highly affects its function as a repressor of TCF transcriptional activity.

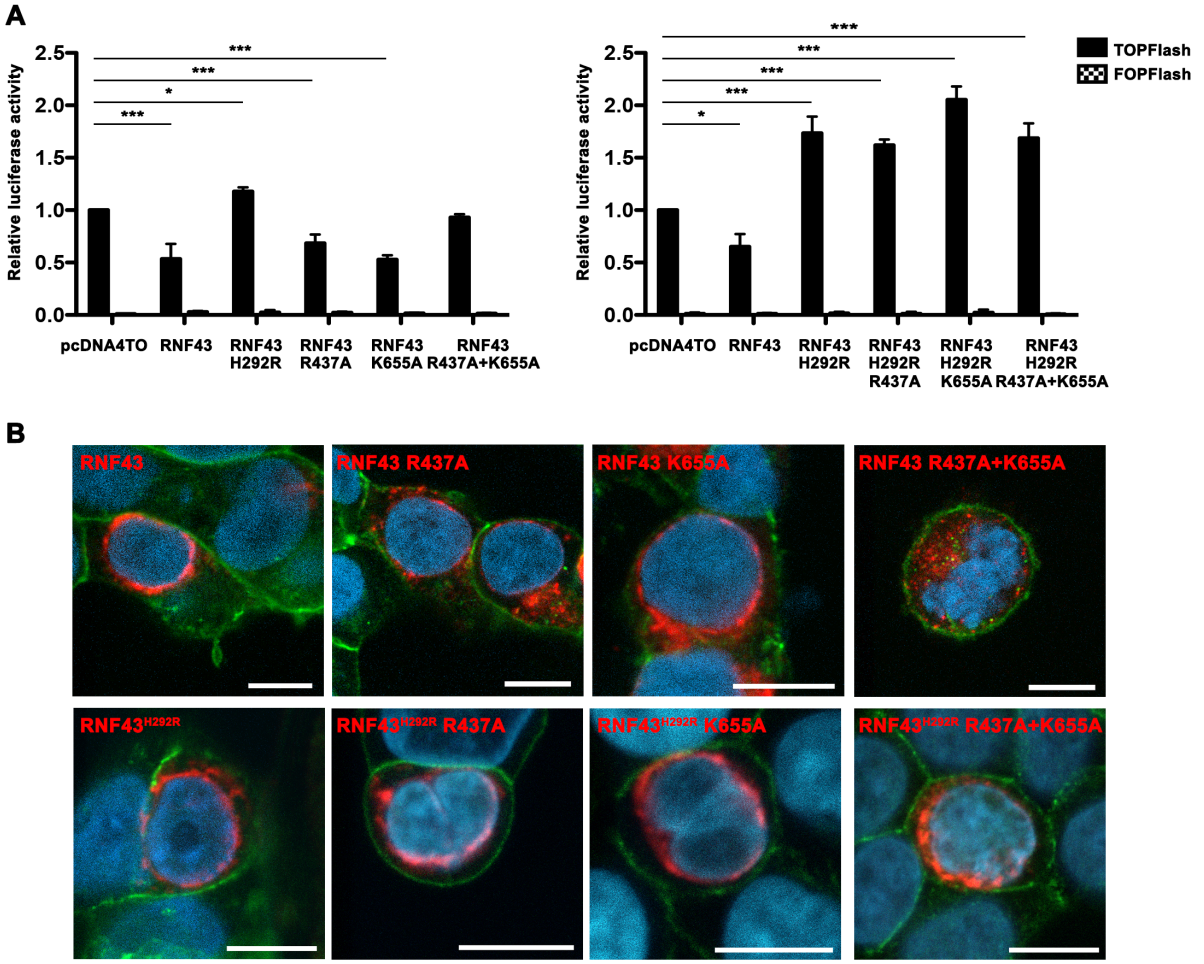

Figure 41: Nuclear leading sequences are essential for activity and localization of RNF43.
(A) TOP/FOP luciferase reporter assay in HCT116 cells transfected with RNF43 or RNF43^{H292R} NLS constructs (R437A, K655A, or R437A + K655A) (n=3). *P<0.05, **P≤0.01, ***P<0.0005, ANOVA with Dunnett's multiple comparison posttest. (B) Confocal immunofluorescence imaging of HCT116 cells transfected with RNF43 or RNF43^{H292R} NLS constructs (red) and β-catenin (green). Scale bars, 10 µm. From Loregger and Grandl *et al*. The E3 ligase RNF43 inhibits Wnt signaling downstream of mutated β-catenin by sequestering TCF4 to the nuclear membrane. *Sci. Signal.* 8, ra90 (2015). Reprinted with permission from AAAS

4.5.9 RNF43 suppresses tumorigenic capacity of cancer cells

To further substantiate the role of RNF43 as tumor suppressor, the tumorigenic capacity of cancer cells after RNF43 depletion were analyzed. Increased proliferation rates were observed in HT29, MCF7 and Caco2 cells with knocked down wild-type RNF43. Interestingly, LS174T cells, which express mutant RNF43$^{K108E,\ R389H}$, showed no changes in proliferation upon knockdown of RNF43 $^{K108E,\ R389H}$ (**Figure 42**).

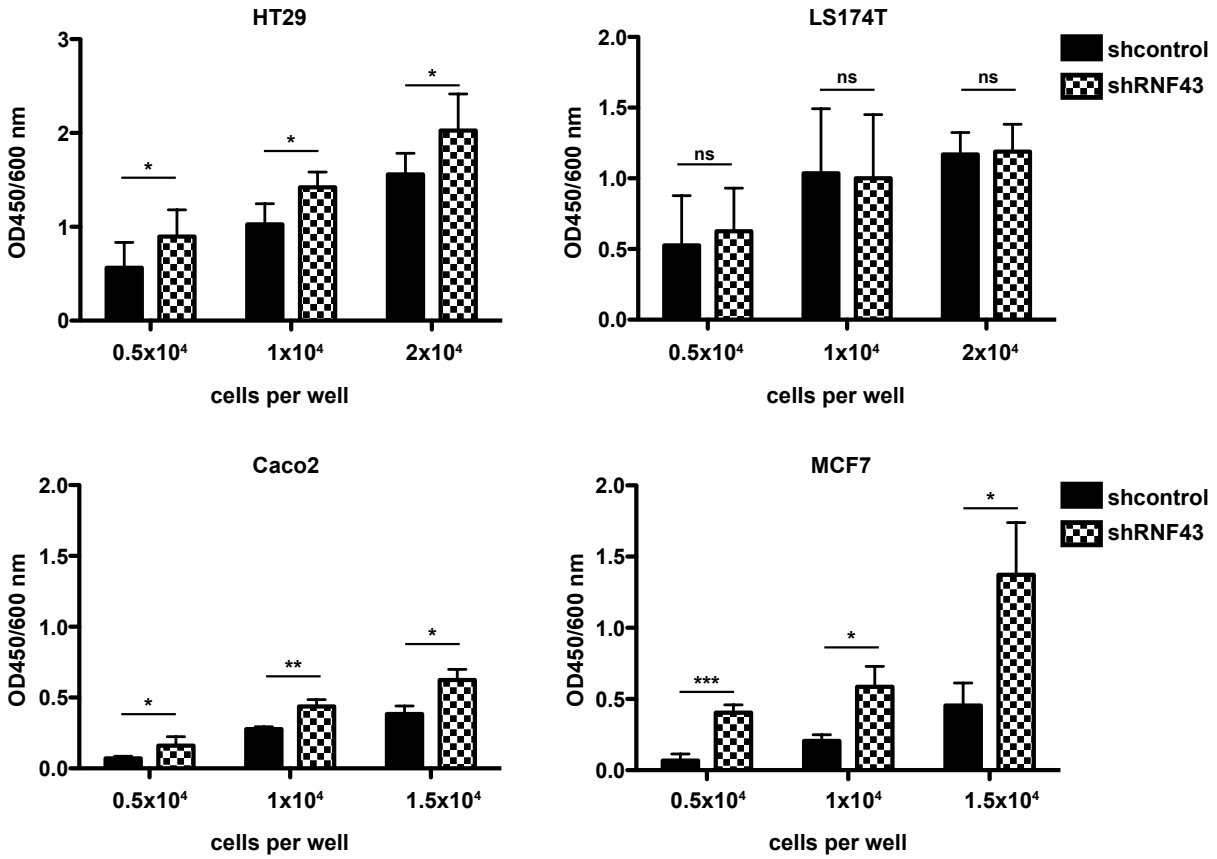

Figure 42: Depletion of wild-type RNF43 promotes cell proliferation.

Cell proliferation analysis of HT29, Caco2, LS174T, and MCF7 after lentiviral knockdown of endogenous RNF43 (n=4). *P<0.05, **P≤0.01, ***P<0.0005, Student's *t*-test.

Furthermore, the colony growth of cells expressing low levels of RNF43 was notably higher than in cells expressing wild-type RNF43 (**Figure 43A**), despite the number of colonies was the same (**Figure 43B**). No changes in colony growth were detected between LS174T with and without mutant RNF43$^{K108E,\ R389H}$.

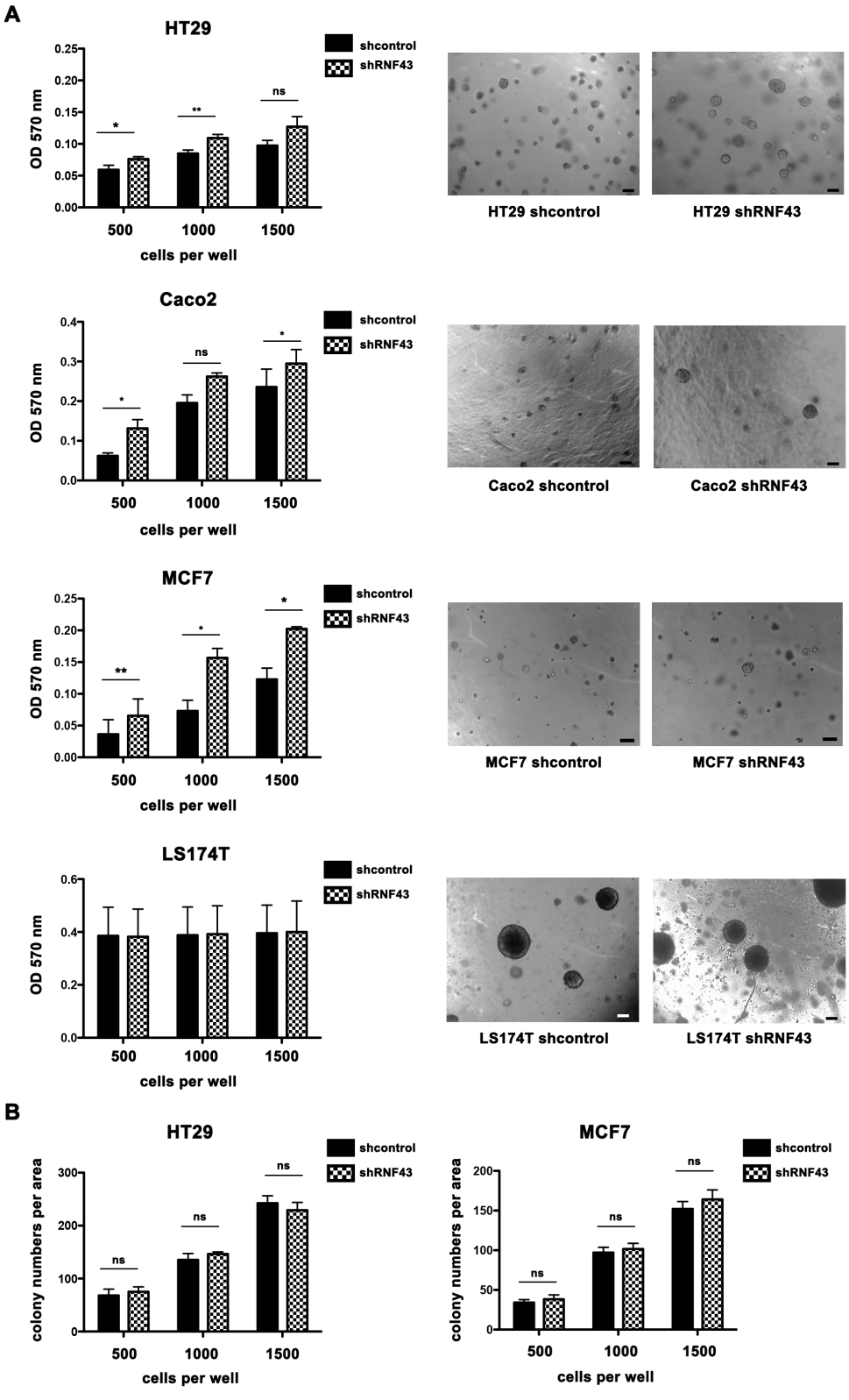

Figure 43: Knockdown of wild-type RNF43 increases colony formation.

(A) Single colony growth of HT29, Caco2, MCF7, and LS174T after knockdown of endogenous RNF43 by lentiviral treatment using softagar analysis (n=3). Colonies were stained with MTT and absorbance was measured at OD 570 nm (left). Pictures of unstained single colonies (right). Scale bars, 100 µm. (B) Numbers of grown colonies of one representative softagar using ImageJ software. *P<0.05, **P≤0.01, ***P<0.0005, Student's *t*-test.

After observing stronger proliferation and colony growth in cells lacking RNF43, the invasive capacity of the cells was investigated using the Boyden-Chamber matrigel invasion assay. Notably, HT29, MCF7 and Caco2 cells showed a stronger invasive potential when lacking wild-type RNF43 (**Figure 44**). The colon cancer cell line LS174T did not show any invasive ability at all. Altogether, these data indicate a tumor suppressor function for the endogenous wild-type RNF43.

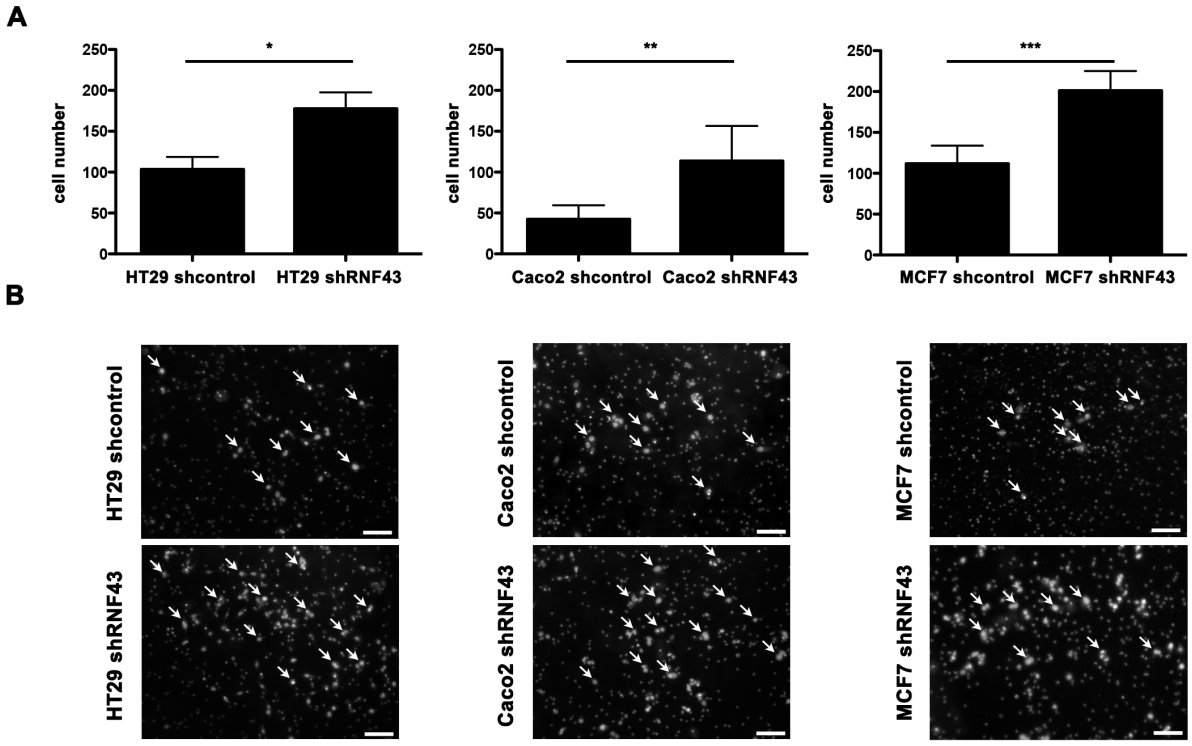

Figure 44: Wild-type RNF43 knockdown enhances cell invasiveness.
(A) Analysis of invasive capacity of HT29, Caco2, and MCF7 cells after knockdown of endogenous RNF43 using the Boyden Chamber Assay supported by a matrix of collagen IV and matrigel. *P<0.05, **P≤0.01, ***P<0.0005, Student's *t*-test. (B) Pictures of migrated HT29, Caco2 and MCF7 cells stained with DAPI (white arrow). Scale bars, 100 µm.

4.5.10 *In vivo* RNF43 knockout model

Since the *in vitro* analyses demonstrated a tumor suppressor function of wild-type RNF43, a murine Rnf43 knock out model was generated using the CRISPR/Cas9 system to confirm the result *in vivo*. To obtain a specific Rnf43 loss of function, its RING domain was targeted with Cas9 nickase (**Figure 45A**). Cas9 nickase can be used to efficiently mutate genes without detectable damage at known off-target sites[276]. After pronuclear injection of plasmids containing guide RNAs and cas9 nickase, a homozygous deletion of 57 base pairs in the RING domain was obtained in one female mouse out of seven FVB/N (**Figure 45B**).

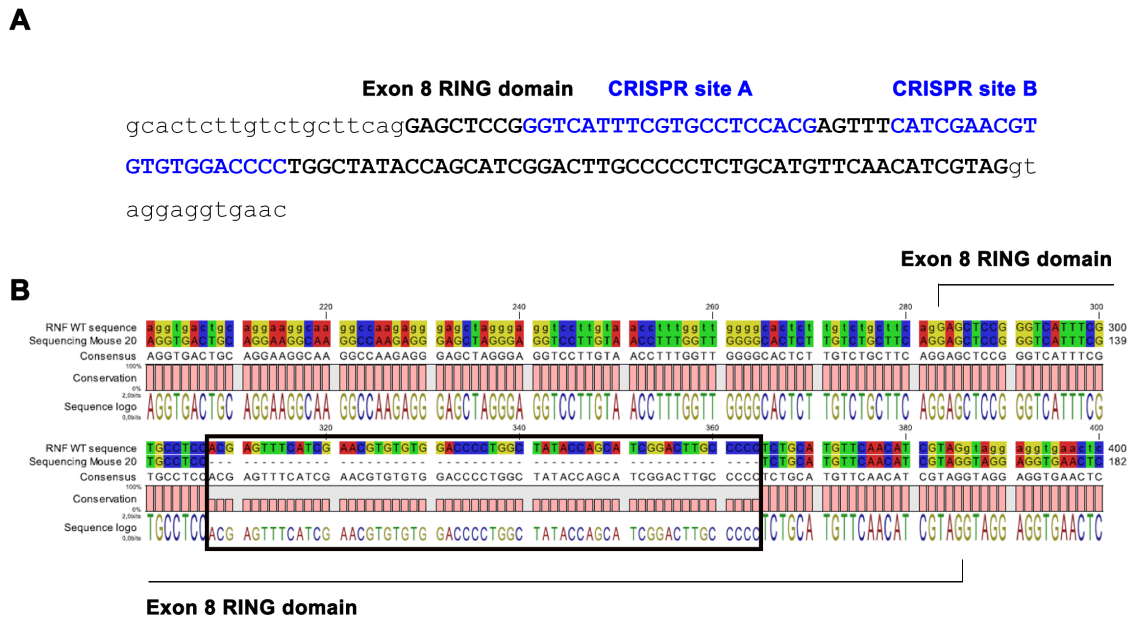

Figure 45: Schematic representation of CRISPR/Cas9 nickase induced RNF43 knockout in FVB/N mice.
(A) Genomic murine *Rnf43* sequence of exon 8 (capital letters) coding the RING domain. Specific sequences targeted by guide RNAs (gRNA) for cas9 nickase is indicated in blue. (B) Alignment of female murine DNA lacking 57 base pairs in exon 8 with wild-type Rnf43 sequence.

Analysis of murine intestinal sections revealed that depletion of 57 bp in the RING domain of Rnf43 induced no phenotype in homozygous mice. No differences in crypt formation and histology could be detected. In addition, immunohistochemical staining for Ki67 was similar in the intestinal tissues of wild-type and Rnf43 knock out mice (**Figure 46**). Taken together, these *in vivo* data showed that inactivation of Rnf43 by deletion of the RING domain did not have an impact on intestinal proliferation.

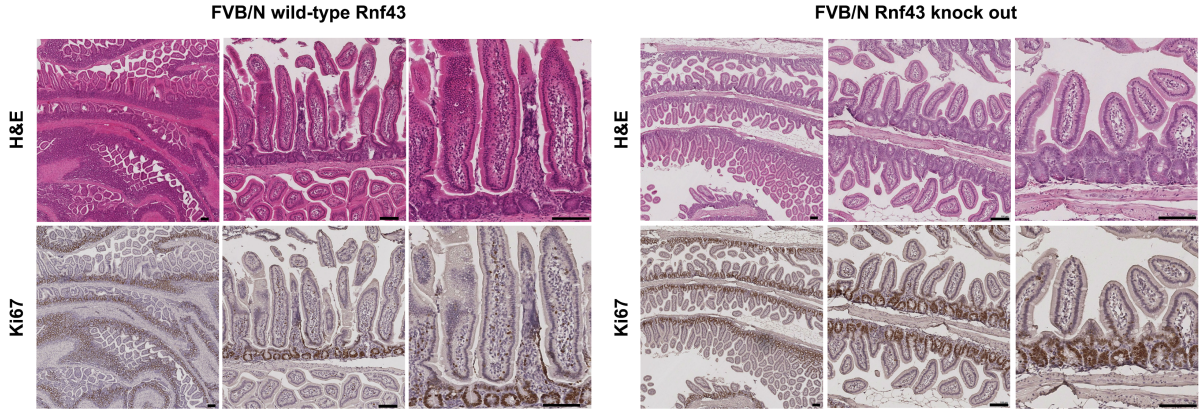

Figure 46: Rnf43 knock out induce no intestinal phenotype.
Immunohistochemical staining of small intestine tissue from wild-type Rnf43 and homozygous Rnf43 knock out FVB/N mice using H&E and Ki67 staining. Scale bars, 100 µm.

4.6 Analysis of RNF43 mutations

4.6.1 RNF43 is highly mutated in tumors

Endogenous RNF43 acts as a tumor suppressor. Inactivation of tumor suppressors due to mutations is a frequently observed event in tumorigenesis[277]. Indeed, several publications studying gastrointestinal tumors[250,251,253,278,279] described that the *RNF43* gene is frequently mutated over the entire open reading frame (**Figure 47A**). According to these studies and the Cosmic database of the Sanger Institute, *RNF43* exhibits a high number of point mutations leading to a missense transcription (47 %), to frameshift mutations due to base pair deletions (32 %) and nonsense mutations resulting in a truncated protein (15 %) (**Figure 47B**).

A

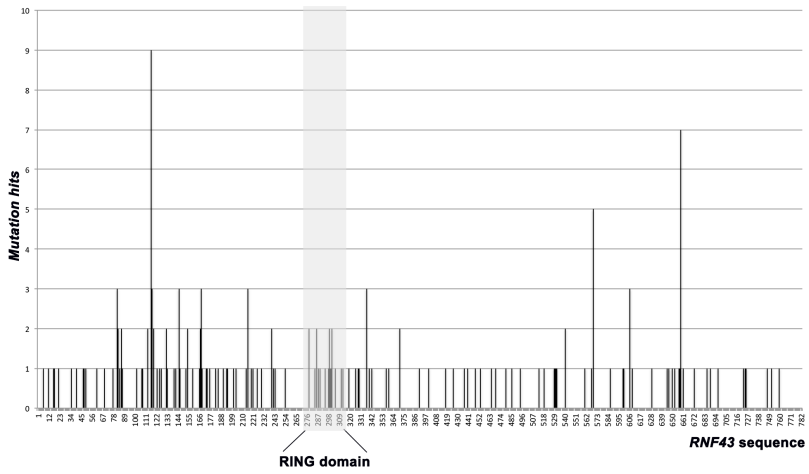

B

Color	Mutation Type	Mutant samples	Percentage
	Substitution nonsense	56	15.01
	Substitution missense	175	46.92
	Insertion frameshift	21	5.63
	Deletion frameshift	119	31.9
	Other	2	0.54

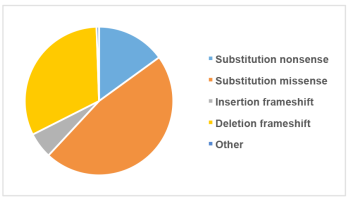

Figure 47: Schematic representation of *RNF43* mutations.
(A) RNF43 mutations described in the Cosmic database. The x- axis shows RNF43 amino acid sequence, while the number of samples showing a specific mutation is shown on the y-axis. (B) Table showing the percentage of different mutation types notated in the Cosmic database.

Next generation sequencing of a Union for International Cancer Control (UICC) tumor cohort was performed to identify and functionally assess *RNF43* mutations in colon cancer. Substitute, frameshift, and stop mutations were found. The impact of some of these mutations as well as of different mutations annotated in literature was studied in functional assays. Specifically, two stop mutations (R113X and S216X) and two amino acid substitutions (R127P and A169T) described in neoplastic cysts of pancreatic tumor samples[250] (**Figure 48A**) were

individually cloned as well as four point mutations (A33T, I48T, R219H, and R343H), one stop mutation G133X, and four frameshift mutations (G102fs, G282fs, H306fs, and K559fs) identified in the UICC tumor cohort (**Figure 48B**). It has to be noted that the mutation R113X was reported as germline mutation in multiple sessile serrated adenomas[263].

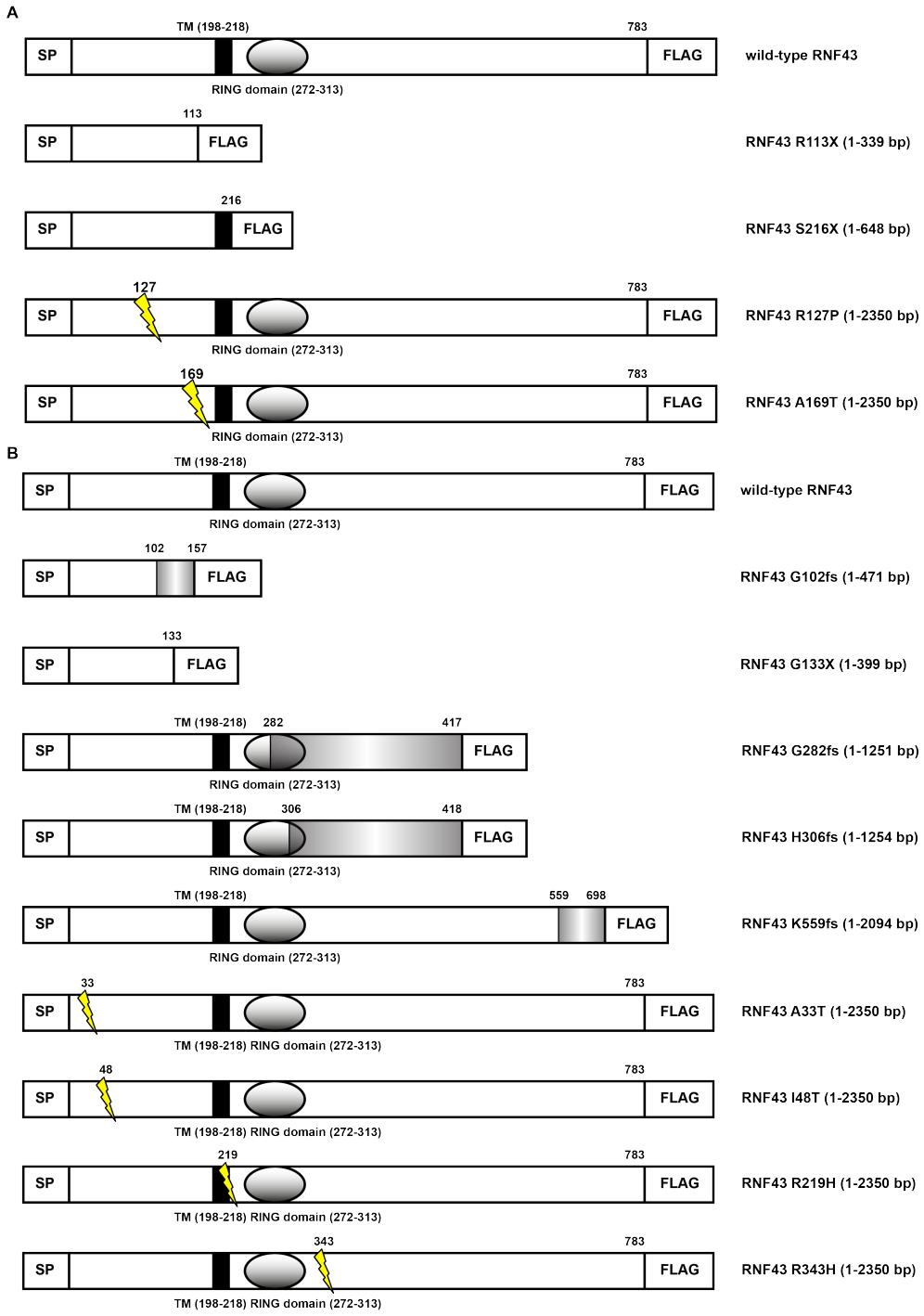

Figure 48: Schematic representation of mutated RNF43 constructs.
SP, signal peptide; TM, putative transmembrane domain; FLAG, Flag-tag; bp, base pair; yellow lightning indicates position of mutation; gray field indicates frameshift sequence; numbers indicate amino acid position

4.6.2 Subcellular localization of mutated RNF43

The expression of the generated mutants was first confirmed in transfected HCT116 cells by Western blot analysis (**Figure 49**). The shortest variants of RNF43^{G102fs} and RNF43^{G133X} were not detected.

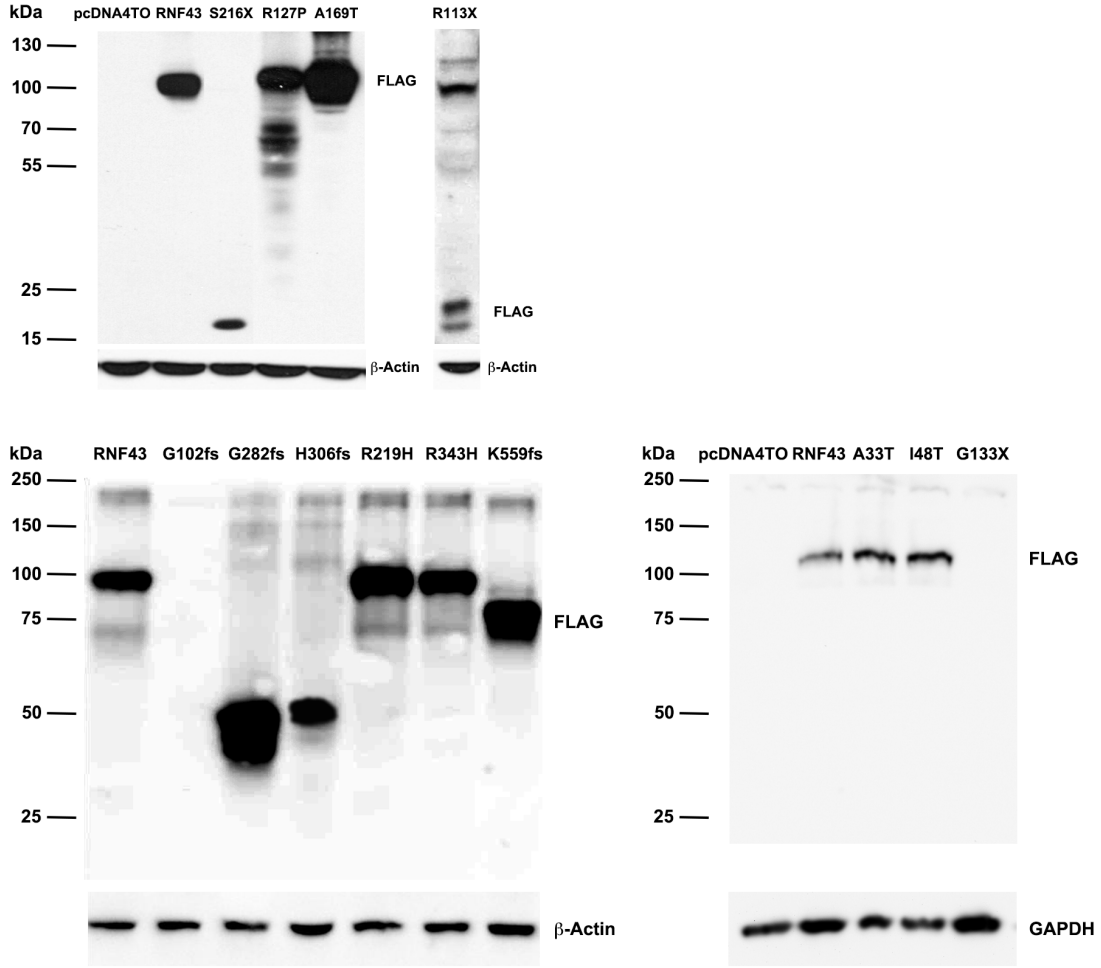

Figure 49: RNF43 constructs are expressed after transfection.
Expression of different mutated RNF43 constructs after transfection in HCT116 cells analyzed by Western blot

RNF43 is expressed in the nuclear compartment of cells, where its localization was shown to be important for the function of the protein. Therefore, confocal microscopy was carried out to analyze subcellular localization of the mutants. The R113X, G282fs, H306fs, and R127P mutations induced a relocalization of RNF43 into the cytoplasm. Interestingly, although the expression of RNF43^{G133X} was not confirmed by Western blot analysis, the protein was still detected in the cytoplasm by immunofluorescence. RNF43^{G102fs} was neither detected by western blot analysis nor by immunofluorescence staining, suggesting that this mutation prevents protein expression. RNF43^{A33T}, RNF43^{I48T}, RNF43^{S216X}, RNF43^{R219H}, RNF43^{A169T},

RNF43^{R343H}, and RNF43^{K559fs} mutations did not influence the localization of the protein at the nuclear envelope (**Figure 50**). These results show that some mutations of RNF43 induce mislocalization of the protein, suggesting that a loss of function could occur.

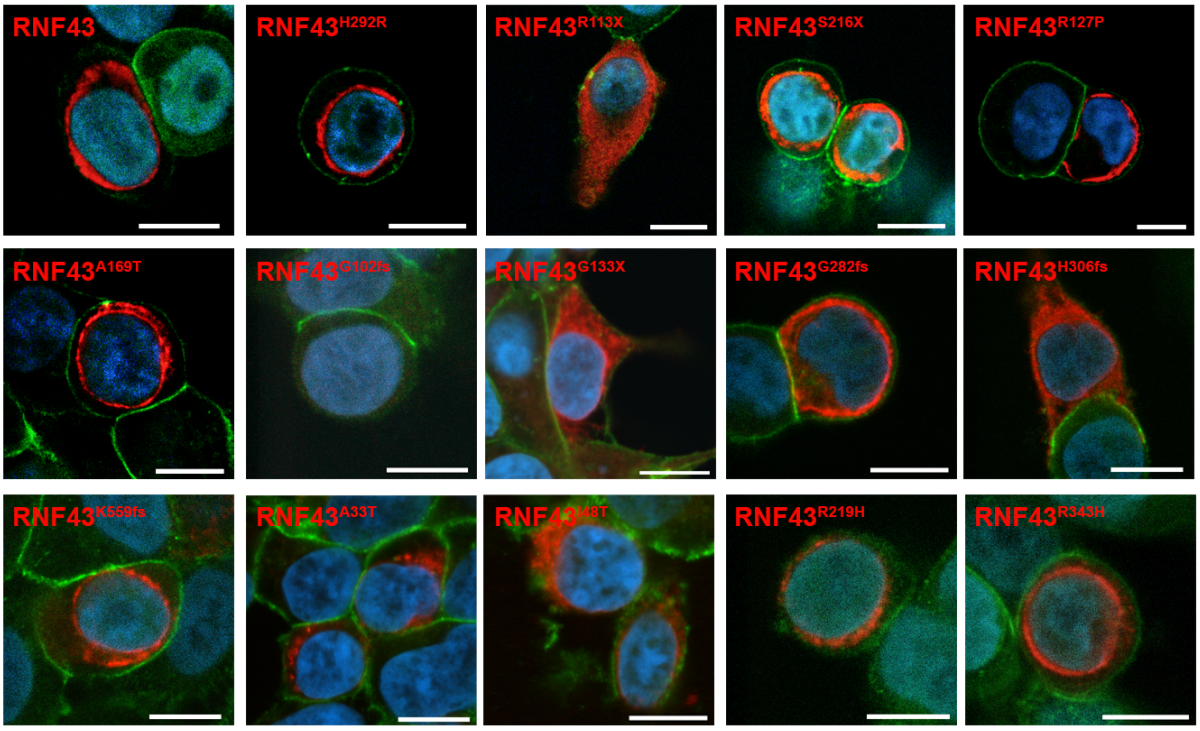

Figure 50: Subcellular localization of RNF43 mutants.
Confocal immunofluorescence of RNF43 mutants (red) after transfection and β-catenin (green) in HCT116 cells. Scale bars, 10 μm. From Loregger and Grandl *et al*. The E3 ligase RNF43 inhibits Wnt signaling downstream of mutated β-catenin by sequestering TCF4 to the nuclear membrane. *Sci. Signal.* 8, ra90 (2015). Reprinted with permission from AAAS

4.6.3 Mutations in RNF43 induce loss of function

When measuring TCF/LEF transcriptional activity, RNF43^{R113X,} RNF43^{S216X}, RNF43^{A169T}, and RNF43^{R127P} could not inhibit Wnt signaling after transfection in HCT116 cells. Similar results were obtained when overexpressing the RNF43 variants A33T, I48T, G133X, G282fs, and H306fs. Interestingly, the R219H, R343H, and K559fs forms were still active (**Figure 51**). These data indicate that mislocalized mutants of RNF43 affect the inhibitory effect on Wnt signaling, resulting in a loss of function of the tumor suppressor.

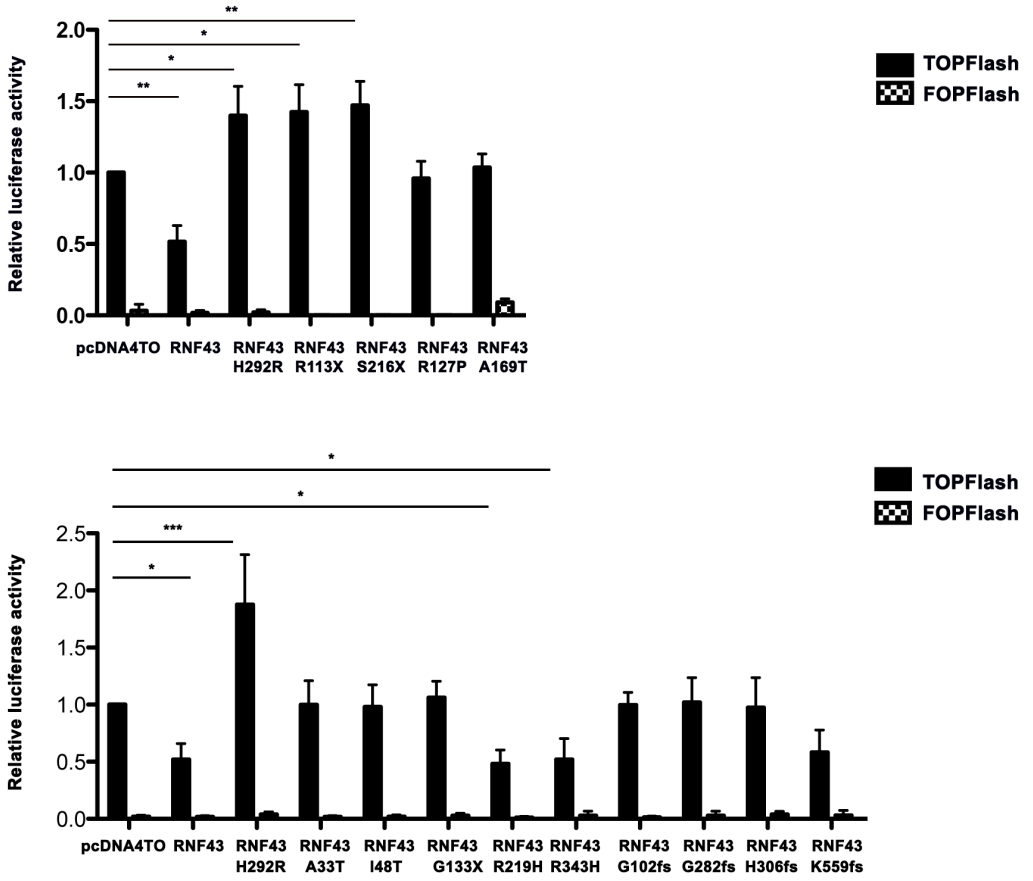

Figure 51: Mutations in RNF43 abolish WNT-inhibitory effect of wild-type RNF43.
TCF/LEF transcriptional activity of RNF43 mutants after overexpression in HCT116 cells (n=3). *P<0.05, **P≤0.01, ***P<0.0005, ANOVA with Dunnett's multiple comparison posttest.

4.6.4 Mutations in RNF43 disrupt the interaction with TCF4

To test whether the loss of function mechanistically occurs through the impaired capacity to relocalize TCF4, colocalization staining of RNF43 mutants with TCF4 was performed. No colocalization was observed between TCF4 and the different RNF43 mutants, with the exception of $RNF43^{R219H}$ and $RNF43^{R343H}$ (**Figure 52A**). Both mutants also showed a similar inhibitory effect on TCF/LEF transcriptional activity as wild-type RNF43, suggesting that these point mutations have no impact on the activity of RNF43 (**Figure 51**). Coimmunoprecipitation was performed between non-active mutants $RNF43^{R127P}$ or $RNF43^{A169T}$ and TCF4. No interaction was observed (**Figure 52B**). Together these findings demonstrate that most of the investigated mutations in *RNF43* impair its inhibitory effect on Wnt signaling due to TCF4 relocalization.

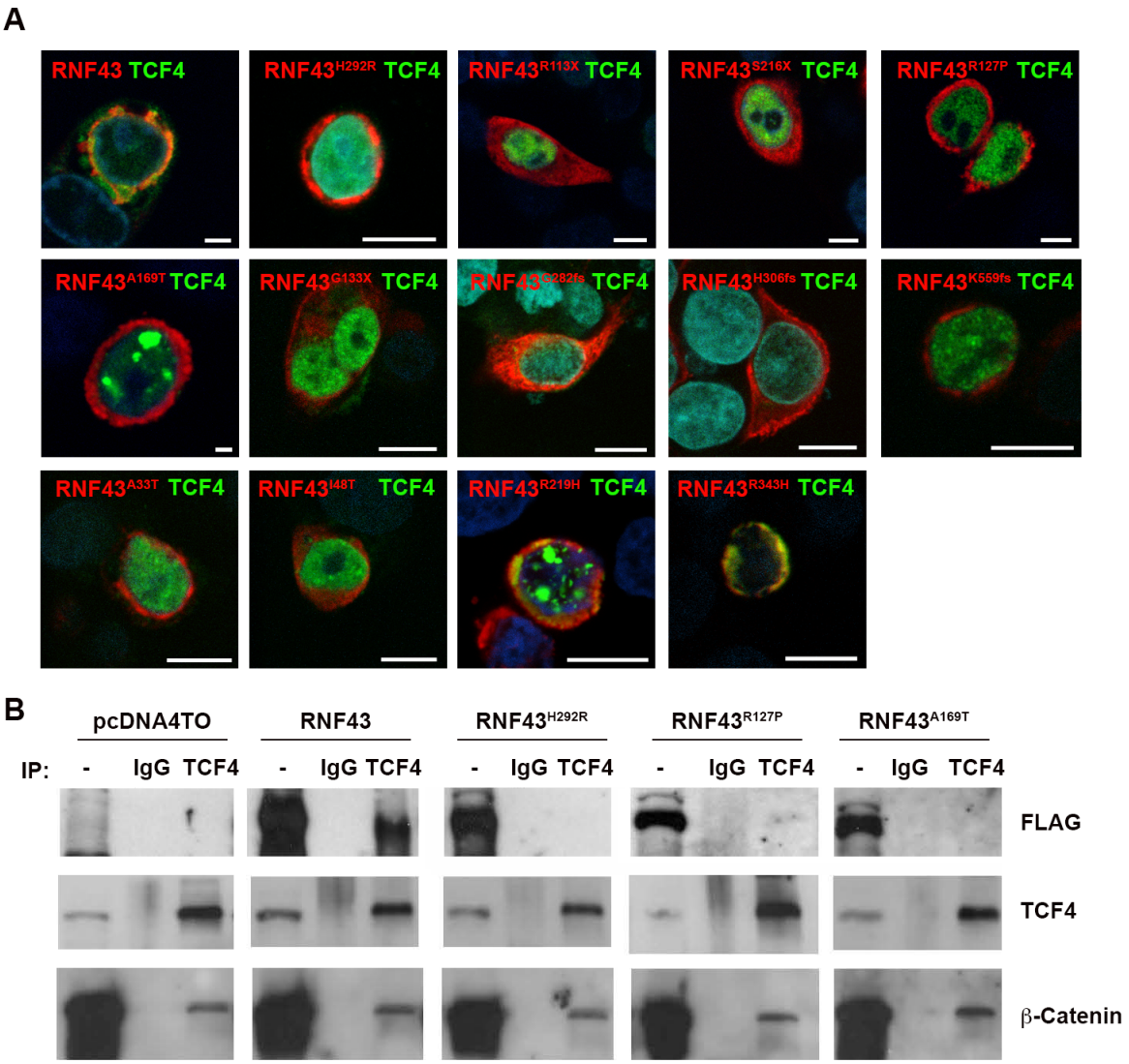

Figure 52: RNF43 mutants do not interact with TCF4.

(A) Confocal immunofluorescence analysis of TCF4 (green) andRNF43 (red) in HCT116 cells cotransfected with TCF4 and wild-type or mutant RNF43. Scale bars, 10 µm. (B) Immunoprecipitation of TCF4 from HCT116 cells transfected with Flag-tagged wild-type or mutant RNF43, followed by Western blot analysis. From Loregger and Grandl *et al*. The E3 ligase RNF43 inhibits Wnt signaling downstream of mutated β-catenin by sequestering TCF4 to the nuclear membrane. *Sci. Signal.* 8, ra90 (2015). Reprinted with permission from AAAS

4.6.5 Analysis of Rnf43^{H292R} mutation *in vivo*

4.6.5.1 Generation of Rnf43^{H292R} mouse using CRISPR/Cas9

In vitro characterization of several mutations found in tumor samples revealed an increased effect or a loss of function of RNF43. Specifically, the mutation RNF43^{H292R} led to increased TCF/LEF transcriptional activity. In order to recapitulate this promoting effect of RNF43^{H292R} on Wnt signaling *in vivo*, the double mutation H292R / H295R was introduced in the genomic

locus of *Rnf43* in mice by using the Cas9 nickase of the CRISPR/Cas9 system[276]. In addition, a new specific restriction site for BsmA1 inducing a silent mutation was introduced to facilitate the screening of the offspring (**Figure 53A**). After pronuclear injection in FVB/N oocytes, one male homozygous Rnf43^{H292R} mouse out of seven mice was obtained. In addition, one female heterozygous Rnf43^{H292R} out of thirteen mice was obtained using C57BL6 oocytes (**Figure 53B**).

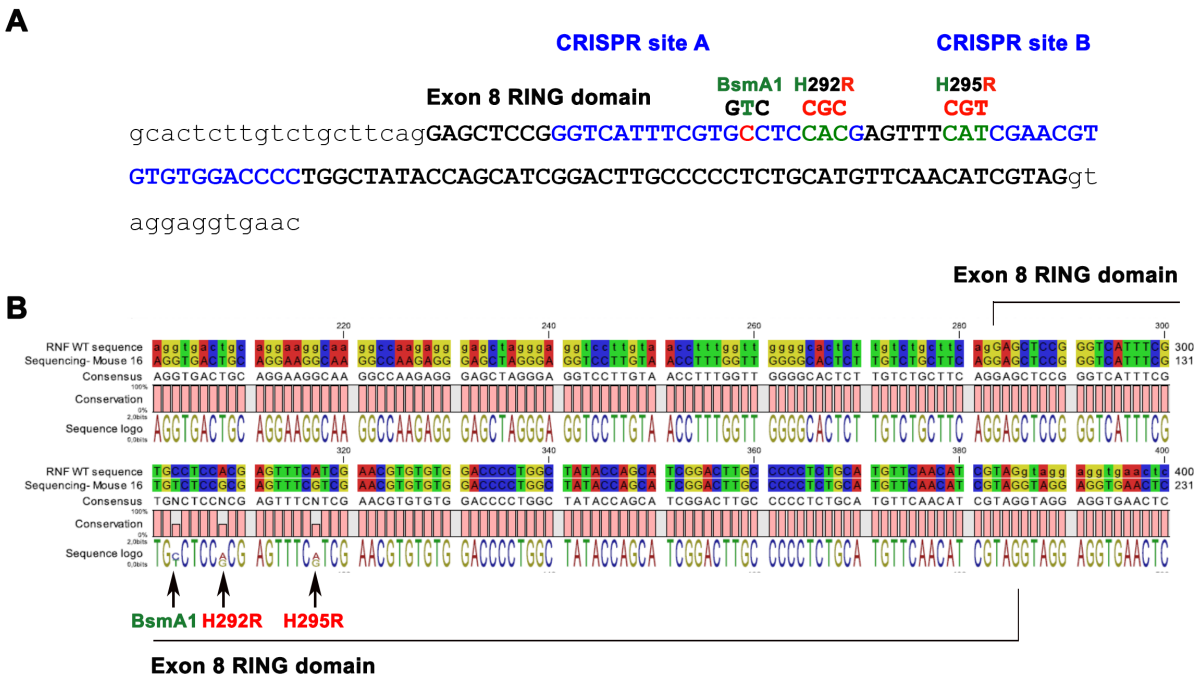

Figure 53: Schematic representation of CRISPR/Cas9 nickase induced H292R and H295R mutation in the genomic sequence of murine Rnf43.

(A) Genomic murine *Rnf43* sequence of exon 8 (capital letters). Specific sequences targeted by guide RNA (CRISPR site) for cas9 nickase are indicated in blue. *Rnf43* wild-type sequence is marked in red letters, while mutations are shown in green. BsmA1 restriction site for screening is indicated in green. (B) Alignment of female murine DNA with H292R, H295R (red), and BsmA1 (green) mutation site in exon 8 with wild-type Rnf43 sequence.

4.6.5.2 Phenotypical characterization of the Rnf43^{H292R} mouse

When analyzing intestinal tissue of Rnf43^{H292R} mice, pathological changes were observed already after 21 weeks in heterozygous mice. Crypt abscesses, erosions with focal mucosal inflammation and crypt distortions were observed in the intestine of 27 week old heterozygous mice. After 70 weeks, crypt abscesses were not detected in homozygous mice, but they presented partial necrosis of the mucosa. The adjacent intact mucosa showed elevated cell count in the tunica propria. In addition, increased number of intraepithelial apoptosis as well as Paneth cell metaplasia was detected. Enhanced cell proliferation was assessed in the

same tissue samples by Ki67 staining (**Figure 54**). Together, these results indicate that the H292R/H295R mutations in Rnf43 induce proliferative activity of crypt cells.

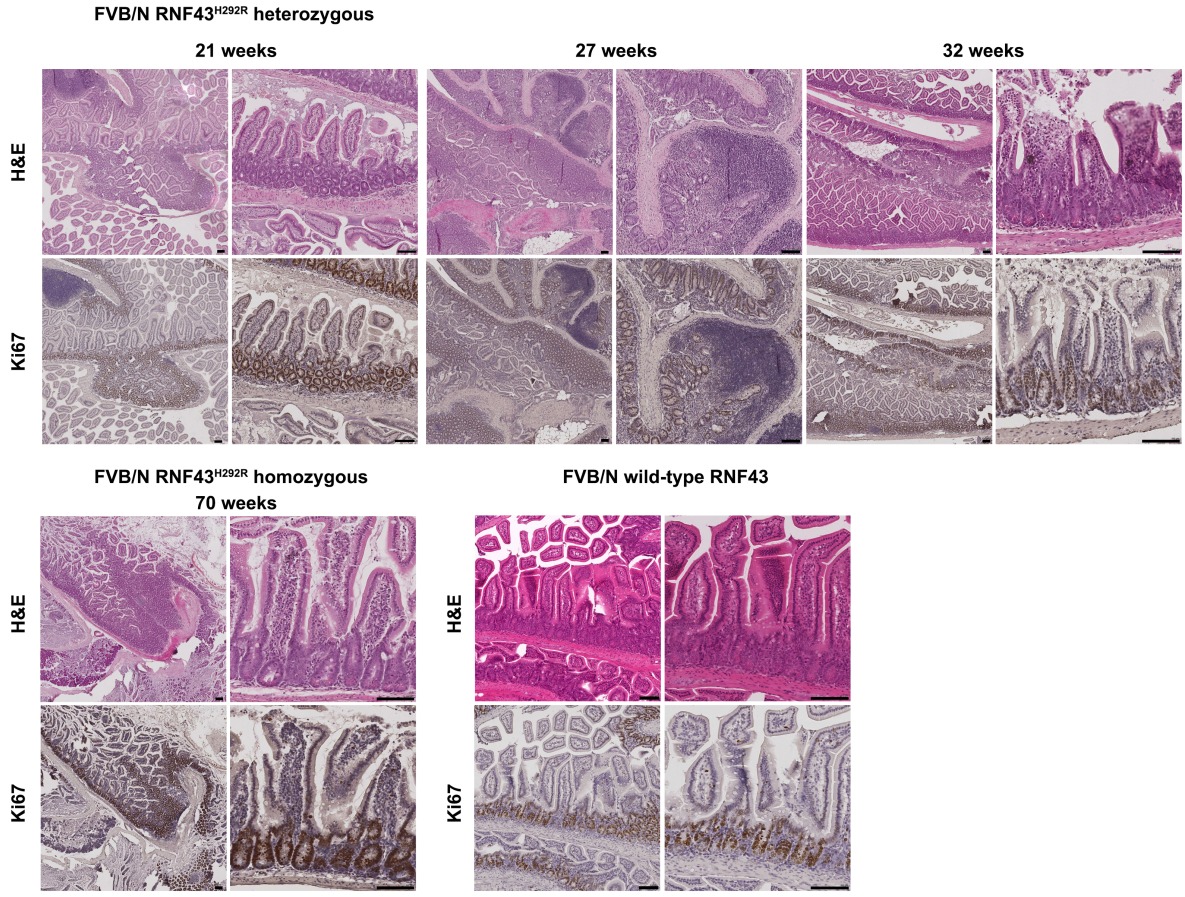

Figure 54: Rnf43 H292R / H295R mutation induce hyperplasia formation in murine intestine. Immunohistochemical staining of small intestine tissue from heterozygous and homozygous Rnf43$^{H292R/H295R}$ FVB/N mice using H&E and Ki67 staining. Scale bars, 100 µm.

4.6.5.3 Characterization of intestinal crypts of Rnf43^{H292R} mouse

In order to investigate the impact of the *Rnf43^{H292R}* mutation on intestinal stem cells, crypts from the small intestine of 12-week old male FVB/N wild-type Rnf43, Rnf43^{H292R} heterozygous and homozygous mice were isolated and cultured over 12 days. 24 h after isolation no difference was detected between the organoids, generated from isolated intestinal crypts. After 4 days *in vitro* culture organoids derived from homozygous Rnf43^{H292R} crypts were bigger in size and showed first crypt-like protrusions compared to heterozygous Rnf43^{H292R} or wild-type RNF43. Compared to organoids of heterozygous Rnf43^{H292R} or wild-type RNF43, organoids derived from homozygous Rnf43^{H292R} crypts were notably bigger after 8 days. The same trend was observed after 12 days of organoid culture (**Figure 55**), indicating that the introduced H292R/H295R mutations promote growth of organoids.

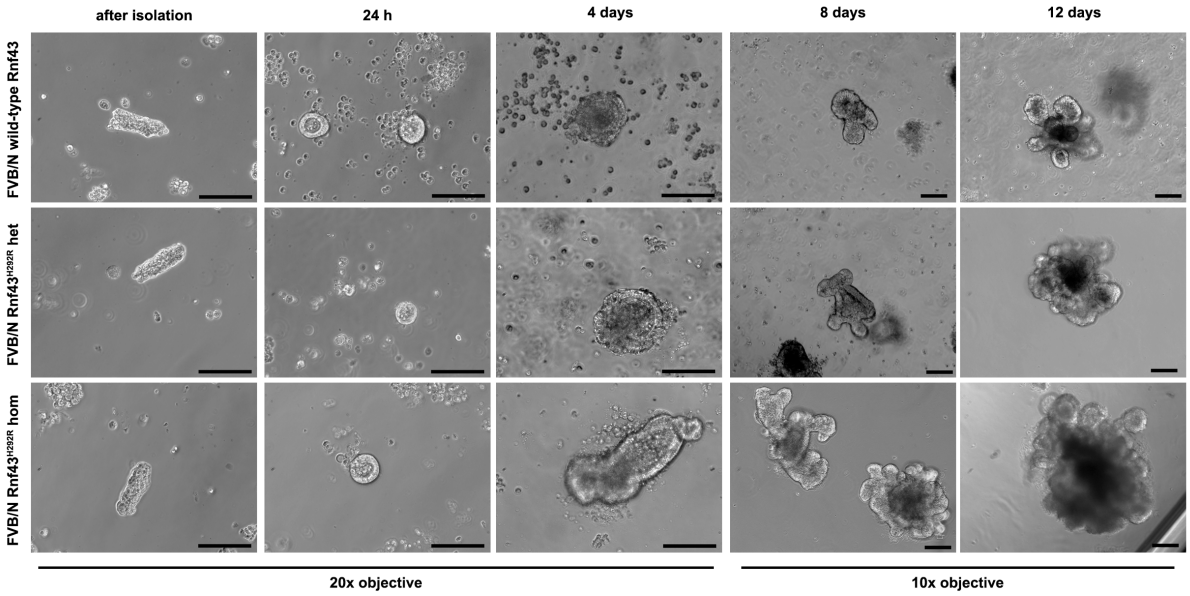

Figure 55: Rnf43^{H292R} mutation promotes growth of intestinal stem cells.
Organoid culture over 12 days of crypts isolated from 12-weeks old wild-type Rnf43, heterozygous (het) Rnf43^{H292R}, and homozygous (hom) Rnf43^{H292R} FVB/N mice. Scale bars, 50 µm

4.7 RNF43 interacts with other nuclear proteins

RNF43 was described being highly mutated in organs where Wnt signaling is not prevalent[251,265,254]. For instance, deregulated Notch signaling is involved in pancreatic cancer, and impaired signal transducer and activator of transcription 3 (STAT3) and nuclear factor kappa-light-chain-enhancer of activated B cells (NFκB) signaling is important for stomach cancer. This suggests a different mode of action for RNF43 in these organs. To investigate whether RNF43 is also connected to other tumor related pathways, luciferase reporter assays of signaling pathways were performed. Interestingly, STAT3 signaling was clearly reduced in presence of RNF43 in cSTAT3-induced HCT116 cells, whereas overexpression of RNF43^{H292R} did not change the luciferase activity (**Figure 56A**). Investigating the impact of RNF43 in Notch1 and 2 signaling resulted also in decreased reporter signaling consequent to Notch induction in HCT116 and HEK293 cells. RNF43^{H292R} overexpression did not alter the activated signaling intensity (**Figure 56B**). In addition, canonical NFκB signaling was studied under the influence of RNF43. In contrast to STAT3 and Notch signaling neither RNF43 nor RNF43^{H292R} affected tumor necrosis factor alpha (TNFα) - induced luciferase activity (**Figure 56C**). These data suggest a role of RNF43 in certain tumor related pathways of the gastrointestinal tract.

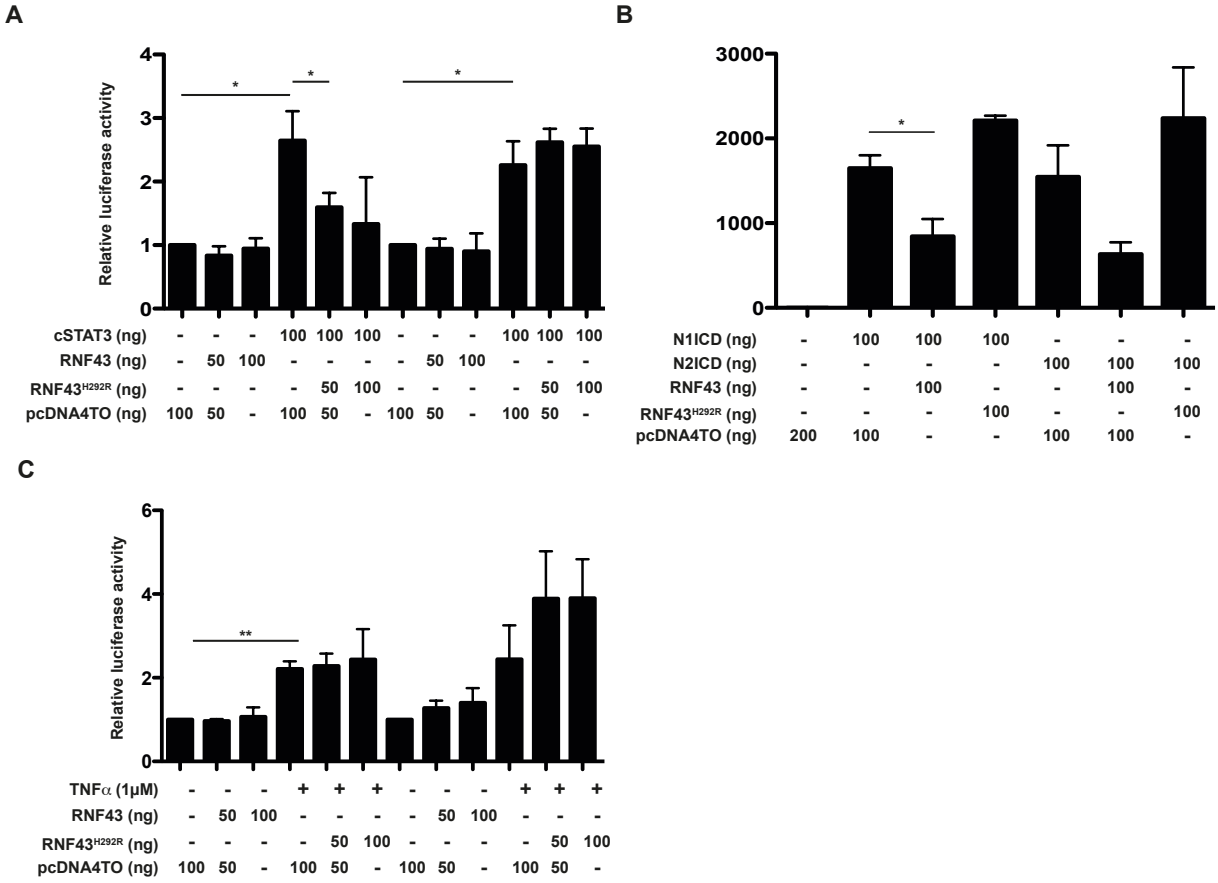

Figure 56: RNF43 acts in different tumor associated pathways.

(A) Luciferase reporter assay measuring STAT3 activity in presence of RNF43 or mutant RNF43^{H292R} in HCT116 cells (n=3). cSTAT3, constitutive active form of STAT3. (B) Luciferase reporter assay measuring Notch1 or Notch 2 activity in presence of RNF43 or mutant RNF43^{H292R} after stimulation with intracellular domain of Notch 1 (N1ICD) or Notch 2 (N2ICD) in HCT116 cells (n=3). (C) Luciferase reporter assay measuring NFκB activity in presence of RNF43 or mutant RNF43^{H292R} after stimulation of TNFα in HCT116 cells (n=3). *P<0.05, **P≤0.01, ***P<0.0005, ANOVA with Dunnett's multiple comparison posttest.

.

5 Discussion

The function and localization of the RING finger ubiquitin ligase 43 are controversially discussed. RNF43 has been described as an oncogene[248,249,261] as well as a tumor suppressor[214,278,280], being localized either in the nucleus[247,261,262,281], in the cytoplasm[248], or at the cellular membrane[148,214,282]. Given its increasingly recognized role in human gastrointestinal cancer, this study analyzed in detail the expression, localization, and function of endogenous and overexpressed RNF43 in murine and human tissue as well as in human cancer cells.

5.1 Subcellular expression of endogenous RNF43

The subcellular localization of RNF43 is still unclear. Initial studies of RNF43 reported a nuclear expression[247,261,262,264,283]. More recently, studies linked RNF ubiquitin ligases, including RNF43, to DDR signaling and chromatin remodeling[263,284]. In addition, RNF43 was found to affect the cell cycle by regulating the expression of pRB, Cyclin D1 and MDM2 proteins of the p53 pathway in hepatocellular cancer cells[283]. In line with this, RNF43 was reported to interact with nucleoprotein of influenza A virus and modulating p53-dependent signaling and apoptosis[262]. In contrast to these data, Koo *et al*. (2012) described RNF43 being expressed at the cellular membrane[214]. They detected doxycycline-induced RNF43 overexpression at the cellular membrane after measuring the surface proteome of cells by mass spectrometry. Moreover, they detected a rapid internalization of frizzled receptors after coexpression of RNF43 and Fzd5 using flow cytometry. Colocalization analysis of overexpressed GFP-coupled RNF43 and Fzd5 localized RNF43 at cell membrane and to lower amounts in the cytoplasm. In line with this report, some studies investigated ZNRF3, the homologue of RNF43, showing that ZNRF3-GFP promotes Wnt receptor turnover in an R-spondin-sensitive manner[148,285].

When studying the subcellular expression of RNF43, subcellular fractionation experiments performed with overexpressed RNF43 in human cancer cells unambiguously detected RNF43 in the nuclear fractions. Furthermore, immunofluorescence staining in different cancer cells confirmed this observation, being in line with reports suggesting the nuclear localization of RNF43[247,264]. Moreover, colocalization stainings of overexpressed RNF43 with inner nuclear membrane proteins lamin B and calnexin corroborated the nuclear expression, supporting previous reports showing that RNF43 is located in the ER and in the nuclear membrane[247,264] with occasional presence in the nucleoplasms[247,261]. Specifically, a direct interaction of RNF43 with the nuclear protein PSF has been reported[261], which was confirmed by colocalization staining of both overexpressed proteins.

Many studies investigated RNF43 or ZNRF3 under overexpression conditions, often being conjugated to GFP, since reliable antibodies detecting endogenous RNF43 were not described. The advantage of a GFP-tag is the intrinsic detection and the opportunity to study localization in live cells using techniques such as fluorescence lifetime imaging, bimolecular fluorescence complementation, fluorescence recovery after photobleaching, and photoactivation[286,287]. The fundamental disadvantage of GFP-tag is that it may alter the location and interactions of the native proteins because of its large size[288,289]. Moreover, transient transfected GFP fusion proteins are generally overexpressed relative to endogenous proteins and can thereby affect the protein localization. This might explain the contradictory results of the subcellular localization of RNF43 obtained by using small epitope HA and FLAG-tags in this study in contrast to the GFP-tagged RNF43 of Koo *et al.* To exclude a mislocalization induced by overexpression of HA/FLAG-tagged RNF43, the subcellular localization of endogenous RNF43 was investigated in this study. For this, after screening of supernatants of generated hybridoma cells one antibody was identified, which specifically recognized endogenous RNF43, and therefore was used for further experiments. Subcellular fractionation experiments using the purified monoclonal RNF43 antibody, immunofluorescence and immunocytochemistry in cancer cells as well as immunohistochemical staining of normal intestine and colon cancer tissue demonstrated a clear nuclear localization of endogenous RNF43 not only *in vitro* but even more importantly also *in vivo*. However, the nuclear localization of overexpressed and endogenous RNF43 slightly differed. Overexpressed RNF43 was found in the ER outlining the nuclear membrane and in low amounts in the nucleoplasm in this study as well as by Sugiura *et al* (2008)[247], whereas endogenous RNF43 was distributed throughout the whole nuclear compartment. This observation might be explained by the strong overexpression of RNF43 under the cytomegalovirus (CMV) promoter of pcDNA4/TO vector used in this study and the pCMV-Tag4 vector used by Sugiura *et al* (2008)[247]. This promoter is active in a broad range of cell types and is the most commonly used promoter in mammalian expression plasmids[290-293]. It has been shown that massive overexpression of protein can lead to protein aggregations, which retain in the ER[294-297]. Thus, immunofluorescence staining of overexpressed RNF43 might mostly detect the protein in the ER and in the nuclear membrane than in the nucleoplasm. The usage of expression vectors with moderate promoter strength would minimize the strong overexpression, giving a more accurate result. Still, in this study a clear nuclear localization of overexpressed and endogenous RNF43 *in vitro* and more importantly *in vivo* was detected.

5.2. Function of endogenous RNF43

Overexpressed RNF43 was described to inhibit Wnt signaling when localized at the cellular membrane by ubiquitinating Fzd receptors and targeting them for degradation[214,282]. A similar inhibitory effect of overexpressed RNF43 on Wnt signaling was detected in this study. However, the proposed mechanism cannot explain how RNF43 inhibits Wnt signaling while being primarily expressed in the nucleus. Thus, it seems that RNF43 might have diverse functions depending on its subcellular localization. Analysis of luciferase reporter experiments showed that RNF43 is able to inhibit Wnt signaling downstream of β-catenin. In fact, a physical interaction of RNF43 and TCF4 was found, embracing the region between the RING domain and amino acid G566 of RNF43, which led to a relocalization of TCF4 to the nuclear membrane, resulting in the inhibition of TCF/LEF transcriptional activity for Wnt target genes without disruption of the transcription complex. Increasing evidence demonstrate that subcellular localization of proteins is an important regulator of transcriptional activity. Proteins of the inner nuclear membrane have been shown to sequester transcription factors, thus limiting their transcriptional activity. For instance, interaction of c-Fos with lamin A or C at the nuclear membrane negatively regulates activating protein 1 (AP-1) while inducing cellular quiescence[298]. In addition, sequestering of β-catenin to the inner nuclear membrane by emerin prevents the nuclear accumulation of β-catenin resulting in inhibition of its transcriptional activity[299]. Furthermore, SUMOylation or deSUMOylation of TCF4 by different nuclear pore complex proteins were shown to enhance or inhibit its transcriptional activity, thereby regulating Wnt signaling in colon cancer cells[300].

In this context, a new model is here proposed in which RNF43 prevents TCF4 transcriptional activity by sequestering the transcription complex from the nucleoplasm to the nuclear membrane using a mechanism, which requires direct interaction with, but not degradation of, TCF4 by RNF43 in the nuclear compartment. This is also compatible with the findings that simultaneous mutagenesis of both NLS sites, but not of individual sites, in RNF43 abrogated nuclear localization resulting in translocation of RNF43 to the cytoplasm and impairing its inhibitory effect on Wnt signaling. In contrast, mutagenesis of the NLS sites in combination with the double mutation H292R / H295R in the RING domain of RNF43 did neither influence the subcellular localization nor the transactivating effect of $RNF43^{H292R}$, suggesting that this double mutation prevents the translocation of RNF43 induced by NLS mutations most likely by rearrangement of the protein conformation. Structure rearrangements have been observed due to inherent flexibility of some amino acid side-chains, which show different degrees of flexibility near mutation sites[301].

When analyzing the effect of endogenous RNF43 on Wnt signaling, the increased TCF/LEF transcriptional activity in cells with depleted endogenous wild-type RNF43 confirmed the Wnt inhibitory effect observed with overexpressed RNF43. Moreover, in cells with RNF43

knockdown, no relocalization of TCF4 towards the nuclear membrane was observed. These findings strongly support the new proposed mechanism by which nuclear RNF43 inhibits Wnt signaling, and provide evidence that endogenous RNF43 acts as tumor suppressor. Tumor suppressors are proteins, which restrain cells from uncontrolled cell growth by inhibiting cell proliferation and tumor development[302]. The best-characterized tumor suppressor is p53. Tumor protein 53 responds to diverse stress signals by orchestrating specific cellular responses, including transient cell cycle arrest, cellular senescence and apoptosis[303]. Loss of p53 due to mutations or LOH induced increased cell proliferation[304,305] and invasivness[306-308]. A further prominent example is the tumor suppressor APC. In colorectal cancer one *APC* mutation usually leads to a truncated protein, and the other is either a similar mutation or resulting in allelic loss[309]. In familial adenomatous polyposis a truncating *APC* mutation is inherited [36] and the other allele either harbors a similar mutation or, more rarely, is lost [310]. Loss of APC leads to hyperactivated Wnt signaling resulting in increased transcription of Wnt target genes[311], which drives cell proliferation *in vitro* and *in vivo*[311]. Loss of endogenous RNF43 resulted in enhanced cell proliferation, colony growth as well as invasive capacity of tumor cells. However, *in vivo,* homozygous inactivation of Rnf43 did not induce any discernible intestinal phenotype, suggesting that a backup system restores loss of Rnf43. This is in line with results of Koo *et al*. (2012). They observed no phenotype by deletion of Rnf43, but when Rnf43 and its homologue Znrf3 were deleted simultaneously, the proliferative compartment was clearly expanded[214], resembling the effects of deleted *Apc*[312].

5.3 Functional impact of RNF43 mutations

Mutations in *RNF43* are described in a number of tumors[250,251,256,263,265,281,313], supporting its role as a tumor suppressor. However, little is known about the functional significance of *RNF43* mutations. Recently, Jiang *et al* (2013) studied *RNF43* mutations identified in pancreatic cancer cell lines from the of Fzd receptor perspective. They observed a RNF43-dependend decrease of frizzled receptors in pancreatic cancer cell lines, which was impaired upon overexpression of RNF43^{F69C}, identified in PaTu 8988S cells. Since a new mode of action for RNF43 was identified in colorectal cancer, the impact of reported RNF43 mutations[65,251,263] as well as mutations detected by NGS sequencing were analyzed with regard to this novel mechanism. Overexpressed RNF43 mutants identified in pancreatic cancers were mostly expressed in the cytoplasm or once at the cellular membrane. Investigating the expression of RNF43 mutants detected in colorectal tumors showed protein localization in the cytoplasm or at nuclear membrane. According to the proposed mechanism by which RNF43 sequesters TCF4 to the nuclear membrane, it was expected that mutants found in the cytoplasm or at the cellular membrane would not interact with TCF4 and have no Wnt-inhibitory effect. Indeed, the Wnt inhibitory capacity of RNF43 was lost in these mutants.

Moreover, direct interaction of RNF43 and TCF4 as well as relocalization of TCF4 to the nuclear membrane was not detected. In contrast, two mutants were detected at the nuclear membrane upon overexpression and analysis of the TCF/LEF transcriptional activity showed a similar inhibitory effect as wild-type RNF43. These findings confirmed that inhibition of TCF4 transcriptional activity by RNF43 involves the tethering of the complex to the nuclear envelope. Thus, these mutations may represent a selective growth for colon cancer. *In vitro* analysis of overexpressed RNF43^{H292R} showed not a loss of function but a transactivation of Wnt signaling, indicating that this double mutation changed the tumor suppressor activity of RNF43 to an oncogenic activity. Moreover, secretion of Wnt proteins requires Porcupine, a membrane bound O-acyltransferase dedicated to Wnt posttranslational acylation[314,315]. This study could show that the enhancement of Wnt signaling resulting from the H292R / H295R mutation is not induced by increased autocrine Wnt signaling, since the presence of LGK974, a porcupine inhibitor, did not alter the Wnt transactivating effect of RNF43^{H292R} in colorectal cancer cells. This is compatible with the observation that porcupine inhibitors can reduce increased Wnt signaling, resulting from deletion of RNF43 in absence of constitutive activating mutations in the Wnt pathway[316,317].

In order to study the impact of RNF43 mutations under endogenous conditions, LS174T cells were used as a model cell line since two point mutations (K108E and R389H) were identified in the *RNF43* gene of these colorectal cancer cells. The endogenous mutant protein was detected in the nucleus as well as in the cytoplasm, suggesting that the point mutations induce partially relocalization of the protein toward cytoplasm. Knockdown of the mutated RNF43 did not change the TCF/LEF transcriptional activity in these cells. Moreover, no changes were observed in cell proliferation or invasion as well as colony growth after depletion of the endogenous mutated RNF43, suggesting that the tumor suppressor activity is lost. These findings are in line with results obtained under overexpression conditions, confirming that RNF43 mutations can induce loss of function of RNF43 *in vitro*.

Even more importantly is the functional relevance of such mutations *in vivo*. Since an oncogenic effect of H292R/H295R mutations in RNF43 was postulated due to its transactivating effect on Wnt signaling upon overexpression, these mutations were investigated in mice. Introduction of H292R/H295R mutations in the genomic locus of murine *Rnf43* resulted in intestinal crypt lesions with cell metaplasia as well as mucosa inflammation and increased cell numbers, already taking place in heterozygous mutants. In addition, the larger size of 4 to 12 day cultured organoids, derived from isolated intestinal crypts of homozygous Rnf43^{H292R} mice, compared to wild-type or heterozygous mice, confirmed the increased proliferative capacity of crypt cells having mutated Rnf43 *in vivo*. Moreover, it appears that these mutations generate a dominant Wnt-activating form of Rnf43, since the presence of non-mutated Znrf3 could not overcome the Wnt transactivation as it was

observed when Rnf43 was knocked out. The strong proliferative capacity induced by the H292R/H295R mutation implicate that these mutations might be sufficient to induce development of colorectal cancer. Thus, such mutations might have clinicopathological relevance in terms of a predictive biomarker for colorectal cancer.

5.4 Impact of RNF43 on tumor associated pathways

Continuous renewal of the intestinal epithelium not only requires Wnt signaling but also Notch signaling to maintain the balance between proliferation and differentiation. *In vivo* studies showed that both Notch and Wnt signaling are required for maintaining crypt cells in a proliferative state. Deletion of Notch target gene *Math1* in mice resulted in the loss of the intestinal proliferative compartment, despite high presence of Wnt signaling[318]. Conversely, enhanced Notch signaling is observed in APC^{min} mice, which display hyperactivation of Wnt signaling because of truncated Apc[319]. It is interesting to note that there is a direct molecular crosstalk between Wnt pathway proteins in Notch signaling. Different studies reported that Dvl directly interacts with Notch[320,321] as well as with the transcription factor RBPj[322], which results in inhibition of Notch signaling. In addition, Notch signaling is also regulated by the physically interaction between the intracellular domains of Notch 1 or Notch 2 with GSK3β[323]. Moreover, it has been shown that Hath1, the human homolog of Math1, inhibits cell proliferation and is downregulated by constitutively activated Wnt signaling[324] through proteasome-mediated degradation, initiated by GSK3β dependent phosphorylation[325].

In this context, overexpressed RNF43 was found to inhibit Notch signaling, indicating that RNF43 might act in Notch signaling. However, the mechanism by which RNF43 inhibits Notch signaling remains elusive and needs to be investigated. One possible approach might be to investigate whether RNF43 marks Notch pathway members for proteasomal degradation, fulfilling its E3 ubiquitin ligase function. Another option is to analyze whether RNF43 directly interacts with transcription factor RBPj, inducing a tethering of RBPj to the nuclear membrane, as it occurs with TCF4 in Wnt signaling. Finally, the turnover of Notch receptors at the cellular membrane could be analyzed in presence and absence of RNF43 to study whether RNF43 targets Notch, similar to the mechanism described by Koo *et al.* (2012). This is also compatible with the findings that RNF43 is frequently mutated in pancreatic cancer patients[250,265,281] where Notch signaling plays a more important role than Wnt signaling.

In addition, RNF43 is mutated in gastric tumors[254,255], where deregulated STAT signaling drives tumor formation, indicating that RNF43 might also be involved in the STAT pathway. Furthermore, studies showed that inhibition of Stat3 signaling prevents intestinal tumor growth in APC^{min} mice[326], and conversely WNT3A stimulation of cells activated STAT3 signaling[327]. Overexpression of RNF43 inhibited STAT3 signaling, although the mechanism is not clear until now. A possible mode of action could be that RNF43 ubiquitinates STAT3 for

proteasomal degradation. A physical interaction of RNF43 with Stat3 inhibiting its transcriptional activity could also be considered, similar to RNF43-TCF4 interaction. In contrast, overexpression of RNF43 did not influence NFκB signaling, another important pathway in development of gastric cancer[328]. However, not all gastric tumors have deregulated STAT3 and NFκB signaling, suggesting that only gastric tumors with deregulated Stat3 signaling may benefit from RNF43 activity. Thus, identifying and mimicking the inhibitory activity of RNF43 in Notch and STAT3 signaling may provide a helpful tool to treat gastric and pancreatic cancer.

5.5 Conclusion

Altogether, this study showed that RNF43 is a tumor suppressor under overexpressed and endogenous conditions, which acts by preventing TCF4 transcriptional activity through sequestering the RNF43-TCF4 complex to the nuclear membrane. Moreover, wild-type RNF43 acts in the presence of constitutive activation of Wnt signaling found in many colorectal tumors.

These findings may enable novel therapeutic strategies for the development of colorectal cancers arising from mutation of the Wnt pathway, where previous therapeutic approaches failed because of targeting Wnt signaling upstream of β-catenin. Furthermore, this study showed that loss of RNF43 and mutations in the *RNF43* gene lead to inactivation or transactivation of Wnt signaling, suggesting RNF43 as a biomarker for colorectal cancer. Characterization of murine and human organoids derived from isolated healthy or tumorigenic intestinal samples can give further information about the effects of RNF43/Rnf43 mutations *in vivo*, contributing to the validation of RNF43 as a biomarker. Moreover, the discovery of many frameshift mutations in *RNF43* may open a promising therapeutic approach of exclusively targeting RNF43 neo-epitopes for adoptive T cell transfer. Therefor, the expression and presentation of RNF43 neo-epitopes have to be confirmed *in vitro* as well as *in vivo*, by introducing frameshift mutations in the genomic locus of RNF43/Rnf43 using CRISPR/Cas9. Finally, RNF43 was found to inhibit also Notch and STAT3, but not NFκB, signaling, indicating that RNF43 might be involved in these pathways. This opens the door for a RNF43 based therapeutic treatment for STAT3-dependent gastric cancer patients and more importantly for pancreatic cancer patients.

6 Registers

6.1 Abbreviations

°C	degree Celsius
ab	antibody
ACF	aberrant crypt foci
Amp	ampicillin
AP-1	activating protein 1
APC	adenomatours polyposis
APCDD1	adenomatosis polyposis coli down-regulated 1
APS	ammonium persulfate
Ascl2	Achaete–Scute homologue 2
ATCC	American Type Culture Collection
ATP	adenosine triphosphate
BMP	bone morphogenic protein
bp	base pairs
BRCA1	breast cancer 1
BSA	bovine serum albumin
Ca^{2+}	calcium
CamK2	calmodulin-dependent kinase II
CBC	crypt base columnar
Cbl	Casitas B-lineage Lymphoma
CD	Crohn’s disease
CDC4	cell division control protein 4
cDNA	complementary DNA
CK1	casein kinase
cm	centimeter
CRC	colorectal cancer
CtBP	C-terminal binding protein
DAG	diacylglycerol
ddH_2O	double distilled water
DDR	DNA damage response

Dkk	dickkopf
DMEM	Dulbeccos modified eagle medium
DMSO	dimethylsufoxid
dn	dominant negative
DNA	deoxyribonucleic acid
dNTP	deoxynucleotids
Dsh	dishevelled murine
DTT	dithiotreitol
Dvl	dishevelled human
ECL	enhanced chemoluminescence
EDTA	ethylenediaminetetraacetic acid
EGTA	ethylene glycol tetraacetic acid
EphB2	ephrin receptor B2
ER	endoplasmic reticulum
FAP	familial adenomatous polyposis
FCS	fetal calf serum
FGF	fibroblast growth factor
fs	frameshift
Fzd	frizzled
g	gram
GF	growth factor
GFP	green fluorescence protein
GI	gastrointestinal tract
GPCR	G-protein coupled receptor
gRNA	guide RNA
GSK3β	glycogen synthase kinase 3beta
h	hour
H&E	Hematoxylin and Eosin staining
HEPES	4-(2-hydroxyethyl)-1-piperazineethanesulfonic acid
HNPCC	hereditary non-polyposis colon cancer
HPLC	high performance liquid chromatography

HPP	hyperplastic polyposis
IF	immunofluorescence
IGFBP	insulin-like growth factor binding protein
IMEM	Iscove's Modified Dulbecco's Medium
$InsP_3$	inositol triphosphate
IP	immunoprecipitation
ISC	intestinal stem cell
JNK	Jun kinase
JPS	juvenile polyposis syndrome
kB	kilo bases
kDa	kilo Dalton
KRAS	Kirsten rat sarcoma viral onogocene homolog
LB	Luria Bertani
LDL	low density lipoprotein
LEF	lymphoid enhancer factor
$LGR5^+$	Leucin-rich repeat-containing G protein-coupled receptor 5
LOH	loss of hereozygosity
LRP	low density lipoprotein receptor-related protein
mA	milliampere
MAP	MUTYH-associated polyposis
MAPK	mitogen activated protein kinase
MATH	meprin and TRAF homology
Mdm	Mouse double minute 2 homolog
mg	milligram
min	minute
mL	milliliter
MLH	mutL homolog
mM	millimolar
MMP	matrix metalloprotease
MMR	mismatch repair
mRNA	messenger RNA

MSH	mutS homolog
n	number of replicates
NEB	New England Biolabs
NFAT	nuclear factor of activated T cells
NFκB	nuclear factor kappa-light-chain-enhancer of activated B
ng	nanogram
NGS	Next generation sequencing
NLS	nuclear leading sequence
nm	nanometer
OD_{570}	optical density at 570 nm
Olfm4	olfactomedin 4
PBS	phosphate-buffered saline
PCP	planar cell polarity
PCR	polymerase chain reaction
PFA	p-formaldehyde
PJS	Peuth-Jeghers syndrome
PLC	phospholipase C
PSF	polypyrimidine tract-binding protein-associated splicing factor
$PtdIns(4,5)P_2$	phosphatidylinositol-4,5-bisphosphate
qRT-PCR	quantitative Real-time PCR
RING	Really interesting new gene
RNA	ribonucleic acid
RNF	RING finger
RNF43	human RING finger protein 43
$RNF43^{H292R}$	human RNF43 with mutated RING domain H292R/H295R
Rnf43	murine RING finger protein 43
$Rnf43^{H292R}$	murine RNF43 with mutated RING domain H292R/H295R
ROCK	Rho associated kinase
rpm	rounds per million
Rspo	R-spondin
RT	room temperature

RTK	receptor tyrosine kinase
SCM	Single crypt medium
SDS	Sodium dodecyl sulfate
sec	second
sFRP	secreted frizzled- related proteins
shRNA	short hairpin RNA
siRNA	small interfering RNA
SMAD4	SMAD family member 4
SP	signal peptide
STAT3	human signal transducer and activator of transcription 3
Stat3	murine signal transducer and activator of transcription 3
TA	transit amplifying
TAE	Tris-Acetat-EDTA
TCF	T cell factor
TEMED	N,N,N',N'-tetramethylethylenediamine
TGFβ	transforming growth factor beta
TM	Melting temperature
TM	transmembrane domain
TNF	tumor necrosis factor
TP53	tumor protein 53
TRAF5	tumor necrosis factor receptor-associated factor 5
UC	ulcerative colitits
UICC	Union for International Cancer Control
V	volt
VHL	von Hippel-Lindau
w/v	weight per volume
Waif1/5T4	Wnt-activated inhibitory factor 1
WB	western blot
wg	wingless
WIF-1	Wnt-inhibitory factor 1
wt	wild-type

xg	times Earth's gravitational force
ZNRF3	human Zink and Ring finger 3
Znrf3	murine Zink and Ring finger 3
µL	microliter
µM	micromolar
µm	micrometer

6.2 List of Figures

6.3 List of Tables

6.4 Bibliography

1 *human digestive system. In Encyclopædia Britannica*, <http://www.britannica.com/science/human-digestive-system> (2016).

2 Pavelka, M. & Roth, J. *Funktionelle Ultrastruktur: Atlas der Biologie und Pathologie von Geweben*. 1 edn, (Springer Vienna, 2005).

3 Heath, J. P. Epithelial cell migration in the intestine. *Cell Biol Int* **20**, 139-146, doi:10.1006/cbir.1996.0018 (1996).

4 Porter, E. M., Bevins, C. L., Ghosh, D. & Ganz, T. The multifaceted Paneth cell. *Cellular and molecular life sciences* **59**, 156-170 (2002).

5 Radtke, F., Clevers, H. & Riccio, O. From gut homeostasis to cancer. *Current molecular medicine* **6**, 275-289 (2006).

6 Krause, W. J., Yamada, J. & Cutts, J. H. Quantitative distribution of enteroendocrine cells in the gastrointestinal tract of the adult opossum, Didelphis virginiana. *Journal of anatomy* **140 (Pt 4)**, 591-605 (1985).

7 REHFELD, J. F. The New Biology of Gastrointestinal Hormones. *Physiological Reviews* **78**, 1087-1108 (1998).

8 Ayabe, T. *et al.* Secretion of microbicidal alpha-defensins by intestinal Paneth cells in response to bacteria. *Nature immunology* **1**, 113-118, doi:10.1038/77783 (2000).

9 Ganz, T. Paneth cells--guardians of the gut cell hatchery. *Nature immunology* **1**, 99-100, doi:10.1038/77884 (2000).

10 Gerbe, F., Legraverend, C. & Jay, P. The intestinal epithelium tuft cells: specification and function. *Cell Mol Life Sci* **69**, 2907-2917, doi:10.1007/s00018-012-0984-7 (2012).

11 Valdivia, L. E. *et al.* Lef1-dependent Wnt/β-catenin signalling drives the proliferative engine that maintains tissue homeostasis during lateral line development. *Development* **138**, 3931-3941, doi:10.1242/dev.062695 (2011).

12 Artavanis-Tsakonas, S., Rand, M. D. & Lake, R. J. Notch Signaling: Cell Fate Control and Signal Integration in Development. *Science* **284**, 770-776, doi:10.1126/science.284.5415.770 (1999).

13 Dunker, N. & Krieglstein, K. Targeted mutations of transforming growth factor-beta genes reveal important roles in mouse development and adult homeostasis. *Eur J Biochem* **267**, 6982-6988 (2000).

14 Ingham, P. W. & McMahon, A. P. Hedgehog signaling in animal development: paradigms and principles. *Genes & Development* **15**, 3059-3087, doi:10.1101/gad.938601 (2001).

15 Hooper, J. E. & Scott, M. P. Communicating with Hedgehogs. *Nat Rev Mol Cell Biol* **6**, 306-317, doi:10.1038/nrm1612 (2005).

16 Massagué, J., Blain, S. W. & Lo, R. S. TGF[beta] Signaling in Growth Control, Cancer, and Heritable Disorders. *Cell* **103**, 295-309, doi:doi: 10.1016/S0092-8674(00)00121-5 (2000).

17 Polakis, P. Wnt signaling and cancer. *Genes & development* **14** (2000).

18 Radtke, F. & Raj, K. The role of Notch in tumorigenesis: oncogene or tumour suppressor? *Nat Rev Cancer* **3**, 756-767, doi:10.1038/nrc1186 (2003).

19 Reya, T. & Clevers, H. Wnt signalling in stem cells and cancer. *Nature* **434**, 843-850, doi:10.1038/nature03319 (2005).

20 Fitzmaurice, C. *et al.* The Global Burden of Cancer 2013. *JAMA oncology* **1**, 505-527, doi:10.1001/jamaoncol.2015.0735 (2015).

21 Stewart, B. W., Wild, C., International Agency for Research on Cancer & World Health Organization. *World cancer report 2014*. (International Agency for Research on Cancer, WHO Press, 2014).

22 Torre, L. A. *et al.* Global cancer statistics, 2012. *CA: A Cancer Journal for Clinicians* **65**, 87-108, doi:10.3322/caac.21262 (2015).

23 Cheah, P. Y. Recent advances in colorectal cancer genetics and diagnostics. *Crit Rev Oncol Hematol* **69**, 45-55, doi:10.1016/j.critrevonc.2008.08.001 (2009).

24 Haggar, F. A. & Boushey, R. P. Colorectal Cancer Epidemiology: Incidence, Mortality, Survival, and Risk Factors. *Clinics in Colon and Rectal Surgery* **22**, 191-197, doi:10.1055/s-0029-1242458 (2009).

25 *National Institutes of Health (NIH)*, <http://www.nih.gov/> (

26 Center, M. M., Jemal, A. & Ward, E. International trends in colorectal cancer incidence rates. *Cancer Epidemiol Biomarkers Prev* **18**, 1688-1694, doi:10.1158/1055-9965.EPI-09-0090 (2009).

27 Parkin, D. M., Bray, F. I. & Devesa, S. S. Cancer burden in the year 2000. The global picture. *Eur J Cancer* **37**, 4-66 (2001).

28 Meyerhardt, J. A. *et al.* Association of dietary patterns with cancer recurrence and survival in patients with stage III colon cancer. *JAMA* **298**, 754-764, doi:10.1001/jama.298.7.754 (2007).

29 Tsoi, K. K. *et al.* Cigarette smoking and the risk of colorectal cancer: a meta-analysis of prospective cohort studies. *Clin Gastroenterol Hepatol* **7**, 682-688 e681-685, doi:10.1016/j.cgh.2009.02.016 (2009).

30 Cho, E., Lee, J. E., Rimm, E. B., Fuchs, C. S. & Giovannucci, E. L. Alcohol consumption and the risk of colon cancer by family history of colorectal cancer. *Am J Clin Nutr* **95**, 413-419, doi:10.3945/ajcn.111.022145 (2012).

31 Campos, F. G. *et al.* Diet and colorectal cancer: current evidence for etiology and prevention. *Nutricion hospitalaria* **20**, 18-25 (2005).

32 Takayama, T. *et al.* Aberrant crypt foci: detection, gene abnormalities, and clinical usefulness. *Clin Gastroenterol Hepatol* **3**, S42-45, doi:doi: 10.1016/S1542-3565(05)00257-0 (2005).

33 Thibodeau, S. N., Bren, G. & Schaid, D. Microsatellite instability in cancer of the proximal colon. *Science* **260** (1993).

34 Fearon, E. R., Hamilton, S. R. & Vogelstein, B. Clonal analysis of human colorectal tumors. *Science* **238**, 193-197 (1987).

35 Kalady, M. F. & Heald, B. Diagnostic Approach to Hereditary Colorectal Cancer Syndromes. *Clin Colon Rectal Surg* **28**, 205-214, doi:10.1055/s-0035-1564432 (2015).

36 Galiatsatos, P. & Foulkes, W. D. Familial Adenomatous Polyposis. *Am J Gastroenterol* **101**, 385-398 (2006).

37 Vasen, H. F., den Hartog Jager, F. C., Menko, F. H. & Nagengast, F. M. Screening for hereditary non-polyposis colorectal cancer: a study of 22 kindreds in The Netherlands. *Am J Med* **86**, 278-281 (1989).

38 Stoffel, E. M. Lynch Syndrome/Hereditary Non-polyposis Colorectal Cancer (HNPCC). *Minerva Gastroenterol Dietol* **56**, 45-53 (2010).

39 Lichtenstein, P. *et al.* Environmental and heritable factors in the causation of cancer—analyses of cohorts of twins from Sweden, Denmark, and Finland. *New England Journal of Medicine* **343**, 78-85 (2000).

40 Grady, W. M. & Markowitz, S. D. Hereditary colon cancer genes. *Methods Mol Biol* **222**, 59-83, doi:10.1385/1-59259-328-3:059 (2003).

41 Jasperson, K. W., Tuohy, T. M., Neklason, D. W. & Burt, R. W. Hereditary and familial colon cancer. *Gastroenterology* **138**, 2044-2058, doi:10.1053/j.gastro.2010.01.054 (2010).

42 Baumgart, D. C. & Sandborn, W. J. Crohn's disease. *Lancet (London, England)* **380**, 1590-1605, doi:10.1016/s0140-6736(12)60026-9 (2012).

43 Cho, J. H. & Brant, S. R. Recent insights into the genetics of inflammatory bowel disease. *Gastroenterology* **140**, 1704-1712, doi:10.1053/j.gastro.2011.02.046 (2011).

44 de Miranda, N. F. *et al.* MUTYH-associated polyposis carcinomas frequently lose HLA class I expression - a common event amongst DNA-repair-deficient colorectal cancers. *J Pathol* **219**, 69-76, doi:10.1002/path.2569 (2009).

45 Tomlinson, I. P. & Houlston, R. S. Peutz-Jeghers syndrome. *Journal of medical genetics* **34**, 1007-1011 (1997).

46 Hearle, N. *et al.* Frequency and spectrum of cancers in the Peutz-Jeghers syndrome. *Clin Cancer Res* **12**, 3209-3215, doi:10.1158/1078-0432.ccr-06-0083 (2006).

47 Brosens, L. A., Langeveld, D., van Hattem, W. A., Giardiello, F. M. & Offerhaus, G. J. Juvenile polyposis syndrome. *World J Gastroenterol* **17**, 4839-4844, doi:10.3748/wjg.v17.i44.4839 (2011).

48 Hyman, N. H., Anderson, P. & Blasyk, H. Hyperplastic polyposis and the risk of colorectal cancer. *Diseases of the colon and rectum* **47**, 2101-2104, doi:10.1007/s10350-004-0709-6 (2004).

49 Gala, M. & Chung, D. C. Hereditary Colon Cancer Syndromes. *Seminars in Oncology* **38**, 490-499, doi:doi: 10.1053/j.seminoncol.2011.05.003 (2011).

50 Fearon, E. R., Vogelstein, B. & others. A genetic model for colorectal tumorigenesis. *Cell* **61**, 759-767 (1990).

51 Yang, J. *et al.* Adenomatous polyposis coli (APC) differentially regulates beta-catenin phosphorylation and ubiquitination in colon cancer cells. *The Journal of biological chemistry* **281**, 17751-17757, doi:10.1074/jbc.M600831200 (2006).

52 Powell, S. M. *et al.* APC mutations occur early during colorectal tumorigenesis. *Nature* **359**, 235-237, doi:10.1038/359235a0 (1992).

53 Rijsewijk, F. *et al.* The Drosophila homology of the mouse mammary oncogene int-1 is identical to the segment polarity gene wingless. *Cell* **50**, 649-657 (1987).

54 Solomon, E. *et al.* Chromosome 5 allele loss in human colorectal carcinomas. *Nature* **328**, 616-619, doi:10.1038/328616a0 (1987).

55 Okamoto, M. *et al.* Loss of constitutional heterozygosity in colon carcinoma from patients with familial polyposis coli. *Nature* **331**, 273-277, doi:10.1038/331273a0 (1988).

56 Hahn, S. A. *et al.* DPC4, a candidate tumor suppressor gene at human chromosome 18q21.1. *Science* **271**, 350-353 (1996).

57 Takagi, Y. *et al.* Somatic alterations of the DPC4 gene in human colorectal cancers in vivo. *Gastroenterology* **111**, 1369-1372 (1996).

58 Miyaki, M. & Kuroki, T. Role of Smad4 (DPC4) inactivation in human cancer. *Biochem Biophys Res Commun* **306**, 799-804 (2003).

59 Koyama, M., Ito, M., Nagai, H., Emi, M. & Moriyama, Y. Inactivation of both alleles of the DPC4/SMAD4 gene in advanced colorectal cancers: identification of seven novel somatic mutations in tumors from Japanese patients. *Mutation research* **406**, 71-77 (1999).

60 De Bosscher, K., Hill, C. S. & Nicolas, F. J. Molecular and functional consequences of Smad4 C-terminal missense mutations in colorectal tumour cells. *The Biochemical journal* **379**, 209-216, doi:10.1042/bj20031886 (2004).

61 Watanabe, T. *et al.* Molecular predictors of survival after adjuvant chemotherapy for colon cancer. *N Engl J Med* **344**, 1196-1206, doi:10.1056/nejm200104193441603 (2001).

62 Welcker, M. & Clurman, B. E. FBW7 ubiquitin ligase: a tumour suppressor at the crossroads of cell division, growth and differentiation. *Nat Rev Cancer* **8**, 83-93, doi:10.1038/nrc2290 (2008).

63 Grim, J. E. *et al.* Isoform- and cell cycle-dependent substrate degradation by the Fbw7 ubiquitin ligase. *The Journal of cell biology* **181**, 913-920, doi:10.1083/jcb.200802076 (2008).

64 Miyaki, M. *et al.* Somatic mutations of the CDC4 (FBXW7) gene in hereditary colorectal tumors. *Oncology* **76**, 430-434, doi:10.1159/000217811 (2009).

65 Forbes, S. A. *et al.* COSMIC: exploring the world's knowledge of somatic mutations in human cancer. *Nucleic Acids Res* **43**, D805-811, doi:10.1093/nar/gku1075 (2015).

66 Rajagopalan, H. *et al.* Inactivation of hCDC4 can cause chromosomal instability. *Nature* **428**, 77-81, doi:10.1038/nature02313 (2004).

67 Kemp, Z. *et al.* CDC4 mutations occur in a subset of colorectal cancers but are not predicted to cause loss of function and are not associated with chromosomal instability. *Cancer Res* **65**, 11361-11366, doi:10.1158/0008-5472.can-05-2565 (2005).

68 Isobe, M., Emanuel, B. S., Givol, D., Oren, M. & Croce, C. M. Localization of gene for human p53 tumour antigen to band 17p13. *Nature* **320**, 84-85, doi:10.1038/320084a0 (1986).

69 Baker, S. J. *et al.* p53 gene mutations occur in combination with 17p allelic deletions as late events in colorectal tumorigenesis. *Cancer Res* **50**, 7717-7722 (1990).

70 Iacopetta, B. TP53 mutation in colorectal cancer. *Human mutation* **21**, 271-276, doi:10.1002/humu.10175 (2003).

71 Rodrigues, N. R. *et al.* p53 mutations in colorectal cancer. *Proc Natl Acad Sci U S A* **87**, 7555-7559 (1990).

72 Liu, Y. & Bodmer, W. F. Analysis of P53 mutations and their expression in 56 colorectal cancer cell lines. *Proc Natl Acad Sci U S A* **103**, 976-981, doi:10.1073/pnas.0510146103 (2006).

73 Li, X. L., Zhou, J., Chen, Z. R. & Chng, W. J. P53 mutations in colorectal cancer - molecular pathogenesis and pharmacological reactivation. *World J Gastroenterol* **21**, 84-93, doi:10.3748/wjg.v21.i1.84 (2015).

74 Chang, F. H. *et al.* Mutations in the p53 tumor suppressor gene in colorectal cancer in Taiwan. *Kaohsiung J Med Sci* **19**, 151-158, doi:10.1016/S1607-551X(09)70464-4 (2003).

75 Vogelstein, B. *et al.* Genetic alterations during colorectal-tumor development. *N Engl J Med* **319**, 525-532, doi:10.1056/NEJM198809013190901 (1988).

76 Forrester, K., Almoguera, C., Han, K., Grizzle, W. E. & Perucho, M. Detection of high incidence of K-ras oncogenes during human colon tumorigenesis. *Nature* **327**, 298-303, doi:10.1038/327298a0 (1987).

77 Bos, J. L. *et al.* Prevalence of ras gene mutations in human colorectal cancers. *Nature* **327**, 293-297, doi:10.1038/327293a0 (1987).

78 Andreyev, H. J., Norman, A. R., Cunningham, D., Oates, J. R. & Clarke, P. A. Kirsten ras mutations in patients with colorectal cancer: the multicenter "RASCAL" study. *Journal of the National Cancer Institute* **90**, 675-684 (1998).

79 Andreyev, H. J. *et al.* Kirsten ras mutations in patients with colorectal cancer: the 'RASCAL II' study. *Br J Cancer* **85**, 692-696, doi:10.1054/bjoc.2001.1964 (2001).

80 Vogelstein, B. & Kinzler, K. W. Cancer genes and the pathways they control. *Nat Med* **10**, 789-799 (2004).

81 Pretlow, T. P., Brasitus, T. A., Fulton, N. C., Cheyer, C. & Kaplan, E. L. K-ras mutations in putative preneoplastic lesions in human colon. *Journal of the National Cancer Institute* **85**, 2004-2007 (1993).

82 Jen, J. *et al.* Molecular determinants of dysplasia in colorectal lesions. *Cancer Res* **54**, 5523-5526 (1994).

83 Namba, H. *et al.* Clinical implication of hot spot BRAF mutation, V599E, in papillary thyroid cancers. *The Journal of clinical endocrinology and metabolism* **88**, 4393-4397, doi:10.1210/jc.2003-030305 (2003).

84 Li, W. Q. *et al.* BRAF mutations are associated with distinctive clinical, pathological and molecular features of colorectal cancer independently of microsatellite instability status. *Mol Cancer* **5**, 2, doi:10.1186/1476-4598-5-2 (2006).

85 Benlloch, S. *et al.* Detection of BRAF V600E mutation in colorectal cancer: comparison of automatic sequencing and real-time chemistry methodology. *The Journal of molecular diagnostics : JMD* **8**, 540-543, doi:10.2353/jmoldx.2006.060070 (2006).

86 Rajagopalan, H. *et al.* Tumorigenesis: RAF/RAS oncogenes and mismatch-repair status. *Nature* **418**, 934, doi:10.1038/418934a (2002).

87 Aberle, H., Schwartz, H. & Kemler, R. Cadherin-catenin complex: protein interactions and their implications for cadherin function. *J Cell Biochem* **61**, 514-523, doi:10.1002/(SICI)1097-4644(19960616)61:4<514::AID-JCB4>3.0.CO;2-R (1996).

88 McCrea, P. D., Turck, C. W. & Gumbiner, B. A homolog of the armadillo protein in Drosophila (plakoglobin) associated with E-cadherin. *Science* **254**, 1359-1361 (1991).

89 Behrens, J. *et al.* Functional interaction of beta-catenin with the transcription factor LEF-1. *Nature* **382**, 638-642, doi:10.1038/382638a0 (1996).

90 Morin, P. J. *et al.* Activation of beta-catenin-Tcf signaling in colon cancer by mutations in beta-catenin or APC. *Science* **275**, 1787-1790 (1997).

91 Polakis, P. The oncogenic activation of beta-catenin. *Curr Opin Genet Dev* **9**, 15-21 (1999).

92 Rubinfeld, B. *et al.* Stabilization of beta-catenin by genetic defects in melanoma cell lines. *Science* **275**, 1790-1792 (1997).

93 Muller, O., Nimmrich, I., Finke, U., Friedl, W. & Hoffmann, I. A beta-catenin mutation in a sporadic colorectal tumor of the RER phenotype and absence of beta-catenin germline mutations in FAP patients. *Genes, chromosomes & cancer* **22**, 37-41 (1998).

94 Bronner, C. E. *et al.* Mutation in the DNA mismatch repair gene homologue hMLH1 is associated with hereditary non-polyposis colon cancer. *Nature* **368**, 258-261, doi:10.1038/368258a0 (1994).

95 Drummond, J. T., Li, G. M., Longley, M. J. & Modrich, P. Isolation of an hMSH2-p160 heterodimer that restores DNA mismatch repair to tumor cells. *Science* **268**, 1909-1912 (1995).

96 Fishel, R. *et al.* The human mutator gene homolog MSH2 and its association with hereditary nonpolyposis colon cancer. *Cell* **75**, 1027-1038 (1993).

97 Leach, F. S. *et al.* Mutations of a mutS homolog in hereditary nonpolyposis colorectal cancer. *Cell* **75**, 1215-1225 (1993).

98 Morrison, B. C. B. S., Lescoe, P. W. G. S. L. & Lipford, M. K. M. E. C. Mutation in the DNA mismatch repair gene homologue hMLH1 is associated with hereditary non-polyposis colon cancer. *Nature* **368** (1994).

99 Nicolaides, N. C. *et al.* Mutations of two PMS homologues in hereditary nonpolyposis colon cancer. *Nature* **371**, 75-80, doi:10.1038/371075a0 (1994).

100 Aaltonen, L. A. *et al.* Clues to the pathogenesis of familial colorectal cancer. *Science* **260**, 812-816 (1993).

101 Ionov, Y., Peinado, M. A., Malkhosyan, S., Shibata, D. & Perucho, M. Ubiquitous somatic mutations in simple repeated sequences reveal a new mechanism for colonic carcinogenesis. *Nature* **363**, 558-561, doi:10.1038/363558a0 (1993).

102 Peltomäki, P. Role of DNA Mismatch Repair Defects in the Pathogenesis of Human Cancer. *Journal of Clinical Oncology* **21**, 1174-1179, doi:10.1200/jco.2003.04.060 (2003).

103 Vilar, E. & Gruber, S. B. Microsatellite instability in colorectal cancer-the stable evidence. *Nat Rev Clin Oncol* **7**, 153-162, doi:10.1038/nrclinonc.2009.237 (2010).

104 Peltomaki, P. & Vasen, H. F. Mutations predisposing to hereditary nonpolyposis colorectal cancer: database and results of a collaborative study. The International Collaborative Group on Hereditary Nonpolyposis Colorectal Cancer. *Gastroenterology* **113**, 1146-1158 (1997).

105 Liu, B. *et al.* Mismatch repair gene defects in sporadic colorectal cancers with microsatellite instability. *Nature genetics* **9**, 48-55 (1995).

106 Vogelstein, B. *et al.* Cancer genome landscapes. *Science* **339**, 1546-1558, doi:10.1126/science.1235122 (2013).

107 Lemieux, E., Cagnol, S., Beaudry, K., Carrier, J. & Rivard, N. Oncogenic KRAS signalling promotes the Wnt/beta-catenin pathway through LRP6 in colorectal cancer. *Oncogene* **34**, 4914-4927, doi:10.1038/onc.2014.416 (2015).

108 Nakamura, T., Tsuchiya, K. & Watanabe, M. Crosstalk between Wnt and Notch signaling in intestinal epithelial cell fate decision. *Journal of Gastroenterology* **42**, 705-710, doi:10.1007/s00535-007-2087-z (2007).

109 Massague, J. TGFbeta in Cancer. *Cell* **134**, 215-230, doi:10.1016/j.cell.2008.07.001 (2008).

110 Nandan, M. O. & Yang, V. W. An Update on the Biology of RAS/RAF Mutations in Colorectal Cancer. *Current colorectal cancer reports* **7**, 113-120, doi:10.1007/s11888-011-0086-1 (2011).

111 Bleeker, F. E. *et al.* AKT1(E17K) in human solid tumours. *Oncogene* **27**, 5648-5650, doi:10.1038/onc.2008.170 (2008).

112 Carpten, J. D. *et al.* A transforming mutation in the pleckstrin homology domain of AKT1 in cancer. *Nature* **448**, 439-444, doi:10.1038/nature05933 (2007).

113 Wodarz, A. & Nusse, R. Mechanisms of Wnt signaling in development. *Annu Rev Cell Dev Biol* **14**, 59-88, doi:10.1146/annurev.cellbio.14.1.59 (1998).

114 Huelsken, J. & Birchmeier, W. New aspects of Wnt signaling pathways in higher vertebrates. *Current Opinion in Genetics & Development* **11**, 547-553, doi:doi: 10.1016/S0959-437X(00)00231-8 (2001).

115 van Amerongen, R. & Nusse, R. Towards an integrated view of Wnt signaling in development. *Development* **136**, 3205-3214, doi:10.1242/dev.033910 (2009).

116 Cadigan, K. M. & Nusse, R. Wnt signaling: a common theme in animal development. *Genes & Development* **11**, 3286-3305, doi:10.1101/gad.11.24.3286 (1997).

117 Willert, K. *et al.* Wnt proteins are lipid-modified and can act as stem cell growth factors. *Nature* **423**, 448-452, doi:10.1038/nature01611 (2003).

118 Vinson, C. R., Conover, S. & Adler, P. N. A Drosophila tissue polarity locus encodes a protein containing seven potential transmembrane domains. *Nature* **338**, 263-264, doi:10.1038/338263a0 (1989).

119 Bhanot, P. *et al.* A new member of the frizzled family from Drosophila functions as a Wingless receptor. *Nature* **382**, 225-230, doi:10.1038/382225a0 (1996).

120 Tamai, K. *et al.* LDL-receptor-related proteins in Wnt signal transduction. *Nature* **407**, 530-535, doi:10.1038/35035117 (2000).

121 Mao, J. *et al.* Low-density lipoprotein receptor-related protein-5 binds to Axin and regulates the canonical Wnt signaling pathway. *Mol Cell* **7**, 801-809 (2001).

122 Pinson, K. I., Brennan, J., Monkley, S., Avery, B. J. & Skarnes, W. C. An LDL-receptor-related protein mediates Wnt signalling in mice. *Nature* **407**, 535-538, doi:10.1038/35035124 (2000).

123 Kelly, O. G., Pinson, K. I. & Skarnes, W. C. The Wnt co-receptors Lrp5 and Lrp6 are essential for gastrulation in mice. *Development* **131**, 2803-2815, doi:10.1242/dev.01137 (2004).

124 Wong, H. C. *et al.* Direct binding of the PDZ domain of Dishevelled to a conserved internal sequence in the C-terminal region of Frizzled. *Mol Cell* **12**, 1251-1260 (2003).

125 Stamos, J. L. & Weis, W. I. The beta-catenin destruction complex. *Cold Spring Harbor perspectives in biology* **5**, a007898, doi:10.1101/cshperspect.a007898 (2013).

126 Logan, C. Y. & Nusse, R. The Wnt signaling pathway in development and disease. *Annu. Rev. Cell Dev. Biol.* **20**, 781-810 (2004).

127 He, X., Semenov, M., Tamai, K. & Zeng, X. LDL receptor-related proteins 5 and 6 in Wnt/beta-catenin signaling: arrows point the way. *Development* **131**, 1663-1677, doi:10.1242/dev.01117 (2004).

128 Hart, M. *et al.* The F-box protein β-TrCP associates with phosphorylated β-catenin and regulates its activity in the cell. *Current Biology* **9**, 207-211, doi:10.1016/S0960-9822(99)80091-8.

129 Shitashige, M., Hirohashi, S. & Yamada, T. Wnt signaling inside the nucleus. *Cancer Sci* **99**, 631-637, doi:10.1111/j.1349-7006.2007.00716.x (2008).

130 Gong, Y., Mo, C. & Fraser, S. E. Planar cell polarity signalling controls cell division orientation during zebrafish gastrulation. *Nature* **430**, 689-693 (2004).

131 Adler, P. N. Planar signaling and morphogenesis in Drosophila. *Dev Cell* **2**, 525-535 (2002).

132 Habas, R., Kato, Y. & He, X. Wnt/Frizzled activation of Rho regulates vertebrate gastrulation and requires a novel Formin homology protein Daam1. *Cell* **107**, 843-854 (2001).

133 Marlow, F., Topczewski, J., Sepich, D. & Solnica-Krezel, L. Zebrafish Rho kinase 2 acts downstream of Wnt11 to mediate cell polarity and effective convergence and extension movements. *Current biology : CB* **12**, 876-884 (2002).

134 Kuhl, M., Sheldahl, L. C., Park, M., Miller, J. R. & Moon, R. T. The Wnt/Ca2+ pathway: a new vertebrate Wnt signaling pathway takes shape. *Trends Genet* **16**, 279-283 (2000).

135 Kühl, M., Sheldahl, L. C., Park, M., Miller, J. R. & Moon, R. T. The Wnt/Ca2+ pathway: a new vertebrate Wnt signaling pathway takes shape. *Trends in Genetics* **16**, 279-283, doi:doi: 10.1016/S0168-9525(00)02028-X (2000).

136 Miller, J. R., Hocking, A. M., Brown, J. D. & Moon, R. T. Mechanism and function of signal transduction by the Wnt/beta-catenin and Wnt/Ca2+ pathways. *Oncogene* **18**, 7860-7872, doi:10.1038/sj.onc.1203245 (1999).
137 Xu, Q. *et al.* Vascular development in the retina and inner ear: control by Norrin and Frizzled-4, a high-affinity ligand-receptor pair. *Cell* **116**, 883-895 (2004).
138 Ke, J. *et al.* Structure and function of Norrin in assembly and activation of a Frizzled 4–Lrp5/6 complex. *Genes & Development* **27**, 2305-2319, doi:10.1101/gad.228544.113 (2013).
139 Kazanskaya, O. *et al.* The Wnt signaling regulator R-spondin 3 promotes angioblast and vascular development. *Development* **135**, 3655-3664, doi:10.1242/dev.027284 (2008).
140 Kim, K. A. *et al.* R-Spondin proteins: a novel link to beta-catenin activation. *Cell Cycle* **5**, 23-26 (2006).
141 Wei, Q. *et al.* R-spondin1 is a high affinity ligand for LRP6 and induces LRP6 phosphorylation and beta-catenin signaling. *The Journal of biological chemistry* **282**, 15903-15911, doi:10.1074/jbc.M701927200 (2007).
142 Nam, J. S., Turcotte, T. J., Smith, P. F., Choi, S. & Yoon, J. K. Mouse cristin/R-spondin family proteins are novel ligands for the Frizzled 8 and LRP6 receptors and activate beta-catenin-dependent gene expression. *The Journal of biological chemistry* **281**, 13247-13257, doi:10.1074/jbc.M508324200 (2006).
143 Kazanskaya, O. *et al.* R-Spondin2 is a secreted activator of Wnt/beta-catenin signaling and is required for Xenopus myogenesis. *Dev Cell* **7**, 525-534, doi:10.1016/j.devcel.2004.07.019 (2004).
144 Binnerts, M. E. *et al.* R-Spondin1 regulates Wnt signaling by inhibiting internalization of LRP6. *Proc Natl Acad Sci U S A* **104**, 14700-14705, doi:10.1073/pnas.0702305104 (2007).
145 Carmon, K. S., Lin, Q., Gong, X., Thomas, A. & Liu, Q. LGR5 interacts and cointernalizes with Wnt receptors to modulate Wnt/beta-catenin signaling. *Mol Cell Biol* **32**, 2054-2064, doi:10.1128/mcb.00272-12 (2012).
146 de Lau, W. *et al.* Lgr5 homologues associate with Wnt receptors and mediate R-spondin signalling. *Nature* **476**, 293-297, doi:10.1038/nature10337 (2011).
147 Glinka, A. *et al.* LGR4 and LGR5 are R-spondin receptors mediating Wnt/beta-catenin and Wnt/PCP signalling. *EMBO reports* **12**, 1055-1061, doi:10.1038/embor.2011.175 (2011).
148 Hao, H. X. *et al.* ZNRF3 promotes Wnt receptor turnover in an R-spondin-sensitive manner. *Nature* **485**, 195-200, doi:10.1038/nature11019 (2012).
149 Ohkawara, B., Glinka, A. & Niehrs, C. Rspo3 binds syndecan 4 and induces Wnt/PCP signaling via clathrin-mediated endocytosis to promote morphogenesis. *Dev Cell* **20**, 303-314, doi:10.1016/j.devcel.2011.01.006 (2011).
150 Niehrs, C. Function and biological roles of the Dickkopf family of Wnt modulators. *Oncogene* **25**, 7469-7481, doi:10.1038/sj.onc.1210054 (2006).
151 Wu, W., Glinka, A., Delius, H. & Niehrs, C. Mutual antagonism between dickkopf1 and dickkopf2 regulates Wnt/beta-catenin signalling. *Current biology : CB* **10**, 1611-1614 (2000).
152 Krupnik, V. E. *et al.* Functional and structural diversity of the human Dickkopf gene family. *Gene* **238**, 301-313 (1999).
153 Pinho, S. & Niehrs, C. Dkk3 is required for TGF-beta signaling during Xenopus mesoderm induction. *Differentiation* **75**, 957-967, doi:10.1111/j.1432-0436.2007.00185.x (2007).
154 Surmann-Schmitt, C. *et al.* Wif-1 is expressed at cartilage-mesenchyme interfaces and impedes Wnt3a-mediated inhibition of chondrogenesis. *Journal of cell science* **122**, 3627-3637, doi:10.1242/jcs.048926 (2009).
155 Sato, H. *et al.* Frequent epigenetic inactivation of DICKKOPF family genes in human gastrointestinal tumors. *Carcinogenesis* **28**, 2459-2466, doi:10.1093/carcin/bgm178 (2007).

156 Bovolenta, P., Esteve, P., Ruiz, J. M., Cisneros, E. & Lopez-Rios, J. Beyond Wnt inhibition: new functions of secreted Frizzled-related proteins in development and disease. *Journal of cell science* **121**, 737-746, doi:10.1242/jcs.026096 (2008).

157 Wawrzak, D. *et al.* Wnt3a binds to several sFRPs in the nanomolar range. *Biochem Biophys Res Commun* **357**, 1119-1123, doi:10.1016/j.bbrc.2007.04.069 (2007).

158 Matsuyama, M., Aizawa, S. & Shimono, A. Sfrp controls apicobasal polarity and oriented cell division in developing gut epithelium. *Plos Genet* **5**, e1000427, doi:10.1371/journal.pgen.1000427 (2009).

159 Satoh, W., Matsuyama, M., Takemura, H., Aizawa, S. & Shimono, A. Sfrp1, Sfrp2, and Sfrp5 regulate the Wnt/beta-catenin and the planar cell polarity pathways during early trunk formation in mouse. *Genesis* **46**, 92-103, doi:10.1002/dvg.20369 (2008).

160 Ohazama, A. *et al.* Lrp4 modulates extracellular integration of cell signaling pathways in development. *PLoS One* **3**, e4092, doi:10.1371/journal.pone.0004092 (2008).

161 Itasaki, N. *et al.* Wise, a context-dependent activator and inhibitor of Wnt signalling. *Development* **130**, 4295-4305 (2003).

162 Guidato, S. & Itasaki, N. Wise retained in the endoplasmic reticulum inhibits Wnt signaling by reducing cell surface LRP6. *Dev Biol* **310**, 250-263, doi:10.1016/j.ydbio.2007.07.033 (2007).

163 Piccolo, S. *et al.* The head inducer Cerberus is a multifunctional antagonist of Nodal, BMP and Wnt signals. *Nature* **397**, 707-710, doi:10.1038/17820 (1999).

164 Belo, J. A. *et al.* Cerberus-like is a secreted BMP and nodal antagonist not essential for mouse development. *Genesis* **26**, 265-270 (2000).

165 Zhu, W. *et al.* IGFBP-4 is an inhibitor of canonical Wnt signalling required for cardiogenesis. *Nature* **454**, 345-349 (2008).

166 Ueno, K. *et al.* IGFBP-4 activates the Wnt/beta-catenin signaling pathway and induces M-CAM expression in human renal cell carcinoma. *Int J Cancer* **129**, 2360-2369, doi:10.1002/ijc.25899 (2011).

167 Furushima, K. *et al.* Mouse homologues of Shisa antagonistic to Wnt and Fgf signalings. *Dev Biol* **306**, 480-492, doi:10.1016/j.ydbio.2007.03.028 (2007).

168 Yamamoto, A., Nagano, T., Takehara, S., Hibi, M. & Aizawa, S. Shisa promotes head formation through the inhibition of receptor protein maturation for the caudalizing factors, Wnt and FGF. *Cell* **120**, 223-235, doi:10.1016/j.cell.2004.11.051 (2005).

169 Kagermeier-Schenk, B. *et al.* Waif1/5T4 inhibits Wnt/beta-catenin signaling and activates noncanonical Wnt pathways by modifying LRP6 subcellular localization. *Dev Cell* **21**, 1129-1143, doi:10.1016/j.devcel.2011.10.015 (2011).

170 Takahashi, M. *et al.* Isolation of a novel human gene, APCDD1, as a direct target of the beta-Catenin/T-cell factor 4 complex with probable involvement in colorectal carcinogenesis. *Cancer Res* **62**, 5651-5656 (2002).

171 Shimomura, Y. *et al.* Apcdd1 is a novel Wnt inhibitor Mutated in Hereditary Hypotrichosis Simplex. *Nature* **464**, 1043-1047, doi:10.1038/nature08875 (2010).

172 Zhang, X. *et al.* Tiki1 is required for head formation via Wnt cleavage-oxidation and inactivation. *Cell* **149**, 1565-1577, doi:10.1016/j.cell.2012.04.039 (2012).

173 Niemann, S. *et al.* Homozygous WNT3 mutation causes tetra-amelia in a large consanguineous family. *Am J Hum Genet* **74**, 558-563, doi:10.1086/382196 (2004).

174 Mani, A. *et al.* LRP6 mutation in a family with early coronary disease and metabolic risk factors. *Science* **315**, 1278-1282, doi:10.1126/science.1136370 (2007).

175 Kinzler, K. W. *et al.* Identification of a gene located at chormosome 5q21 that is mutated in colorectal cancer. *Science* **251**, 1366-1370 (1991).

176 Liu, W. *et al.* Mutations in AXIN2 cause colorectal cancer with defective mismatch repair by activating beta-catenin/TCF signalling. *Nat Genet* **26**, 146-147, doi:10.1038/79859 (2000).

177 Morin, P. *et al.* Activation of b-Catenin–Tcf Signaling in Colon Cancer by Mutations in b-Catenin or APC. *Science* **275**, 1787-1790, doi:10.1126/science.275.5307.1787 (1997).

178 Duval, A. *et al.* Frequent Frameshift Mutations of the TCF-4 Gene in Colorectal Cancers with Microsatellite Instability. *Cancer Research* **59**, 4213-4215 (1999).

179 Hovanes, K. *et al.* Beta-catenin-sensitive isoforms of lymphoid enhancer factor-1 are selectively expressed in colon cancer. *Nat Genet* **28**, 53-57, doi:10.1038/88264 (2001).

180 MacDonald, B. T., Tamai, K. & He, X. Wnt/β-Catenin Signaling: Components, Mechanisms, and Diseases. *Developmental Cell* **17**, 9-26, doi:10.1016/j.devcel.2009.06.016 (2009).

181 Laurent-Puig, P., Beroud, C. & Soussi, T. APC gene: database of germline and somatic mutations in human tumors and cell lines. *Nucleic Acids Res* **26**, 269-270 (1998).

182 Henderson, B. R. Nuclear-cytoplasmic shuttling of APC regulates [beta]-catenin subcellular localization and turnover. *Nat Cell Biol* **2**, 653-660 (2000).

183 He, T.-C. *et al.* Identification of c-MYC as a Target of the APC Pathway. *Science* **281**, 1509-1512, doi:10.1126/science.281.5382.1509 (1998).

184 Wilson, C. L., Heppner, K. J., Labosky, P., Hogan, B. L. M. & Matrisian, L. M. Intestinal tumorigenesis is suppressed in mice lacking the metalloproteinase matrilysin. *PNAS* **94**, 1402-1407 (1997).

185 Zhang, T. *et al.* Evidence That APC Regulates Survivin Expression. *Cancer research* **61** (2001).

186 Koh, T. J. *et al.* Gastrin is a target of the β-catenin/TCF-4 growth-signaling pathway in a model of intestinal polyposis. *J Clin Invest* **106**, 533-539 (2000).

187 Pennica, D. *et al.* WISP genes are members of the connective tissue growth factor family that are up-regulated in Wnt-1-transformed cells and aberrantly expressed in human colon tumors. *Proceedings of the National Academy of Sciences* **95**, 14717-14722 (1998).

188 Townsley, F. M., Cliffe, A. & Bienz, M. Pygopus and Legless target Armadillo/beta-catenin to the nucleus to enable its transcriptional co-activator function. *Nat Cell Biol* **6**, 626-633, doi:10.1038/ncb1141 (2004).

189 Roose, J. *et al.* The Xenopus Wnt effector XTcf-3 interacts with Groucho-related transcriptional repressors. *Nature* **395**, 608-612, doi:10.1038/26989 (1998).

190 Brannon, M., Brown, J. D., Bates, R., Kimelman, D. & Moon, R. T. XCtBP is a XTcf-3 co-repressor with roles throughout Xenopus development. *Development* **126**, 3159-3170 (1999).

191 Zhang, W. *et al.* Novel Cross Talk of Krüppel-Like Factor 4 and beta-Catenin Regulates Normal Intestinal Homeostasis and Tumor Repression. *Mol Cell Biol* **26**, 2055-2064 (2006).

192 Bjerknes, M. & Cheng, H. Clonal analysis of mouse intestinal epithelial progenitors. *Gastroenterology* **116**, 7-14 (1999).

193 Hermiston, M. L., Green, R. P. & Gordon, J. I. Chimeric-transgenic mice represent a powerful tool for studying how the proliferation and differentiation programs of intestinal epithelial cell lineages are regulated. *Proc Natl Acad Sci U S A* **90**, 8866-8870 (1993).

194 Roth, K. A., Hermiston, M. L. & Gordon, J. I. Use of transgenic mice to infer the biological properties of small intestinal stem cells and to examine the lineage relationships of their descendants. *Proc Natl Acad Sci U S A* **88**, 9407-9411 (1991).

195 Lopez-Garcia, C., Klein, A. M., Simons, B. D. & Winton, D. J. Intestinal stem cell replacement follows a pattern of neutral drift. *Science* **330**, 822-825, doi:10.1126/science.1196236 (2010).

196 Snippert, H. J. *et al.* Intestinal crypt homeostasis results from neutral competition between symmetrically dividing Lgr5 stem cells. *Cell* **143**, 134-144, doi:10.1016/j.cell.2010.09.016 (2010).

197 Cheng, H. Origin, differentiation and renewal of the four main epithelial cell types in the mouse small intestine. IV. Paneth cells. *Am J Anat* **141**, 521-535, doi:10.1002/aja.1001410406 (1974).

198 Cheng, H. Origin, differentiation and renewal of the four main epithelial cell types in the mouse small intestine. II. Mucous cells. *Am J Anat* **141**, 481-501, doi:10.1002/aja.1001410404 (1974).

199 Cheng, H. & Leblond, C. P. Origin, differentiation and renewal of the four main epithelial cell types in the mouse small intestine. V. Unitarian Theory of the origin of the four epithelial cell types. *Am J Anat* **141**, 537-561, doi:10.1002/aja.1001410407 (1974).

200 Cheng, H. & Leblond, C. P. Origin, differentiation and renewal of the four main epithelial cell types in the mouse small intestine. I. Columnar cell. *Am J Anat* **141**, 461-479, doi:10.1002/aja.1001410403 (1974).

201 Cheng, H. & Leblond, C. P. Origin, differentiation and renewal of the four main epithelial cell types in the mouse small intestine. III. Entero-endocrine cells. *Am J Anat* **141**, 503-519, doi:10.1002/aja.1001410405 (1974).

202 Potten, C. S., Booth, C. & Pritchard, D. M. The intestinal epithelial stem cell: the mucosal governor. *Int J Exp Pathol* **78**, 219-243 (1997).

203 Qiu, J. M., Roberts, S. A. & Potten, C. S. Cell migration in the small and large bowel shows a strong circadian rhythm. *Epithelial Cell Biol* **3**, 137-148 (1994).

204 Potten, C. S., Gandara, R., Mahida, Y. R., Loeffler, M. & Wright, N. A. The stem cells of small intestinal crypts: where are they? *Cell Prolif* **42**, 731-750, doi:10.1111/j.1365-2184.2009.00642.x (2009).

205 Barker, N. *et al.* Identification of stem cells in small intestine and colon by marker gene Lgr5. *Nature* **449**, 1003-1007, doi:10.1038/nature06196 (2007).

206 Snippert, H. J. *et al.* Lgr6 marks stem cells in the hair follicle that generate all cell lineages of the skin. *Science* **327**, 1385-1389, doi:10.1126/science.1184733 (2010).

207 Guo, W. *et al.* Slug and Sox9 cooperatively determine the mammary stem cell state. *Cell* **148**, 1015-1028, doi:10.1016/j.cell.2012.02.008 (2012).

208 van der Flier, L. G. *et al.* Transcription factor achaete scute-like 2 controls intestinal stem cell fate. *Cell* **136**, 903-912, doi:10.1016/j.cell.2009.01.031 (2009).

209 Holmberg, J. *et al.* EphB receptors coordinate migration and proliferation in the intestinal stem cell niche. *Cell* **125**, 1151-1163, doi:10.1016/j.cell.2006.04.030 (2006).

210 van der Flier, L. G., Haegebarth, A., Stange, D. E., van de Wetering, M. & Clevers, H. OLFM4 is a robust marker for stem cells in human intestine and marks a subset of colorectal cancer cells. *Gastroenterology* **137**, 15-17, doi:10.1053/j.gastro.2009.05.035 (2009).

211 Barker, N. *et al.* Crypt stem cells as the cells-of-origin of intestinal cancer. *Nature* **457**, 608-611, doi:10.1038/nature07602 (2009).

212 Nakanishi, Y. *et al.* Dclk1 distinguishes between tumor and normal stem cells in the intestine. *Nat Genet* **45**, 98-103, doi:10.1038/ng.2481 (2013).

213 van der Flier, L. G. *et al.* Transcription Factor Achaete Scute-Like 2 Controls Intestinal Stem Cell Fate. *Cell* **136**, 903-912, doi:doi: 10.1016/j.cell.2009.01.031 (2009).

214 Koo, B.-K. *et al.* Tumour suppressor RNF43 is a stem-cell E3 ligase that induces endocytosis of Wnt receptors. *Nature* **488**, 665-669, doi:10.1038/nature11308 (2012).

215 Freemont, P. S., Hanson, I. M. & Trowsdale, J. A novel cysteine-rich sequence motif. *Cell* **64**, 483-484, doi:doi: 10.1016/0092-8674(91)90229-R (1991).

216 *Bioinformatics Databases | EBI*, <http://www.ebi.ac.uk/Databases/files/161/Databases.html>

217 Borden, K. L. & Freemont, P. S. The RING finger domain: a recent example of a sequence-structure family. *Curr Opin Struct Biol* **6**, 395-401 (1996).

218 Cheng, G. *et al.* Involvement of CRAF1, a relative of TRAF, in CD40 signaling. *Science* **267**, 1494-1498 (1995).

219 The UniProt, C. The Universal Protein Resource (UniProt). *Nucleic Acids Research* **36**, D190-D195, doi:10.1093/nar/gkm895 (2008).

220 UniProt. <http://www.uniprot.org/uniprot/O00463> (

221 Saurin, A. J., Borden, K., Boddy, M. N. & Freemont, P. S. Does this have a familiar RING? *Trens Biochem Sci.* **21**, 208-214 (1996).

222 Peng, H. *et al.* Reconstitution of the KRAB-KAP-1 repressor complex: a model system for defining the molecular anatomy of RING-B box-coiled-coil domain-mediated protein-protein interactions. *J Mol Biol* **295**, 1139-1162, doi:10.1006/jmbi.1999.3402 (2000).

223 Cohen, N. *et al.* PML RING suppresses oncogenic transformation by reducing the affinity of eIF4E for mRNA. *EMBO J* **20**, 4547-4559, doi:10.1093/emboj/20.16.4547 (2001).
224 Joazeiro, C. A. P. & Weissman, A. M. RING Finger Proteins: Mediators of Ubiquitin Ligase Activity. *Cell* **102**, 549-552, doi:doi: 10.1016/S0092-8674(00)00077-5 (2000).
225 Kang, H. C. *et al.* Iduna is a poly(ADP-ribose) (PAR)-dependent E3 ubiquitin ligase that regulates DNA damage. *Proceedings of the National Academy of Sciences* **108**, 14103-14108, doi:10.1073/pnas.1108799108 (2011).
226 Zhang, Y. *et al.* RNF146 is a poly(ADP-ribose)-directed E3 ligase that regulates axin degradation and Wnt signalling. *Nature Cell Biology* **13**, 623-629, doi:10.1038/ncb2222 (2011).
227 Nakayama, K. *et al.* Siah2 regulates stability of prolyl-hydroxylases, controls HIF1alpha abundance, and modulates physiological responses to hypoxia. *Cell* **117**, 941-952, doi:10.1016/j.cell.2004.06.001 (2004).
228 van Wijk, S. J. L. *et al.* A comprehensive framework of E2–RING E3 interactions of the human ubiquitin–proteasome system. *Molecular Systems Biology* **5**, doi:10.1038/msb.2009.55 (2009).
229 Hashizume, R. *et al.* The RING heterodimer BRCA1-BARD1 is a ubiquitin ligase inactivated by a breast cancer-derived mutation. *The Journal of biological chemistry* **276**, 14537-14540, doi:10.1074/jbc.C000881200 (2001).
230 Wang, H. *et al.* Role of histone H2A ubiquitination in Polycomb silencing. *Nature* **431**, 873-878, doi:10.1038/nature02985 (2004).
231 Linares, L. K., Hengstermann, A., Ciechanover, A., Muller, S. & Scheffner, M. HdmX stimulates Hdm2-mediated ubiquitination and degradation of p53. *Proc Natl Acad Sci U S A* **100**, 12009-12014, doi:10.1073/pnas.2030930100 (2003).
232 Larochelle, S. *et al.* T‐loop phosphorylation stabilizes the CDK7–cyclin H–MAT1 complex in vivo and regulates its CTD kinase activity. *The EMBO Journal* **20**, 3749-3759, doi:10.1093/emboj/20.14.3749 (2001).
233 Inouye, C., Dhillon, N. & Thorner, J. Ste5 RING-H2 Domain: Role in Ste4-Promoted Oligomerization for Yeast Pheromone Signaling. *Science* **278**, 103-106, doi:10.1126/science.278.5335.103 (1997).
234 Kales, S. C., Ryan, P. E., Nau, M. M. & Lipkowitz, S. Cbl and human myeloid neoplasms: the Cbl oncogene comes of age. *Cancer Res* **70**, 4789-4794, doi:10.1158/0008-5472.CAN-10-0610 (2010).
235 Oliner, J. D., Kinzler, K. W., Meltzer, P. S., George, D. L. & Vogelstein, B. Amplification of a gene encoding a p53-associated protein in human sarcomas. *Nature* **358**, 80-83, doi:10.1038/358080a0 (1992).
236 Wade, M., Wang, Y. V. & Wahl, G. M. The p53 orchestra: Mdm2 and Mdmx set the tone. *Trends Cell Biol* **20**, 299-309, doi:10.1016/j.tcb.2010.01.009 (2010).
237 Welcsh, P. L. & King, M. C. BRCA1 and BRCA2 and the genetics of breast and ovarian cancer. *Hum Mol Genet* **10**, 705-713 (2001).
238 Gnarra, J. R. *et al.* Mutations of the VHL tumour suppressor gene in renal carcinoma. *Nat Genet* **7**, 85-90, doi:10.1038/ng0594-85 (1994).
239 Latif, F. *et al.* Identification of the von Hippel-Lindau disease tumor suppressor gene. *Science* **260**, 1317-1320 (1993).
240 Marikawa, Y. & Elinson, R. P. beta-TrCP is a negative regulator of Wnt/beta-catenin signaling pathway and dorsal axis formation in Xenopus embryos. *Mechanisms of development* **77**, 75-80 (1998).
241 Ougolkov, A. *et al.* Associations among beta-TrCP, an E3 ubiquitin ligase receptor, beta-catenin, and NF-kappaB in colorectal cancer. *Journal of the National Cancer Institute* **96**, 1161-1170, doi:10.1093/jnci/djh219 (2004).
242 Muerkoster, S. *et al.* Increased expression of the E3-ubiquitin ligase receptor subunit betaTRCP1 relates to constitutive nuclear factor-kappaB activation and chemoresistance in pancreatic carcinoma cells. *Cancer Res* **65**, 1316-1324, doi:10.1158/0008-5472.can-04-1626 (2005).

243 Liu, J. *et al.* Oncogenic BRAF regulates beta-Trcp expression and NF-kappaB activity in human melanoma cells. *Oncogene* **26**, 1954-1958, doi:10.1038/sj.onc.1209994 (2007).

244 Saitoh, T. & Katoh, M. Expression profiles of betaTRCP1 and betaTRCP2, and mutation analysis of betaTRCP2 in gastric cancer. *Int J Oncol* **18**, 959-964 (2001).

245 Gerstein, A. V. *et al.* APC/CTNNB1 (beta-catenin) pathway alterations in human prostate cancers. *Genes, chromosomes & cancer* **34**, 9-16 (2002).

246 *UCSC Genome Browser database*, <https://genome.ucsc.edu/>

247 Sugiura, T., Yamaguchi, A. & Miyamoto, K. A cancer-associated RING finger protein, RNF43, is an ubiquitin ligase that interacts with a nuclear protein, HAP95. *Experimental cell research* **314**, 1519-1528 (2008).

248 Yagyu, R. *et al.* A novel oncoprotein RNF43 functions in an autocrine manner in colorectal cancer. *Int J Oncol* **25**, 1343-1348 (2004).

249 Xing, C. *et al.* Reversing Effect of Ring Finger Protein 43 Inhibition on Malignant Phenotypes of human Hepatocellular Carcinoma. *Molecular cancer therapeutics*, doi:10.1158/1535-7163.MCT-12-0672 (2012).

250 Wu, J. *et al.* Whole-exome sequencing of neoplastic cysts of the pancreas reveals recurrent mutations in components of ubiquitin-dependent pathways. *Proceedings of the National Academy of Sciences* **108**, 21188-21193, doi:10.1073/pnas.1118046108 (2011).

251 Furukawa, T. *et al.* Whole-exome sequencing uncovers frequent GNAS mutations in intraductal papillary mucinous neoplasms of the pancreas. *Scientific Reports* **1**, doi:10.1038/srep00161 (2011).

252 Ryland, G. L. *et al.* RNF43 is a tumour suppressor gene mutated in mucinous tumours of the ovary. *The Journal of Pathology*, n/a-n/a, doi:10.1002/path.4134 (2012).

253 Ong, C. K. *et al.* Exome sequencing of liver fluke-associated cholangiocarcinoma. *Nat Genet* **44**, 690-693, doi:10.1038/ng.2273 (2012).

254 Jo, Y. S. *et al.* Frequent frameshift mutations in 2 mononucleotide repeats of RNF43 gene and its regional heterogeneity in gastric and colorectal cancers. *Hum Pathol*, doi:10.1016/j.humpath.2015.07.004 (2015).

255 Wang, K. *et al.* Whole-genome sequencing and comprehensive molecular profiling identify new driver mutations in gastric cancer. *Nat Genet* **46**, 573-582, doi:10.1038/ng.2983 (2014).

256 Giannakis, M. *et al.* RNF43 is frequently mutated in colorectal and endometrial cancers. *Nat Genet*, doi:10.1038/ng.3127 (2014).

257 Jiang, X., Charlat, O., Zamponi, R., Yang, Y. & Cong, F. Dishevelled Promotes Wnt Receptor Degradation through Recruitment of ZNRF3/RNF43 E3 Ubiquitin Ligases. *Mol Cell*, doi:10.1016/j.molcel.2015.03.015 (2015).

258 Peng, W. C. *et al.* Structures of Wnt-Antagonist ZNRF3 and Its Complex with R-Spondin 1 and Implications for Signaling. *PLoS One* **8**, e83110, doi:10.1371/journal.pone.0083110 (2013).

259 Zebisch, M. *et al.* Structural and molecular basis of ZNRF3/RNF43 transmembrane ubiquitin ligase inhibition by the Wnt agonist R-spondin. *Nature communications* **4**, 2787, doi:10.1038/ncomms3787 (2013).

260 Zebisch, M. & Yvonne Jones, E. Crystal structure of R-spondin 2 in complex with the ectodomains of its receptors LGR5 and ZNRF3. *J Struct Biol*, doi:10.1016/j.jsb.2015.05.008 (2015).

261 Miyamoto, K., Sakurai, H. & Sugiura, T. Proteomic identification of a PSF/p54nrb heterodimer as RNF43 oncoprotein-interacting proteins. *Proteomics* **8**, 2907-2910, doi:10.1002/pmic.200800083 (2008).

262 Nailwal, H., Sharma, S., Mayank, A. K. & Lal, S. K. The nucleoprotein of influenza A virus induces p53 signaling and apoptosis via attenuation of host ubiquitin ligase RNF43. *Cell death & disease* **6**, e1768, doi:10.1038/cddis.2015.131 (2015).

263 Gala, M. K. *et al.* Germline mutations in oncogene-induced senescence pathways are associated with multiple sessile serrated adenomas. *Gastroenterology* **146**, 520-529, doi:10.1053/j.gastro.2013.10.045 (2014).

264 Shinada, K. *et al.* RNF43 interacts with NEDL1 and regulates p53-mediated transcription. *Biochemical and Biophysical Research Communications* (2010).

265 Jiang, X. *et al.* Inactivating mutations of RNF43 confer Wnt dependency in pancreatic ductal adenocarcinoma. *Proc Natl Acad Sci U S A* **110**, 12649-12654, doi:10.1073/pnas.1307218110 (2013).

266 Degenhart, K. *Charakterisierung genetischer un epigenetischer Veränderungen von RNF43 in kolorektalen Karzinomen* M.Sc. Biologie thesis, TU München, (2012).

267 Takahashi, N., Yamaguchi, K., Ikenoue, T., Fujii, T. & Furukawa, Y. Identification of two Wnt-responsive elements in the intron of RING finger protein 43 (RNF43) gene. *PLoS One* **9**, e86582, doi:10.1371/journal.pone.0086582 (2014).

268 Loregger, A. *et al.* The E3 ligase RNF43 inhibits Wnt signaling downstream of mutated beta-catenin by sequestering TCF4 to the nuclear membrane. *Science signaling* **8**, ra90, doi:10.1126/scisignal.aac6757 (2015).

269 Cuilliere-Dartigues, P. *et al.* TCF-4 isoforms absent in TCF-4 mutated MSI-H colorectal cancer cells colocalize with nuclear CtBP and repress TCF-4-mediated transcription. *Oncogene* **25**, 4441-4448, doi:10.1038/sj.onc.1209471 (2006).

270 Korinek, V. *et al.* Two members of the Tcf family implicated in Wnt/beta-catenin signaling during embryogenesis in the mouse. *Mol Cell Biol* **18**, 1248-1256 (1998).

271 Valenta, T., Lukas, J. & Korinek, V. HMG box transcription factor TCF-4's interaction with CtBP1 controls the expression of the Wnt target Axin2/Conductin in human embryonic kidney cells. *Nucleic Acids Res* **31**, 2369-2380, doi:10.1093/nar/gkg346 (2003).

272 Yan, D. *et al.* Elevated expression of axin2 and hnkd mRNA provides evidence that Wnt/beta -catenin signaling is activated in human colon tumors. *Proc Natl Acad Sci U S A* **98**, 14973-14978, doi:10.1073/pnas.261574498 (2001).

273 Howe, L. R., Watanabe, O., Leonard, J. & Brown, A. M. Twist is up-regulated in response to Wnt1 and inhibits mouse mammary cell differentiation. *Cancer Res* **63**, 1906-1913 (2003).

274 Brabletz, T., Jung, A., Dag, S., Hlubek, F. & Kirchner, T. beta-catenin regulates the expression of the matrix metalloproteinase-7 in human colorectal cancer. *The American journal of pathology* **155**, 1033-1038 (1999).

275 PSORTII. <http://psort.hgc.jp/form2.html>

276 Shen, B. *et al.* Efficient genome modification by CRISPR-Cas9 nickase with minimal off-target effects. *Nat Meth* **11**, 399-402, doi:10.1038/nmeth.2857 (2014).

277 Rivlin, N., Brosh, R., Oren, M. & Rotter, V. Mutations in the p53 Tumor Suppressor Gene: Important Milestones at the Various Steps of Tumorigenesis. *Genes & Cancer* **2**, 466-474, doi:10.1177/1947601911408889 (2011).

278 Ryland, G. L. *et al.* RNF43 is a tumour suppressor gene mutated in mucinous tumours of the ovary. *J Pathol* **229**, 469-476, doi:Doi 10.1002/Path.4134 (2013).

279 Cancer Genome Atlas, N. Comprehensive molecular characterization of human colon and rectal cancer. *Nature* **487**, 330-337, doi:10.1038/nature11252 (2012).

280 Niu, L. *et al.* RNF43 Inhibits Cancer Cell Proliferation and Could be a Potential Prognostic Factor for Human Gastric Carcinoma. *Cell Physiol Biochem* **36**, 1835-1846, doi:10.1159/000430154 (2015).

281 Sakamoto, H. *et al.* Clinicopathological significance of somatic RNF43 mutation and aberrant expression of ring finger protein 43 in intraductal papillary mucinous neoplasms of the pancreas. *Mod Pathol* **28**, 261-267, doi:10.1038/modpathol.2014.98 (2015).

282 Zebisch, M. & Jones, E. Y. ZNRF3/RNF43--A direct linkage of extracellular recognition and E3 ligase activity to modulate cell surface signalling. *Prog Biophys Mol Biol* **118**, 112-118, doi:10.1016/j.pbiomolbio.2015.04.006 (2015).

283 Xie, H. *et al.* Association of RNF43 with cell cycle proteins involved in p53 pathway. *Int J Clin Exp Pathol* **8**, 14995-15000 (2015).

284 Luijsterburg, M. S. *et al.* A new non-catalytic role for ubiquitin ligase RNF8 in unfolding higher-order chromatin structure. *EMBO J* **31**, 2511-2527, doi:10.1038/emboj.2012.104 (2012).

285 Zhou, Y. *et al.* ZNRF3 acts as a tumour suppressor by the Wnt signalling pathway in human gastric adenocarcinoma. *Journal of molecular histology* **44**, 555-563, doi:10.1007/s10735-013-9504-9 (2013).
286 Fernandez-Suarez, M. & Ting, A. Y. Fluorescent probes for super-resolution imaging in living cells. *Nat Rev Mol Cell Biol* **9**, 929-943, doi:10.1038/nrm2531 (2008).
287 Fricker, M., Runions, J. & Moore, I. Quantitative fluorescence microscopy: from art to science. *Annual review of plant biology* **57**, 79-107, doi:10.1146/annurev.arplant.57.032905.105239 (2006).
288 Skube, S. B., Chaverri, J. M. & Goodson, H. V. Effect of GFP tags on the localization of EB1 and EB1 fragments in vivo. *Cytoskeleton (Hoboken, N.j.)* **67**, 1-12, doi:10.1002/cm.20409 (2010).
289 Lisenbee, C. S., Karnik, S. K. & Trelease, R. N. Overexpression and mislocalization of a tail-anchored GFP redefines the identity of peroxisomal ER. *Traffic* **4**, 491-501 (2003).
290 Boshart, M. *et al.* A very strong enhancer is located upstream of an immediate early gene of human cytomegalovirus. *Cell* **41**, 521-530 (1985).
291 Ghazal, P., Lubon, H., Fleckenstein, B. & Hennighausen, L. Binding of transcription factors and creation of a large nucleoprotein complex on the human cytomegalovirus enhancer. *Proc Natl Acad Sci U S A* **84**, 3658-3662 (1987).
292 Thomsen, D. R., Stenberg, R. M., Goins, W. F. & Stinski, M. F. Promoter-regulatory region of the major immediate early gene of human cytomegalovirus. *Proc Natl Acad Sci U S A* **81**, 659-663 (1984).
293 Xia, W. *et al.* High levels of protein expression using different mammalian CMV promoters in several cell lines. *Protein Expression and Purification* **45**, 115-124 (2006).
294 Gibson, T. J., Seiler, M. & Veitia, R. A. The transience of transient overexpression. *Nat Meth* **10**, 715-721, doi:10.1038/nmeth.2534 (2013).
295 Lord, J. M., Davey, J., Frigerio, L. & Roberts, L. M. Endoplasmic reticulum-associated protein degradation. *Semin Cell Dev Biol* **11**, 159-164, doi:10.1006/scdb.2000.0160 (2000).
296 Moore, I. & Murphy, A. Validating the location of fluorescent protein fusions in the endomembrane system. *Plant Cell* **21**, 1632-1636, doi:10.1105/tpc.109.068668 (2009).
297 Trombetta, E. S. & Parodi, A. J. Quality control and protein folding in the secretory pathway. *Annu Rev Cell Dev Biol* **19**, 649-676, doi:10.1146/annurev.cellbio.19.110701.153949 (2003).
298 Ivorra, C. *et al.* A mechanism of AP-1 suppression through interaction of c-Fos with lamin A/C. *Genes Dev* **20**, 307-320, doi:10.1101/gad.349506 (2006).
299 Markiewicz, E. *et al.* The inner nuclear membrane protein emerin regulates beta-catenin activity by restricting its accumulation in the nucleus. *EMBO J* **25**, 3275-3285, doi:10.1038/sj.emboj.7601230 (2006).
300 Shitashige M Fau - Satow, R. *et al.* Regulation of Wnt signaling by the nuclear pore complex.
301 Eyal, E., Najmanovich, R., Edelman, M. & Sobolev, V. Protein side-chain rearrangement in regions of point mutations. *Proteins* **50**, 272-282, doi:10.1002/prot.10276 (2003).
302 Weinberg, R. Tumor suppressor genes. *Science* **254**, 1138-1146, doi:10.1126/science.1659741 (1991).
303 Zilfou, J. T. & Lowe, S. W. Tumor Suppressive Functions of p53. *Cold Spring Harbor perspectives in biology* **1**, a001883, doi:10.1101/cshperspect.a001883 (2009).
304 Eliyahu, D., Michalovitz, D., Eliyahu, S., Pinhasi-Kimhi, O. & Oren, M. Wild-type p53 can inhibit oncogene-mediated focus formation. *Proc Natl Acad Sci U S A* **86**, 8763-8767 (1989).
305 Finlay, C. A., Hinds, P. W. & Levine, A. J. The p53 proto-oncogene can act as a suppressor of transformation. *Cell* **57**, 1083-1093 (1989).
306 Wang, S.-P. *et al.* p53 controls cancer cell invasion by inducing the MDM2-mediated degradation of Slug. *Nat Cell Biol* **11**, 694-704 (2009).

307 Muller, P. A. J. *et al.* Mutant p53 Drives Invasion by Promoting Integrin Recycling. *Cell* **139**, 1327-1341, (2009).

308 Campbell, C., Quinn, A. G., Ro, Y.-S., Angus, B. & Rees, J. L. p53 Mutations Are Common and Early Events that Precede Tumor Invasion in Squamous Cell Neoplasia of the Skin. *Journal of Investigative Dermatology* **100**, 746-748 (1993).

309 Miyaki, M. *et al.* Characteristics of somatic mutation of the adenomatous polyposis coli gene in colorectal tumors. *Cancer Res* **54**, 3011-3020 (1994).

310 Ichii, S. *et al.* Detailed analysis of genetic alterations in colorectal tumors from patients with and without familial adenomatous polyposis (FAP). *Oncogene* **8**, 2399-2405 (1993).

311 Sansom, O. J. *et al.* Loss of Apc in vivo immediately perturbs Wnt signaling, differentiation, and migration. *Genes Dev* **18**, 1385-1390, doi:10.1101/gad.287404 (2004).

312 Sansom, O. J. *et al.* Myc deletion rescues Apc deficiency in the small intestine. *Nature* **446**, 676-679, doi:10.1038/nature05674 (2007).

313 Taupin, D. *et al.* A deleterious RNF43 germline mutation in a severely affected serrated polyposis kindred. *Human Genome Variation* **2**, 15013, doi:10.1038/hgv.2015.13 (2015).

314 Herr, P., Hausmann, G. & Basler, K. WNT secretion and signalling in human disease. *Trends in molecular medicine* **18**, 483-493, doi:10.1016/j.molmed.2012.06.008 (2012).

315 Takada, R. *et al.* Monounsaturated fatty acid modification of Wnt protein: its role in Wnt secretion. *Dev Cell* **11**, 791-801, doi:10.1016/j.devcel.2006.10.003 (2006).

316 Koo, B. K., van Es, J. H., van den Born, M. & Clevers, H. Porcupine inhibitor suppresses paracrine Wnt-driven growth of Rnf43;Znrf3-mutant neoplasia. *Proc Natl Acad Sci U S A* **112**, 7548-7550, doi:10.1073/pnas.1508113112 (2015).

317 van de Wetering, M. *et al.* Prospective derivation of a living organoid biobank of colorectal cancer patients. *Cell* **161**, 933-945, doi:10.1016/j.cell.2015.03.053 (2015).

318 Yang, Q., Bermingham, N. A., Finegold, M. J. & Zoghbi, H. Y. Requirement of Math1 for secretory cell lineage commitment in the mouse intestine. *Science* **294**, 2155-2158, doi:10.1126/science.1065718 (2001).

319 van Es, J. H. *et al.* Notch/gamma-secretase inhibition turns proliferative cells in intestinal crypts and adenomas into goblet cells. *Nature* **435**, 959-963, doi:10.1038/nature03659 (2005).

320 Axelrod, J. D., Matsuno, K., Artavanis-Tsakonas, S. & Perrimon, N. Interaction between Wingless and Notch signaling pathways mediated by dishevelled. *Science* **271**, 1826-1832 (1996).

321 Munoz-Descalzo, S. *et al.* Wingless modulates the ligand independent traffic of Notch through Dishevelled. *Fly (Austin)* **4**, 182-193, doi:10.4161/fly.4.3.11998 (2010).

322 Collu, G. M. *et al.* Dishevelled limits Notch signalling through inhibition of CSL. *Development* **139**, 4405-4415, doi:10.1242/dev.081885 (2012).

323 Foltz, D. R., Santiago, M. C., Berechid, B. E. & Nye, J. S. Glycogen synthase kinase-3beta modulates notch signaling and stability. *Current biology : CB* **12**, 1006-1011 (2002).

324 Leow, C. C., Romero, M. S., Ross, S., Polakis, P. & Gao, W. Q. Hath1, down-regulated in colon adenocarcinomas, inhibits proliferation and tumorigenesis of colon cancer cells. *Cancer Res* **64**, 6050-6057, doi:10.1158/0008-5472.CAN-04-0290 (2004).

325 Tsuchiya, K., Nakamura, T., Okamoto, R., Kanai, T. & Watanabe, M. Reciprocal targeting of Hath1 and beta-catenin by Wnt glycogen synthase kinase 3beta in human colon cancer. *Gastroenterology* **132**, 208-220, doi:10.1053/j.gastro.2006.10.031 (2007).

326 Phesse, T. J. *et al.* Partial inhibition of gp130-Jak-Stat3 signaling prevents Wnt-beta-catenin-mediated intestinal tumor growth and regeneration. *Science signaling* **7**, ra92, doi:10.1126/scisignal.2005411 (2014).

327 Fragoso, M. A. *et al.* The Wnt/beta-catenin pathway cross-talks with STAT3 signaling to regulate survival of retinal pigment epithelium cells. *PLoS One* **7**, e46892, doi:10.1371/journal.pone.0046892 (2012).

328 Katoh, M. & Katoh, M. Transcriptional mechanisms of WNT5A based on NF-kappaB, Hedgehog, TGFbeta, and Notch signaling cascades. *International journal of molecular medicine* **23**, 763-769 (2009).

Publications

First author:

Loregger A*, Grandl M*, Mejías-Luque R, Allgäuer M, Degenhart K, Haselmann V, Oikonomou C, Hatzis P, Janssen KP, Nitsche U, Gradl D, van den Broek O, Destree O, Ulm K, Neumaier M, Kalali B, Jung A, Varela I, Schmid RM, Rad R, Busch DH, Gerhard M.; **The E3 ligase RNF43 inhibits Wnt signaling downstream of mutated β-catenin by sequestering TCF4 to the nuclear membrane**. *Sci Signal.* Sep 8;8(393):ra90. doi: 10.1126/scisignal.aac6757 (2015)

Co-author:

Beil-Wagner J, Dössinger G, Schober K, Vom Berg J, Tresch A, Grandl M, Palle P, Mair F, Gerhard M, Becher B, Busch DH, Buch T.: **T cell-specific inactivation of mouse CD2 by CRISPR/Cas9.** *Sci Rep*. Feb 23;6:21377. doi: 10.1038/srep21377. (2016)

Schelter F, Grandl M, Seubert B, Schaten S, Hauser S, Gerg M, Boccaccio C, Comoglio P, Krüger A.: **Tumor cell-derived Timp-1 is necessary for maintaining metastasis-promoting Met-signaling via inhibition of Adam-10.** *Clin Exp Metastasis*. Dec;28(8):793-802. doi: 10.1007/s10585-011-9410-z. (2011)

Declaration

I, Martina Grandl, hereby declare that I independently prepared the present thesis, using only the references and resources stated. This work has not been submitted to any examination board yet.

Danksagung

Mein besonderer Dank gilt:

Herrn Prof. Dr. med. Markus Gerhard für die interessante Themenstellung, die Aufnahme in seinen Arbeitskreis, seine fachlichen Ratschläge und das große Interesse, dass er meiner Arbeit entgegenbrachte, sowie den wertvollen wissenschaftlichen Gesprächen, die maßgeblich zum Gelingen dieser Arbeit beigetragen haben.

Ich danke **Herrn Prof. Dr. Martin Hrabé de Angelis** für die Zweitbetreuung, Unterstützung und die hilfreichen Diskussionen in den Committee Meetings.

Weiterhin möchte ich mich ganz herzlich bedanken:

bei **Frau Dr. Raquel Mejías-Luque** für die hervorragende wissenschaftliche Betreuung und die motivierende Zusammenarbeit in einem Projekt mit vielen Höhen und Tiefen. Von ihrem fachlichen Wissen, den ausgiebigen lehrreichen Diskussionen und wertvollen Ratschläge sowie dem kritischen Korrekturlesen dieser Arbeit konnte ich in vielfältiger Weise profitieren.

bei **Herrn Dr. Pantelis Hatzis,** meinem Mentor, für seine großartige wissenschaftliche Betreuung und die warmherzige, motivierende Zusammenarbeit und Diskussionen sowie für den äußerst lehrreichen und wunderbaren Aufenthalt in seiner Arbeitsgruppe am Alexander Fleming Institut in Vari, Griechenland.

bei **Herrn Dr. Behnam Kalali** für die Einführung, Hilfe und Unterstützung bei der Generierung der RNF43 Mäuse mittels CRISPR/Cas9, und seiner hilfreichen Ratschläge und Diskussionen.

bei **Frau Dr. Martina Anton** von der Experimentellen Onkologie und Therapieforschung am Klinikum rechts der Isar für die Einführung und Hilfe im Umgang mit lentiviraler shRNA.

bei **Herrn PD Dr. Klaus-Peter Janssen** und **Herrn Dr. Ulrich Nitzsche** von der II Medizinischen Klinik und Poliklinik am Klinikum rechts der Isar für die Bereitstellung der humanen Tumorproben und den vielen wertvollen Diskussionen und Informationen.

bei **Herrn Prof. Dr. Roland Rad** (der II Medizinischen Klinik und Poliklinik am Klinikum rechts der Isar) und **Herrn Dr. Ignacio Varela** (Instituto de Biomedicina y Biotecnología de Cantabira, Spanien) sowie **Frau Dr. Verena Haselmann** (Institut für Klinische Chemie, Universität Mannheim) für die Kooperation zur Messung und Auswertung vieler Proben mittels Next-Generation-Sequencing und den anregenden Austausch und hilfreiche Diskussionen.

Frau Dr. Elisabeth Kremmer (Institut für Molekulare Immunologie am Helmholtz Zentrum München) für die Kooperation zur Herstellung monoklonaler Antikörper gegen endogenes RNF43.

bei **Herrn Prof. Dr. Dirk Busch** für die Möglichkeit, mein Projekt am Institut für Medizinische Mikrobiologie, Immunologie und Hygiene bearbeiten zu dürfen

Des Weiteren möchte ich mich bedanken bei:

Frau Dr. Anke Loregger für ihre Hilfe bei der Einführung in das Thema und wertvollen Beiträge in den Diskussionen.

Frau Kathrin Degenhart, Herrn Michael Allgäuer und **Frau Victoria Neumeyer** für Ihre entspannte Unterstützung und der tollen Zusammenarbeit im Kampf rund um das RNF43 Projekt.

Frau Jane Beil-Wagner aus der Gruppe von Herrn Prof. Dr. Thorsten Buch für ihre großartige Unterstützung, den hilfreichen Tipps und Troubleshooting und rund um das CRISPRN.

Frau Agnieszka Pastuła aus der Gruppe von Herrn Prof. Dr. Michael Quante (II Medizinische Klinik und Poliklinik am Klinikum rechts der Isar) für die Einführung und die großartige Unterstützung bei der Isolation von murinen Darmkrypten und der Kultivierung der Organoide.

Herrn Dr. Christian Bolz und **Herrn Tobias Kruse** aus der Firma Imevax für ihre Hilfe bei der Antikörperaufreinigung.

Mein Dank gilt ferner:

Frau Jeannette Koch, **Frau Ina Sebald, Frau Daniela Scheikl, Frau Ramona Nitiu** und **Frau Karin Mink** für ihre Hilfsbereitschaft, Unterstützung in der Zellkultur, im Labor sowie bei den Mäusen.

Herrn Martin Skerhut für die geduldige Einführung, endlose Unterstützung und Hilfe bei der Mäusezucht.

Frau Karin Mink und **Frau Katarzyna Jopek** (Kasia) für die zahlreichen, geduldigen Injektionen zur Herstellung der RNF43 Mäuse.

Meinen beiden großartigen Helferinnen **Frau Abirami Rathakrishnan** und **Frau Alexandra Hambsch** für den Zusammenhalt im Labor und die gemeinsame Bewältigung alltäglicher und außergewöhnlicher Herausforderungen.

Insbesondere danke ich der „RNF43-Gruppe“ für den anregenden Austausch und die vielen kleinen Hilfen mit herausfordernden Experimenten und Daten.

Darüber hinaus möchte ich mich bei **allen Mitgliedern der Arbeitsgruppe Gerhard** für die außergewöhnliche Hilfsbereitschaft, die tatkräftige Unterstützung und entspannte Atmosphäre bedanken.

★★★

Ganz besonders danke ...

... ich **meinen Eltern**, **meiner Schwester Pia** und **meinem Schwager Andreas**, ohne deren grenzenlose Unterstützung nichts möglich gewesen wäre. Danke für alles!